

**ADVANCED CHARACTERISATION OF RAILWAY BALLAST  
ROUNDNESS**

**GCULISILE MAVIS MVELASE**

**A dissertation submitted in partial fulfilment of the requirements for the degree of**

**MASTER OF ENGINEERING (GEOTECHNICAL ENGINEERING)**

**In the**

**FACULTY OF ENGINEERING**

**UNIVERSITY OF PRETORIA**

**August 2017**

## DISSERTATION SUMMARY

### ADVANCED CHARACTERISATION OF RAILWAY BALLAST ROUNDNESS

GM MVELASE

<b>Supervisor:</b>	Professor PJ Gräbe
<b>Co- Supervisor:</b>	Doctor JK Anochie-Boateng
<b>Department:</b>	Civil Engineering
<b>University:</b>	University of Pretoria
<b>Degree:</b>	Master of Engineering (Geotechnical Engineering)

The performance of a railway track structure is significantly influenced by ballast shape properties such as roundness, flatness, elongation, sphericity, angularity and surface texture. Railway ballast materials have to comply with several quality requirements and shape properties. Accurate measurement of the shape properties is important for developing and revising specifications for quality control and quality assurance in the selection of ballast materials for railway construction. However, the current test methods for determining these properties have severe shortcomings such as poor repeatability and subjectivity. In addition, they are often based on visual measurements and empirically developed charts, which lack scientific standing.

In this study, an advanced three-dimensional (3D) laser scanning was used to quantify the shapes of railway ballast materials from a heavy haul coal line in South Africa. This study complements the current research by the Council for Scientific and Industrial Research (CSIR) that is aimed at introducing advancement and scientific approach (i.e. 3D-laser scanning and numerical techniques) to effectively model the shape of crushed stones i.e. aggregates for roads and ballast for railways used in transport infrastructure. The primary objective was to investigate the effect of ballast particle shape, determined from a modern 3D-laser scanning technique, on the performance characteristics (i.e. shear strength and permanent deformation) of ballast materials. Overall, five ballast materials (four recycled ballast materials from the coal line and one freshly crushed ballast) and one river aggregate were investigated for this study.

All six materials were scanned in the 3D-laser scanning system and the data were processed to reconstruct three dimensional models of the ballast and the river pebble particles. The models were further analysed to determine the roundness, flatness, elongation, and sphericity shape properties of the particles. The results obtained were used to develop different charts to characterise ballast shapes. An ANOVA (Analysis of variance) statistical analysis was conducted on the three dimensional data to establish which individual ballast particles contributed significantly to the overall shape parameters.

To evaluate the effects of the shape properties on the behaviour of ballast in the track structure, a laboratory testing programme was conducted to determine the settlement behaviour and shear strength of the ballast materials. Repeated load permanent deformation tests were conducted to evaluate the overall settlement behaviour, whereas monotonic static triaxial tests were used to determine the shear strength properties of the ballast materials. The results indicated that ballast materials with low roundness values exhibited low shear strength and high permanent deformation (settlement). Although this was expected, the use of the automated 3D-laser scanning approach introduced a high level of accuracy and confidence in the results.

Based on the laser results, a new empirical model was developed to determine the surface area of the ballast materials. The surface area values were further used to develop a chart to assess different particle shapes with varying degrees of roundness. Triaxial tests were conducted to determine the effect of the roundness on the shear strength properties of the materials. A Mohr-Coulomb failure model was successfully developed from the results to represent the individual materials tested. The overall results show that the angle of internal friction decreases with an increase in the roundness index of the particles. More rounded particles have roundness index values of between 1.4 and 1.7 whereas less rounded particles have roundness index values of between 0.8 and 1.3. The outcomes of this study would assist with quality control in the field as to whether or not to replace degraded ballast in the track layer. It is anticipated that this study will enhance improved guidelines, test methods and specifications for the selection of ballast materials, and consequently ensure good performance of railway infrastructure in South Africa.

## **DECLARATION**

I, the undersigned hereby declare that:

- I understand what plagiarism is and I am aware of the University's policy in this regard;
- The work contained in this thesis is my own original work;
- I did not refer to work of current or previous students, lecture notes, handbooks or any other study material without proper referencing;
- Where other people's work has been used, this has been properly acknowledged and referenced;
- I have not allowed anyone to copy any part of my thesis; and
- I have not previously in its entirety or in part submitted this thesis at any university for a degree.

### **Signature of student**

#### **Name of student**

Gculisile Mavis Mvelase

#### **Student number**

28449887

#### **Date**

17 August 2017

## ACKNOWLEDGEMENT

I wish to express my appreciation to the following organisations and persons who made this research possible:

- a) Professor Hannes Gräbe, my supervisor, for his guidance and support during the study.
- b) Doctor Joseph Anochie-Boateng, my co-supervisor and mentor on this study, for his invaluable guidance and supervision throughout the whole research. This dissertation would not have been completed without his immense support.
- c) This project is based on a research project of Council of Scientific Industrial Research (CSIR). My study was mainly funded under a CSIR R&D Strategic Research Panel (SRP) project TA-2011-001 led by Dr JK Anochie-Boateng as the Principal Investigator (PI).
- d) Transnet Freight Rail (TFR) for financial support, as well as the use of laboratory facilities during the course of the study.
- e) The University of Pretoria for the use of laboratory facilities during the course of this study.
- f) The following persons are gratefully acknowledged for their assistance during the course of the study:
  1. Dr M de Beer from CSIR who introduced me to the CSIR laser scanning research group.
  2. Mr L Msibi, Principal Engineer of TFR, for his support during the finalisation of the dissertation.
  3. Mr JS Maree, Principal Engineer of TFR, for his initiation of the laser scanning research collaboration work on railway ballast with the CSIR.
  4. Mr P Kawula from TFR Vryheid Depot for funding the sampling of the ballast materials from the field.
  5. Mr J Komba and Mr Lucyboy Mohale from the CSIR for providing training on laser scanning and assistance in the scanning of the ballast materials.
  6. Mr V Zitholele, technician of TFR, who was involved in the scanning of the ballast samples.
- g) My parents, my daughter and all family members for their constant support, belief, and encouragement during this study.

## TABLE OF CONTENTS

1	INTRODUCTION .....	1-1
1.1	BACKGROUND .....	1-1
1.2	PROBLEM STATEMENT .....	1-2
1.3	OBJECTIVES OF THE STUDY .....	1-3
1.4	HYPOTHESIS.....	1-3
1.5	SCOPE OF THE STUDY .....	1-3
1.6	METHODOLOGY .....	1-4
1.7	ORGANISATION OF THE REPORT.....	1-4
2	LITERATURE REVIEW .....	2-1
2.1	INTRODUCTION.....	2-1
2.2	BALLAST.....	2-1
2.2.1	Effect of ballast characteristics on behaviour .....	2-4
2.2.2	Ballast selection tests .....	2-6
2.3	TECHNIQUES TO DETERMINE BALLAST SHAPE PROPERTIES.....	2-7
2.3.1	Advanced three dimensional laser based technique.....	2-8
2.3.2	Image-based techniques .....	2-9
2.4	KEY BALLAST SHAPE PROPERTIES.....	2-10
2.4.1	Parameters of ballast particle shape.....	2-12
2.4.2	Sphericity in 2D.....	2-14
2.4.3	Sphericity in three dimensional .....	2-15
2.4.4	Current approach to derive ballast roundness using 2D images .....	2-15
2.4.5	Current approach to derive ballast roundness using 3D models .....	2-18
2.4.6	Current standard test to determine the flakiness index .....	2-20
2.4.7	Current standard test to determine flat and elongated ratio .....	2-22
2.4.8	Laser-based determination of flakiness index.....	2-23

2.5	PROPERTIES OF BALLAST MATERIAL.....	2-24
2.5.1	Ballast shear strength.....	2-25
2.5.2	Ballast settlement.....	2-26
2.6	LOSS OF CANT HOLDING ON CURVES.....	2-28
2.7	EFFECTS OF PARTICLE CHARACTERISTICS ON TRACK PERFORMANCE	2-29
3	METHODOLOGY.....	3-1
3.1	INTRODUCTION.....	3-1
3.2	SAMPLING AND SAMPLE DESCRIPTION.....	3-1
3.3	PHYSICAL PROPERTIES OF BALLAST MATERIALS.....	3-6
3.4	GRADING ANALYSIS.....	3-6
3.5	REPRESENTATIVE SAMPLE SIZE.....	3-8
3.6	LASER APPROACH TO DETERMINE SHAPE PROPERTIES.....	3-14
3.6.1	Description of samples for scanning process.....	3-16
3.6.2	Laser scanning mode.....	3-18
3.7	TRIAXIAL TESTING OF BALLAST SAMPLES.....	3-19
3.7.1	Experimental set-up and procedure.....	3-19
3.7.2	Triaxial shear strength testing of ballast samples.....	3-20
3.7.3	Repeated load triaxial testing.....	3-22
4	DATA ANALYSIS AND DISCUSSION OF LASER SCANNING RESULTS.....	4-1
4.1	INTRODUCTION.....	4-1
4.2	SURFACE AREA, VOLUME AND DIMENSIONS.....	4-1
4.3	PROCESSING LASER SCANNED DATA.....	4-5
4.4	RESULTS OF SCANNED BALLAST PARTICLES.....	4-5
4.5	DETERMINATION OF BALLAST SHAPE INDICES BY USING PHYSICAL PROPERTIES.....	4-8
4.5.1	Flat and elongated particles.....	4-9

4.5.2	Development of shape chart classification .....	4-11
4.5.3	Sphericity computed using principal dimensions .....	4-14
4.5.4	Sphericity computed using surface area and volume.....	4-15
4.6	DEVELOPMENT OF BALLAST SURFACE AREA MODEL .....	4-17
4.7	ROUNDNESS COMPUTED USING SURFACE AREAS.....	4-20
4.8	CORRELATION OF FLAKINESS INDEX WITH BALLAST SHAPE INDICES .	4-23
4.9	BALLAST SHAPE STATISTICAL ANALYSIS .....	4-26
4.9.1	ANOVA test results of ballast shape .....	4-27
4.10	VALIDATION OF LASER-BASED SHAPE PROPERTIES .....	4-28
4.10.1	Mill Abrasion results of sphericity and roundness validation .....	4-30
4.10.2	Relationship of sphericity and roundness index .....	4-32
5	DATA ANALYSIS AND DISCUSSION OF TRIAXIAL TEST RESULTS .....	5-34
5.1	INTRODUCTION.....	5-34
5.2	DISCUSSION OF TRIAXIAL TEST RESULTS.....	5-34
5.3	SHAPE EFFECTS ON SHEAR STRENGTH.....	5-42
5.4	RESULTS AND DISCUSSION OF PERMANENT DEFORMATION .....	5-44
6	CONCLUSIONS AND RECOMMENDATIONS .....	6-1
6.1	CONCLUSIONS .....	6-1
6.1.1	Development of shape descriptors to quantify ballast characteristics .....	6-1
6.1.2	The effect of ballast shape on performance-related properties .....	6-1
6.2	RECOMMENDATIONS AND ASPECTS FOR FUTURE STUDY .....	6-2
7	REFERENCES .....	7-1
8	APPENDIX A: TRIAXIAL SAMPLE PREPARATION .....	8-1
9	APPENDIX B: MATLAB CODE FOR PROCESSING LASER SCAN DATA .....	9-8
10	APPENDIX C: BALLAST SCAN RESULTS.....	10-1



## LIST OF TABLES

Table 2.1: Particle shape classification (modified after Zingg, 1935) .....	2-5
Table 2.2: Standard characterisation test references (S406, 2011) .....	2-7
Table 2. 3: Specifications for flat and elongated particles (Asphalt Institute, 1996) .....	2-22
Table 2. 4: Slots of specified width with appropriate sieve size (TMH1 & SANS 3001) .....	2-23
Table 3.1: Physical characteristics of fresh crushed dolerite ballast .....	3-6
Table 3.2: Summary of grain size characteristics of ballast and pebble material .....	3-8
Table 3.3: Statistical representative samples of ballast and pebble.....	3-9
Table 4.1: Area verification of the laser results .....	4-4
Table 4. 2: Statistical parameters for flatness ratio .....	4-10
Table 4. 3: Statistical parameters for elongation ratio.....	4-11
Table 4.4: Average parameters for shape chart.....	4-14
Table 4. 5: Statistical parameters for sphericity computed using principal dimensions .....	4-14
Table 4. 6: Ballast surface area model parameter .....	4-19
Table 4.7: Ballast roundness chart developed using three dimensional laser models.....	4-23
Table 4. 8: Ballast shape indices computed from laser results.....	4-23
Table 4.9: Analysis of variance for sphericity .....	4-27
Table 4.10: Analysis of variance ANOVA for Roundness .....	4-27
Table 4.11: Analysis of variance for Flatness .....	4-28
Table 4.12: Analysis of variance for Elongation.....	4-28
Table 4.13: ANOVA sphericity validation.....	4-31
Table 4.14: ANOVA roundness validation .....	4-32
Table 8.1: Scanned particles of recycled ballast from Km 9.....	10-1
Table 8.2: Scanned particles of recycled ballast from Km 17.....	10-4
Table 8.3: Scanned particles of recycled ballast from Km 31.....	10-7
Table 8.4: Scanned particles of recycled ballast from Km 32.....	10-9
Table 8.5: Scanned particles of freshly crushed.....	10-11
Table 8.6: Scanned particles of river pebbles.....	10-13
Table 8.7: Summary of average results of scanned particles .....	10-15

## LIST OF FIGURES

Figure 2. 1: A transverse photograph of ballast track structure .....	2-2
Figure 2. 2: Ballast material types used in South Africa (courtesy, Transnet Freight Rail).....	2-3
Figure 2.3: Variation of ballast shape and surface texture .....	2-4
Figure 2.4: 3D-laser scanning set-up at CSIR.....	2-9
Figure 2.5: The Aggregate Imaging System (Masad et al., 2007) .....	2-10
Figure 2.6: Graphical presentation of ballast shape or surface properties .....	2-11
Figure 2.7: Principal dimensions of ballast particle scanned at CSIR .....	2-13
Figure 2.8: Chart to characterise particle shape (redrawn from Zingg, 1935) .....	2-14
Figure 2.9: Visual assessment of particle shape (Quiroga & Fowler, 2003).....	2-17
Figure 2.10: A well-rounded pebble approximated by an ellipsoid with semi-axis.....	2-18
Figure 2.11: Spherical coordinates.....	2-19
Figure 2.12: Current test method using a flat gauge (Courtesy of TFR).....	2-21
Figure 2.13: Proportional calliper device.....	2-23
Figure 2.14: Effect of particle shape on stress strain characteristics (Modified after Holz & Gibbs, 1956).....	2-25
Figure 2.15: Ballast, sub-ballast and subgrade contributions to total settlement (modified from Selig & Waters, 1994).....	2-27
Figure 2.16: Cant visible of track around curve.....	2-28
Figure 3.1: Ballast sampling positions along the heavy haul coal export route and sources of other sample materials.....	3-3
Figure 3.2: Illustration of sample position in the ballast layer .....	3-4
Figure 3.3: View of undisturbed recycled samples at different positions on the coal line, fresh ballast and river pebbles.....	3-5
Figure 3.4: Grading analysis result of the six materials compared to TFR specs .....	3-7
Figure 3.5: three dimensional modelled recycled ballast particles.....	3-9
Figure 3.6: Normal distribution of the sample size to be scanned .....	3-10
Figure 3.7: Grading analysis of recycled ballast (Km 9) to be scanned.....	3-11
Figure 3.8: Grading analysis of recycled ballast (Km 17) to be scanned.....	3-11
Figure 3.9: Grading analysis of recycled ballast (Km 31) to be scanned.....	3-12
Figure 3.10: Grading analysis of recycled ballast (Km 32) to be scanned.....	3-12
Figure 3.11: Grading analysis of fresh crushed ballast to be scanned.....	3-13
Figure 3.12: Grading analysis of river pebbles to be scanned.....	3-13
Figure 3.13: Aggregate and ballast scanning process (Anochie-Boateng et al., 2014).....	3-15

Figure 3.14: Process used for 3D laser-based measurements of ballast particles .....	3-17
Figure 3.15: Typical planer scanning mode of the four- and two-side faces .....	3-18
Figure 3. 16: Ballast particles of samples and triaxial specimen .....	3-21
Figure 4.1: Wire frame with surface triangles obtained from the laser scanner.....	4-1
Figure 4.2: Mesh of poly-faces to determine surface area and volume.....	4-5
Figure 4.3: Actual images versus modelled river pebbles.....	4-6
Figure 4. 4: Actual ballast particles versus modelled recycled ballast.....	4-7
Figure 4. 5: Distributions of flatness ratio.....	4-10
Figure 4. 6: Distributions of elongation ratio .....	4-11
Figure 4. 7: Actual vs scanned particles for shape classification .....	4-12
Figure 4.8: A shape chart classification for all scanned particles .....	4-13
Figure 4.9: Distributions of sphericity computed using principal dimensions.....	4-15
Figure 4.10: Box and whisker plot for the sphericity values of six samples scanned.....	4-16
Figure 4.11: Distributions of sphericity computed using surface area and volume .....	4-17
Figure 4. 12: Plots of surface area versus volume results of scanned particles.....	4-19
Figure 4.13: Relationship between scanned surface area and the mathematical model.....	4-20
Figure 4.14: Distributions of ballast roundness index.....	4-21
Figure 4. 15: Box and whisker plot for the roundness values of six samples scanned.....	4-22
Figure 4.16: Flakiness index versus sphericity computed by using volume and surface area .	4-24
Figure 4.17: Flakiness index versus sphericity computed by using principal dimensions .....	4-25
Figure 4. 18: Flakiness index versus flatness ratio.....	4-25
Figure 4. 19: Flakiness index versus roundness index .....	4-26
Figure 4.20: Typical Mill Abrasion test machine used for this study .....	4-29
Figure 4.21: Ballast sample before and after a Mill Abrasion test.....	4-29
Figure 4.22: Sphericity validation results.....	4-30
Figure 4.23: Roundness validation results .....	4-31
Figure 4. 24: Relationship between roundness and sphericity .....	4-32
Figure 5.1: Shear test results for recycled ballast from Km 9 .....	5-36
Figure 5.2: Mohr circles and failure envelop of recycled ballast from Km 9 .....	5-36
Figure 5.3: Shear test results for recycled ballast from Km 17 .....	5-37
Figure 5.4: Mohr circles and failure envelop of recycled ballast from Km 17 .....	5-37
Figure 5.5: Shear test results for recycled ballast from Km 31 .....	5-38
Figure 5.6: Mohr circles and failure envelop of recycled ballast from Km 31 .....	5-38
Figure 5.7: Shear test results for recycled ballast from Km 32 .....	5-39
Figure 5.8: Mohr circles and failure envelop of recycled ballast from Km 32 .....	5-39

Figure 5.9: Shear test results of freshly crushed ballast .....	5-40
Figure 5.10: Mohr circles and failure envelop of freshly crushed ballast .....	5-40
Figure 5.11: Shear test results of river pebbles .....	5-41
Figure 5.12: Mohr circles and failure envelop of river pebbles .....	5-41
Figure 5.13: Effect of sphericity index on internal friction angle .....	5-43
Figure 5.14: Effect of roundness index on internal friction angle.....	5-43
Figure 5.15: Effect of flakiness index on internal friction angle.....	5-44
Figure 5.16: Measured permanent deformation of recycled ballast from Km 9 .....	5-45
Figure 5.17: Measured permanent deformation of recycled ballast from Km 17 .....	5-45
Figure 5.18: Measured permanent deformation of recycled ballast from Km 31 .....	5-46
Figure 5.19: Measured permanent deformation of recycled ballast from Km 32 .....	5-46
Figure 5.20: Measured permanent deformation of freshly crushed ballast.....	5-47
Figure 5.21: Measured permanent deformation of river pebbles .....	5-47
Figure 5.22: Second-stage permanent deformation of tested materials .....	5-48
Figure 5.23: Effect of flatness ratio on permanent deformation .....	5-49
Figure 5. 24: Effect of sphericity index on permanent deformation .....	5-50
Figure 5.25: Effect of roundness index on permanent deformation.....	5-50

## LIST OF ABBREVIATIONS

$L$	longest dimension of a particle
$I$	intermediate dimension of a particle
$S$	shortest dimension of a particle
$\Psi$	working sphericity
$A$	surface area
$V$	volume
$r_i$	individual corner radius
$R$	radius of a circle inscribed about the particle
$N$	number of corners on the particle
$R_a$	average roundness
$n_i$	number of particles in group i
$m_i$	mid-point roundness of group i
$N_t$	total number of particles
$R_s$	Folk's roundness index
$R_u$	Wadell's roundness index
$A$	area of the particle image
$P$	perimeter of the particle 2-D image
$\rho$	individual particle roundness
$SA_e$	surface area of an ellipsoid
$SA_p$	surface area of ballast particle
$FI$	flakiness index
$M_p$	total mass of aggregate passing a bar sieve slots
$M_T$	total mass of aggregate retained on a specific sieve size (grading analysis)
$FI_v$	flakiness index based on volume
$V_p$	total volume of flaky aggregates scanned
$V_T$	total volume of the aggregate sample
$S_B$	ballast settlement
$\varepsilon_B$	plastic ballast strain
$H_B$	ballast layer thickness
$E_s$	plastic sub-ballast strain
$H_s$	sub-ballast layer thickness
$S_N$	settlement of ballast
$N$	number of load cycles

$a$	settlement at first cycle
$k$	empirical constant
$C_c$	coefficient of curvature
$C_u$	coefficient of uniformity
$D$	particle diameter at any % finer
$D_{10}$	particle diameter at 10 % finer
$D_{30}$	particle diameter at 30 % finer
$D_{50}$	particle diameter at 50 % finer (mean particle size)
$D_{60}$	particle diameter at 60 % finer
$D_{max}$	maximum particle size at % finer
$D_{min}$	minimum particle size at % finer
$RI$	roundness index
$SA_e$	surface area of an ellipsoid
$SA_{pm}$	surface area of the particle model
$\sigma_1$	major principal (or axial) stress
$\sigma_3$	minor principal (or radial or confining) stress
$\sigma_d$	deviator stress
$\tau$	shear strength of the material
$\sigma$	applied normal stress
$c$	cohesion
$\phi$	angle of internal friction of the material

# 1 INTRODUCTION

## 1.1 BACKGROUND

Railway ballast has several functions as part of the track structure, including the transfer of the applied load from the wheel to the subgrade. Ballasted track has remained virtually unchanged for centuries and is still the most cost-effective and maintainable design. A common problem in the rail industry is the degradation of ballast under cyclic loading, especially on heavy haul lines. According to Li et al. (2015) shape, angularity and surface texture are critical elements that affect ballast performance since they affect ballast interlocking, which contributes to ballast strength and deformation behaviour. Ballast deformation can be due to settlement and particle rearrangement, ballast fracture/crushing and ballast wearing of sharp corners.

The challenge with regard to ballast performance is to accurately measure the shape properties of ballast materials and to directly link these to performance. Mathematical descriptors are common and useful due the reproducibility of the measurements and these can be used to measure ballast shape properties with confidence. Flakiness, roundness and sphericity are important shape parameters that have been used to quantify ballast shape properties. However, the irregular shape of ballast stones presents a modelling challenge.

The increasing demand for higher axle loads and annual tonnages implies that understanding railway ballast behaviour and its interactions with track components remain critical for minimizing maintenance activities. Therefore, characterisation and modelling of ballast properties and their behaviour have to be researched and discussed in a more systematic and scientific way. For example, during the past few years some researchers have investigated the aggregate shape effects on ballast tamping and railroad track stability, as well as modelled and validated railroad ballast settlement (Tutumluer et al., 2006; Tutumluer et al., 2007; Tutumluer et al., 2011).

The Council for Scientific and Industrial Research (CSIR) in South Africa recently embarked on an extensive research and development programme on the use of modern three-dimensional (3D) laser scanning and numerical modelling techniques to improve measurements of the shape properties of aggregates and ballast materials (Anochie-Boateng et al., 2013; Mvelase et al., 2012; Anochie-Boateng et al., 2012). The overall goal was to link the shape parameters of aggregates and ballast obtained from the laser system to engineering properties and performance. The laser device has been evaluated for accuracy and precision, and calibrated to

determine basic shape properties of aggregates and ballast materials used in roads and railways (Anochie-Boateng et al., 2011; Anochie-Boateng et al., 2011; Anochie-Boateng et al., 2010). This study focuses on the effect of rounded particles on shear strength properties and the permanent deformation of railway ballast. The overall goal was to link the shape parameters of aggregates and ballast obtained from the laser system to engineering properties and performance. The major problem is that ballast particles have irregular shapes with variable surface textures. An accurate measurement of the shape properties is important for developing and revising specifications for quality control and quality assurance of ballast.

In South Africa, the railway system plays a significant role in hauling bulk commodities to ports and transporting freight along major corridors. Transnet Freight Rail operates the two heavy haul lines, namely the Coal Line from Broodsniersplaas to Richards Bay and the Iron Ore Line from Sishen to Saldanha. Railway ballast materials must comply with several quality requirements, including shape properties. The source of ballast (parent rock) varies from quarry to quarry and even within the rock mass at a single quarry depending on the quality and availability of the rock, regulations and economic considerations. According to Indraratna et al. (2005), the maintenance cost of track sections can significantly be reduced if there is a better understanding of the physical and mechanical properties of ballast.

This study focuses on the development of shape properties (roundness, flakiness, elongation and sphericity) of ballast materials using the 3D-laser scanning technique. The selected ballast materials are being investigated by Transnet Freight Rail (TFR) in South Africa. The effect of these shape properties on performance were further investigated through triaxial testing of the ballast materials. In addition, abrasion tests were conducted to verify the shape properties determined from the laser scanning system. It is anticipated that this study will lead to the development of new and improved national standards for ballast materials. These standards will have significant impact on the track structure and the railway industry in an effort to provide better performing railway track structures in order to lower maintenance cost and improve safety on the railway tracks.

## **1.2 PROBLEM STATEMENT**

The fundamental measurements of railway ballast shape characteristics are essential for good quality control and, ultimately, for understanding their influence on the performance of the track structure. The performance of the railway track structure can be significantly influenced



by the ballast shape properties, which are roundness, flatness, elongation, sphericity, angularity and surface texture. These are important properties to quantify ballast shapes. The abrasion and wearing of sharp corners of ballast because of heavy dynamic loading conditions often leads to round particle shapes, causing differential track settlement and geometry deterioration.

It is well known that the current test methods for determining the shape properties of railway ballast have some limitations, i.e. they are laborious and subjective, which could lead to poor repeatability of test results. Current track ballast specifications do not address in a direct manner the measurement of shape properties, thus leading to inconsistent interpretation of test results. The major challenge is how to discriminate between different shapes and their effect on performance. The optimal shape of ballast used in railway construction must preferably be angular rather than rounded. This enables it to interlock for increased strength, as opposed to particles with rounded edges, which allow for settlement leading to instability. Therefore, there is a need to address these problems in order to minimise maintenance costs that are normally associated with ballast replacement, and to ensure better performing track structures as well as ensuring safety of the railway infrastructure.

### **1.3 OBJECTIVES OF THE STUDY**

The main objectives of this study were to:

- Develop three dimensional shape descriptors to accurately quantify ballast characteristics.
- Investigate the effect of ballast shape on performance-related properties of the five different ballast materials and one-pebble material using triaxial testing.

### **1.4 HYPOTHESIS**

The underlying hypothesis of this study is that a modern three dimensional measurement technique can improve the accuracy and repeatability, as well as introduce automation in the determination of ballast shapes beyond that of the traditional 2D measurement techniques.

### **1.5 SCOPE OF THE STUDY**

The scope of the study is summarised as follows:

- review of existing data and related documents;
- selection of ballast materials to be studied;

- scanning of ballast using the three dimensional laser, scanning device at CSIR and TFR;
- processing of scan data to reconstruct three dimensional models of the ballast;
- analysis of the laser scan results to determine ballast shape properties and validation of the shape properties by Mill Abrasion tests of ballast particles;
- static and repeated load triaxial testing of the ballast samples; and
- correlation of ballast roundness with track performance (shear strength and permanent deformation).

Limitations of the scope:

- this study was limited to one type of ballast, ruling out factors such as size, shape and durability characteristics;
- evaluation of surface texture and angularity was not included; and
- mathematical modelling of ballast particles using the Discrete-element method (DEM) was not done.

## **1.6 METHODOLOGY**

The detailed methodology for the study is presented in Chapter 3. The methodology for the study can be summarised as follows:

- literature review;
- sampling and sample description;
- physical properties of track ballast;
- laser-based method to quantify ballast shape properties;
- triaxial testing;
- data analysis, and shape effect correlation

## **1.7 ORGANISATION OF THE REPORT**

The report consists of the following chapters and appendices:

- Chapter 1 entails the introduction to the dissertation.
- Chapter 2 contains the review of available literature that pertains to this study.
- Chapter 3 describes the detailed approach / methodology followed to achieve the objectives of the study.

- Chapter 4 presents laser scanning and laboratory testing results with limited discussion of the results.
- Chapter 5 describes detailed analyses of laser scanning and laboratory testing results.
- Chapter 6 contains the conclusions and recommendations of the study.
- The list of references follows at the end of the document.
- Finally, the dissertation ends with the appendices of the study.

## **2 LITERATURE REVIEW**

### **2.1 INTRODUCTION**

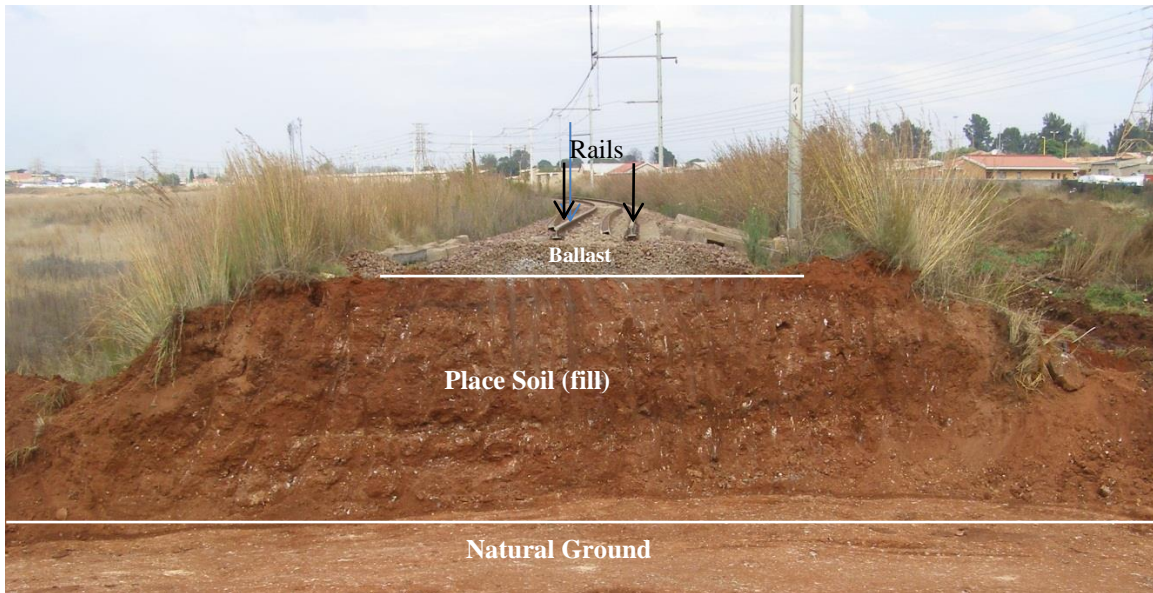
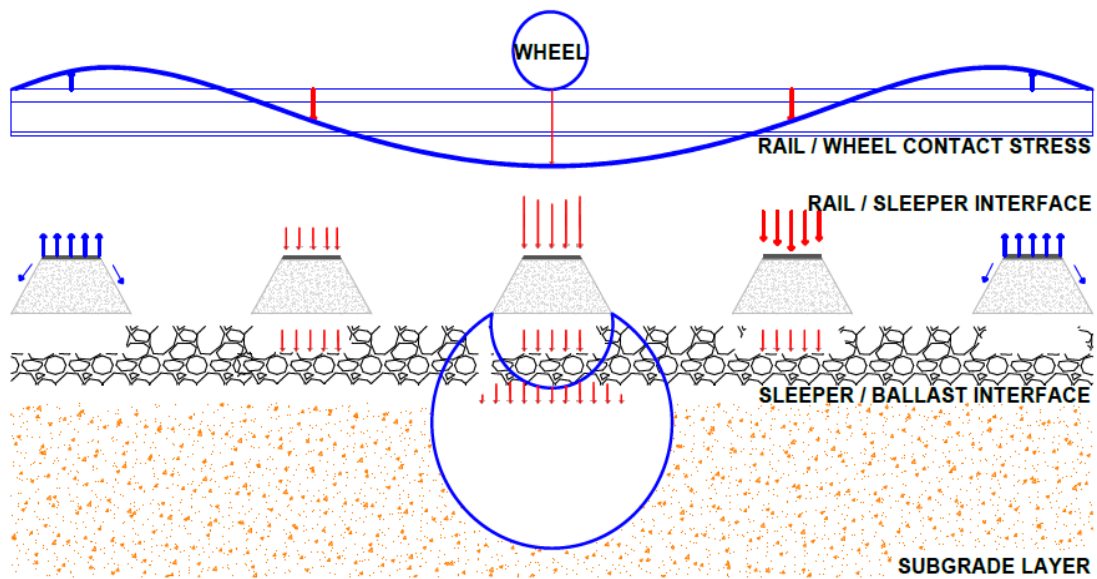
The purpose of a railway track structure is to provide safe and economical train transportation. This requires the track to serve as a stable guideway with appropriate vertical and horizontal alignment. To achieve this role, each component of the system must perform its specific functions in response to the traffic loads and environmental factors imposed on the system. These are rails, fastening systems, sleepers, ballast, fill material and the subgrade.

The development of a method for quantifying shape properties of ballast is a new development. Specifications, terminology, processes and methods differ to some extent from one railway organisation to another. The literature focuses on ballast particle characteristics that are likely to influence track performance. The literature search also covers imaging techniques for characterising ballast shape properties, and three dimensional laser, scanning technology currently used in South Africa and overseas. A brief description of the track substructure components and the current ballast testing methods and their associated shortcomings will also be presented.

### **2.2 BALLAST**

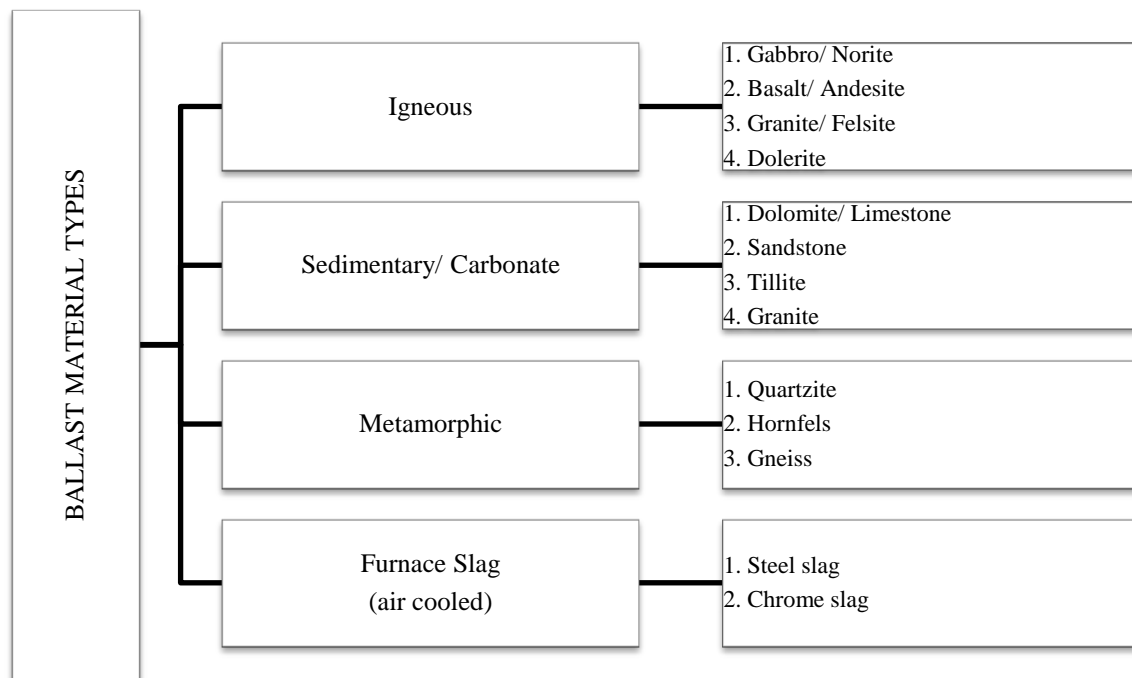
Ballast is the main structural part of the railway that distributes the trainloads to the underlying supporting structure. Track components are grouped into two main categories: the superstructure and substructure. The superstructure refers to the top part of the track, which is the rails, the fastening system and sleepers, while the substructure refers to the lower part of the track, which is ballast, the sub-ballast and subgrade. Figure 2.1 shows the components of a typical ballasted track. For in-depth descriptions of each of the components, the reader is referred to the text by Selig and Waters (1994).

The component of interest in this study is ballast. Ballast comprises of selected crushed granular material in which the sleepers are embedded into a ballast layer that is typically 200 mm – 300 mm thick. Ballast is a free draining granular material used as a load-bearing material in railway tracks.



**Figure 2. 1: A transverse photograph of ballast track structure**

Traditionally, angular, crushed hard stones and rocks, uniformly graded and free from dust have been used as ballast material. Therefore, wide varieties of minerals are used as ballast throughout the world. The commonly used ballast materials in South Africa are summarised in Figure 2.2.

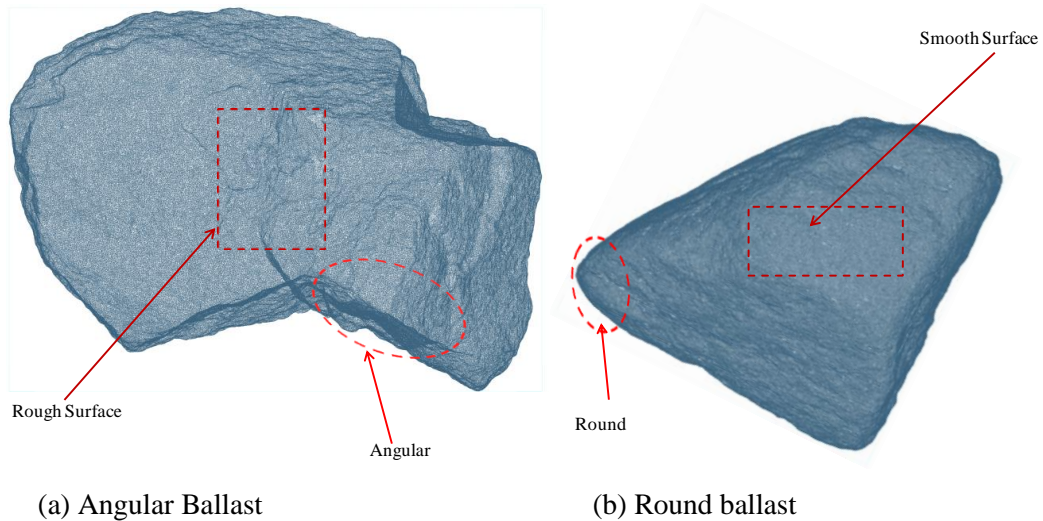


**Figure 2. 2: Ballast material types used in South Africa (courtesy, Transnet Freight Rail)**

Kumar (2010) mentioned the following properties of track ballast in the track specification for high axle load. Ballast should have high wear and abrasive qualities to withstand the impact of train dynamic traffic loads and excessive degradation. Excessive abrasion loss of an aggregate will result in reduction of particle size, fouling of the ballast, reduction of drainage and loss of supporting strength of the ballast. Ballast should be hard, durable and as far as possible angular along edges/corners, free from weathered portions of parent rock, organic impurities and inorganic residues. The shape of ballast particles is a product of the rock type, depositional environment and quarrying and production process. For example, hard, tough or brittle rocks will often generate more flakes, whereas softer rocks produce more fines. Ballast should have sharp corners and cubical fragments with minimum particles that are round, flat and elongated. Angular or nearly cubical particles having a rough surface texture are preferred over round, smooth particles. The ballast particle should have high internal shearing strength to have high stability. The ballast material should possess sufficient unit weight to provide a stable ballast section and in turn provide support and alignment stability to the track structure. The ballast material should have less absorption of water, as excessive absorption can result in rapid deterioration during alternate wetting and drying cycles.

### 2.2.1 Effect of ballast characteristics on behaviour

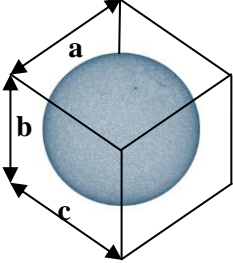
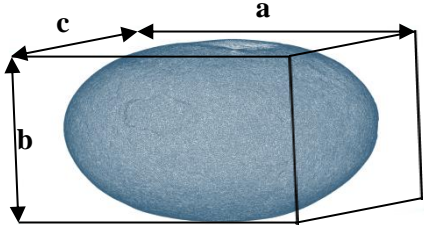
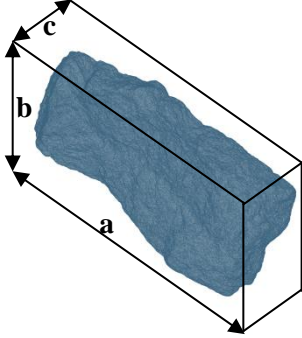
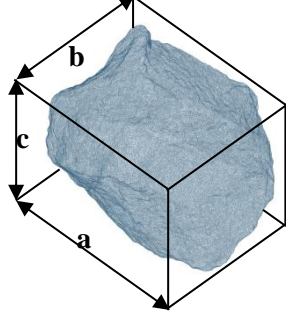
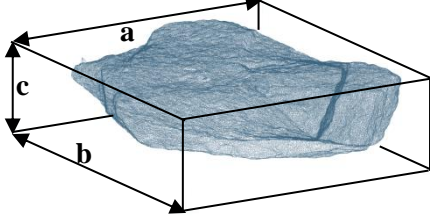
No single characteristic controls ballast behaviour. Instead, the behaviour is the net effect of combined characteristics. Ballast characteristics can be identified by three independent components, namely angularity (roundness), surface texture, and shape (form). Factors that cause deterioration of ballast include repeated train loading and vibrations of varying frequencies and intensities. Therefore, it is important to evaluate the effect of ballast shape on the overall behaviour of the ballast layer. Figure 2.3 presents a typical variation of ballast shape and surface texture between freshly supplied ballast and recycled ballast from the field. Shape and surface characteristics are important for interlocking properties of the ballast.



**Figure 2.3: Variation of ballast shape and surface texture**

Zingg (1935) developed a classification chart based on the relationship between the three axes. In this way, it is easy to determine the main form of the particles as equidimensional, spherical, elongated or flat (see Table 2.1).

**Table 2.1: Particle shape classification (modified after Zingg, 1935)**

Shape category	Particle dimensions	Explanation	Examples
<b>Sphere</b>	$a = b = c$	<b>High Sphericity:</b> all dimensions are equal	
<b>Scalene ellipsoid</b>	$a > b > c$	<b>Low Sphericity/ Flat &amp; Elongated:</b> all dimensions are very different	
<b>Prolate spheroid</b>	$a > b$	<b>Elongated:</b> one dimension is much longer	
<b>Equant</b>	$a \approx b \approx c$	<b>Cubic:</b> all dimensions are comparable	
<b>Oblate spheroid</b>	$b > c$	<b>Flaky:</b> one dimension is much shorter	



### **2.2.2 Ballast selection tests**

These tests are concerned with establishing a quantitative estimate of the resistance to in-track stability under loading. Tests include form (flakiness, elongation, sphericity and roundness) and surface (surface area, surface texture, grain size and angularity) examination. The standard tests and the corresponding reference are included in Table 2.2. The S406 ballast specification (2011) is a material requirement for the purchase of crushed rock as ballast on the TFR rail network in South Africa. The specification ensures the functional use of ballast. Many tests have been carried out to define the ballast particle characteristics and they are defined in detail in the S406 specification.

The Los Angeles Abrasion (LA) test is a dry test to measure the material's toughness or tendency towards coarse breakage. Steel balls are placed in a rotating drum along with a sample of ballast. After a number of cycles, the material is removed and washed through a 4.25 mm sieve. The LA value is the amount of material less than 4.25 mm generated by the test as a percentage of the original sample weight. The Mill Abrasion (MA) test is where a sample of ballast is placed in a rotating drum with water. The Mill Abrasion value is the amount of material finer than 0.075 mm generated by the test as a percentage of the original sample weight.

The ballast grading size is determined through sieving and washing. A clean ballast grading has a grading envelope of 63 mm – 13.2 mm (for ordinary lines) and 73 mm – 19 mm (for heavy axle lines) (S406, 2011). The shape of the grading curves is a function of the particle size. 'Uniformly graded' means a narrow range of particles while 'broadly graded' means a wide range of particles. A 'gap-graded' material contains a relatively small amount of particles of a given range. Clean ballast is uniformly graded. An important factor influencing the ballast unit weight is the specific gravity. Specific gravity is determined by the water displacement method, and water absorption is determined at the same time. Water absorption is an indication of the rock porosity, which relates to its strength.

Shape and surface characteristics are important for interlocking properties of the ballast. These characteristics include flakiness, elongation and roundness. A ballast particle is flat or flaky if the ratio of thickness to width is  $< 0.6$ . The flakiness index is the percentage by weight of flaky particles in a sample. The British Standard defines an elongated particle as one with a length to width  $> 1.8$ . The elongation index is the percentage by weight of elongated particles in a

sample. Angularity (or roundness) measures the sharpness of the edges (visual test are usually used).

**Table 2.2: Standard characterisation test references (S406, 2011)**

Characteristic	Test	Test Reference								
Durability	Los Angeles abrasion	< 22; LA value determined in accordance with ASTM C131-89 grading B								
	Mill abrasion	< 7; measured in accordance with S406								
Unit weight & environmental	Water absorption	< 1; measured in accordance with SABS 1083 (latest version)								
	Sulphate soundness	< 5; the loss in mass shall not exceed 5% after 20 cycles of the test								
	Relative density	> 2.5; measured in accordance with SABS 1083 (latest version)								
	Void content	> 40; measured in accordance with SABS 1083 (latest version)								
Shape and surface	Flakiness index	< 30; measured in accordance with SANS 3001-AG4 (2009)								
	Roundness Index	<b>No spec</b>								
	Elongation index	<b>No spec</b>								
	Surface texture	<b>No spec</b>								
Grading	size	<table border="1"> <tr> <td>Sieve size (mm)</td> <td>75</td> <td>63</td> <td>53</td> <td>37.5</td> <td>26.5</td> <td>19</td> <td>13.2</td> </tr> </table>	Sieve size (mm)	75	63	53	37.5	26.5	19	13.2
	Sieve size (mm)	75	63	53	37.5	26.5	19	13.2		
Size distribution	<table border="1"> <tr> <td>Passing (%)</td> <td>100</td> <td>90-100</td> <td>40-70</td> <td>10-30</td> <td>0-5</td> <td>0-1</td> <td>0</td> </tr> </table>	Passing (%)	100	90-100	40-70	10-30	0-5	0-1	0	
Passing (%)	100	90-100	40-70	10-30	0-5	0-1	0			

### 2.3 TECHNIQUES TO DETERMINE BALLAST SHAPE PROPERTIES

There are several shape descriptors and various techniques to capture the particle profile (3D and 2D). Each technique presents advantages and disadvantages. three dimensional is probably the technique that provides more information about the particle shape but the precision also lies in the resolution.

### **2.3.1 Advanced three dimensional laser based technique**

The major problem is aggregate or ballast particles have irregular and non-ideal shapes with variable surface textures. Hayakawa et al. (2005) and Tolppanen et al. (2008) reported that digital modelling of gravel particles based on three-dimensional (3D) laser scanning could be useful, reliable, repeatable and relatively fast to evaluate the properties of ballast material. Recently, the Council for Scientific and Industrial Research (CSIR) acquired a 3D laser, scanning device to accurately quantify aggregates and ballast shape and surface properties.

The 3D laser, scanning device used for this study is available at CSIR and TFR. The device is currently being used in an R&D project that employs laser scanning and numerical techniques to effectively address a number of difficulties associated with characterisation of aggregate and ballast shape and surface properties, as well as their influence on the performance of transport infrastructure in South Africa. The laser device has been evaluated for accuracy and precision, and calibrated to determine basic shape properties of conventional and non-conventional aggregates used in pavements and railways (Anochie-Boateng et al., 2010; Anochie-Boateng et al., 2011b, 2011c, 2011d). In addition, the laser device has been validated for direct measurements of shape and surface properties of aggregates (Komba, 2013; Anochie-Boateng et al., 2010).

The device uses an advanced non-contact sensor to capture flat areas, hollow objects, oblique angles and fine details of scanned objects in three dimensions, with scanning resolutions that range from 1 mm (1 000  $\mu\text{m}$ ) to 0.1 mm (100  $\mu\text{m}$ ). Figure 2.4 shows a photograph of the three dimensional laser device at the CSIR. An integral part of the laser device is advanced data processing software that is used for obtaining accurate shape properties of the ballast particles.

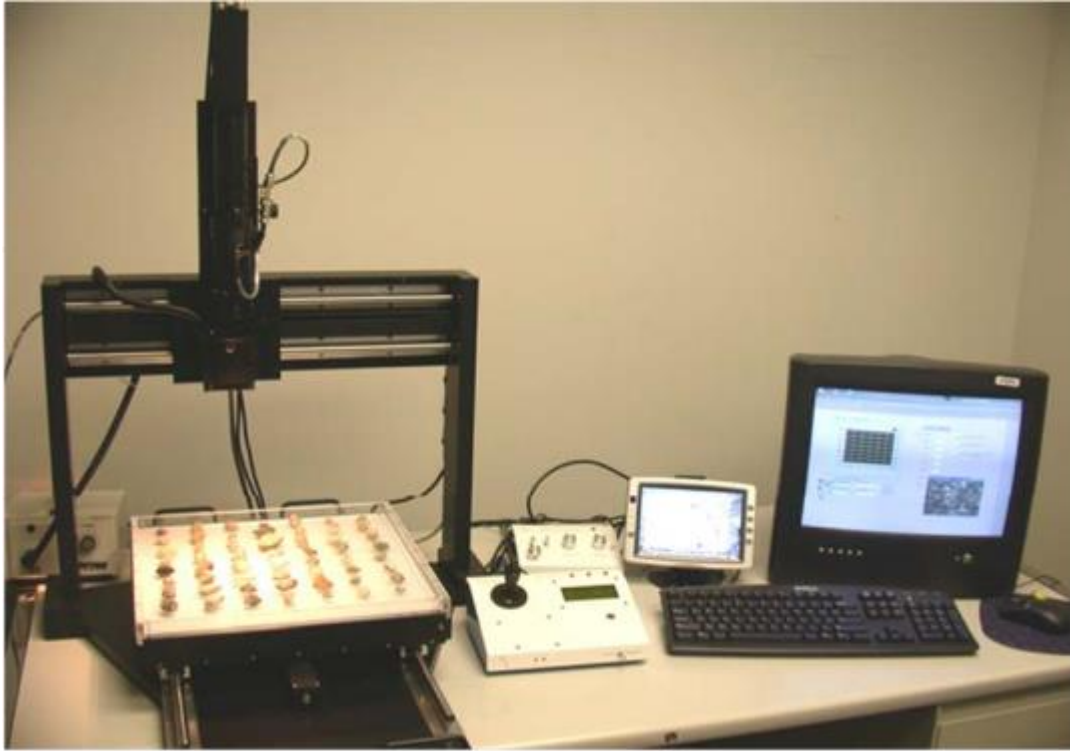


**Figure 2.4: 3D-laser scanning set-up at CSIR**

### **2.3.2 Image-based techniques**

Some image-based techniques provide only 2D information about the aggregate shape, which makes it difficult to accurately determine aggregates shape properties in a three dimensions. The 2D method has recently become a concern for most agencies and stakeholders in the road industry (Anochie-Boateng et al., 2010).

The imaging system that has been used for measurement of aggregate shape properties is the Aggregate Imaging System (AIMS), developed by Masad (2003). The AIMS is used to measure shape properties of coarse and fine aggregates. The system as shown in Figure 2.5 consists of a camera, video microscope, lighting systems, aggregate tray, computer automated data acquisition system and processing software for analysis of aggregate shape properties (Masad, 2003; Masad, 2004). Masad et al. (2007) evaluated test methods for characterising aggregate shape properties. They proposed the AIMS to be suitable for quantification of aggregate form, angularity and surface texture.



**Figure 2.5: The Aggregate Imaging System (Masad et al., 2007)**

Although aggregate imaging has been used extensively for direct measurement of aggregate shape properties, as well as have provided a better understanding of the distinction between aggregate form, angularity and surface texture, some inherent limitations of the technique do exist. The main limitation is that most available image-based systems provide information that facilitates characterisation of aggregate form, angularity and surface texture in 2D. In reality, an aggregate particle is a three dimensional object. Therefore, characterisation of aggregate shape properties should ideally be three dimensional based. The use of a more advanced technique such as laser scanning could alleviate some limitations of image-based aggregate analysis.

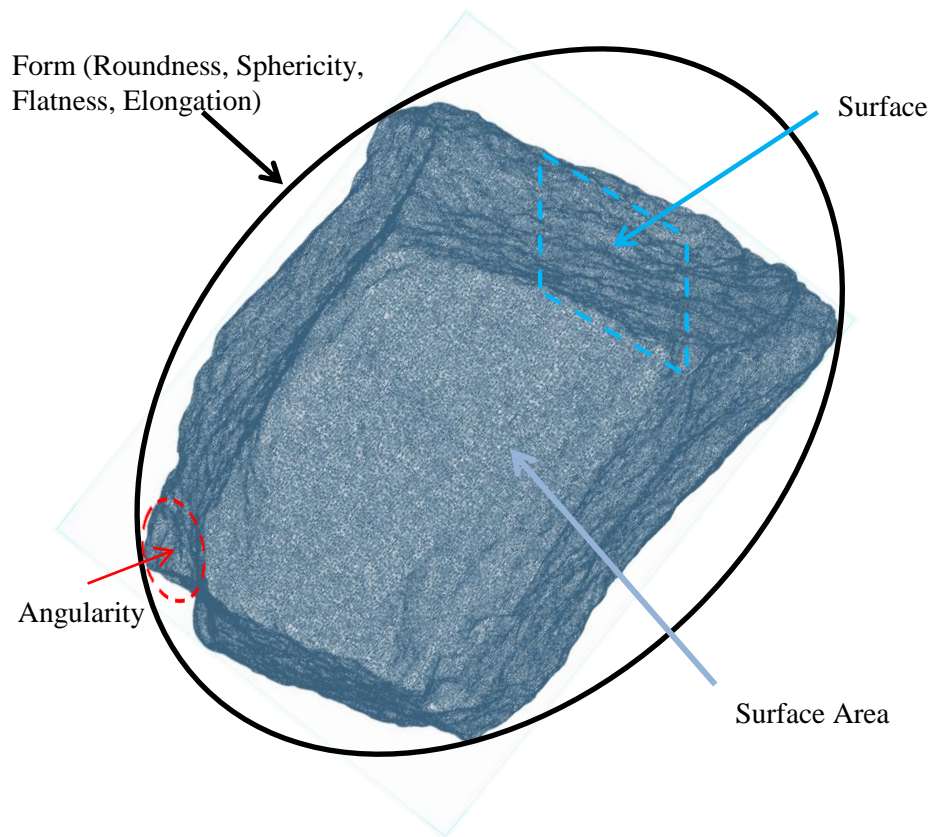
## **2.4 KEY BALLAST SHAPE PROPERTIES**

In order to describe the particle shape in detail, there are a number of terms, quantities and definitions used in the literature. During the historical development of shape descriptors, the terminology has been used differently among the published studies. Several attempts to introduce methodology to measure the particles' shape were developed over the years. Manual measurement of particle form is too labor intensive so it is costly, thus, visual charts were

developed early to diminish the measuring time (Krumbein, 1941; Krumbein & Sloss, 1963; Aschenbrenner, 1956; Pye & Pye, 1943).

The performance of the railway track structure can be significantly influenced by the ballast shape properties of roundness, flatness, elongation, sphericity, angularity and surface texture. Railway ballast materials must fulfil several quality requirements including shape properties. Figure 2.6 shows typical shape properties of a railway ballast particle.

An accurate measurement of the shape properties is important for developing and revising specifications for quality control and quality assurance of ballast. Current track ballast specifications do not address the measurement of shape properties in a direct manner, thus leading to inconsistent interpretation of test results. If rounded ballast were to be avoided, then an even more restrictive specification of ballast shape properties would be required.



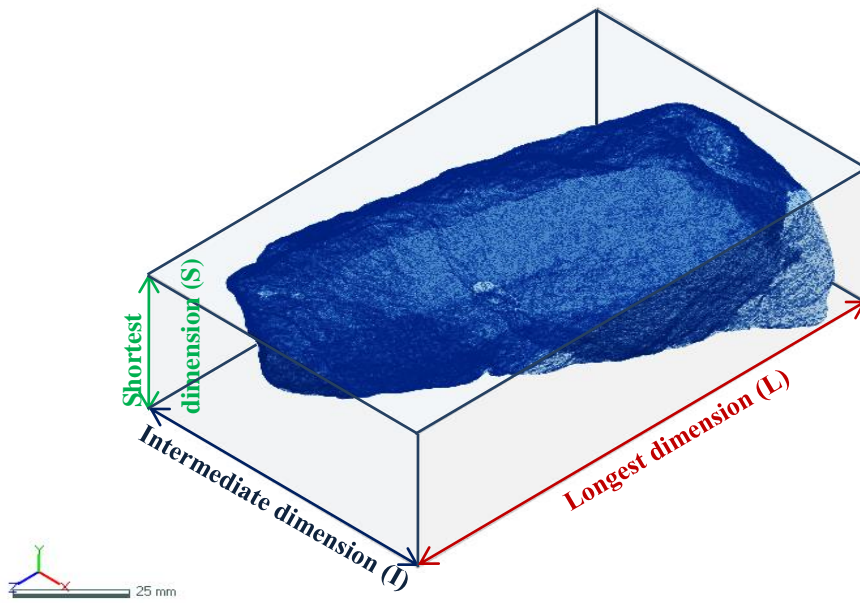
**Figure 2.6: Graphical presentation of ballast shape or surface properties**

Overtime, due to traffic and maintenance procedures, the ballast material is subjected to breakage phenomena and degradation by means of wear which tends to make ballast round. It is the main reason why problems associated with ballast layer in the railway track, structure system need to be addressed based on scientific approaches or techniques. The increasing demand of higher axle loads means that understanding railway ballast behaviour and its interactions with track components remains a critical element in order to minimise maintenance activities. Therefore, characterisation and modelling of ballast properties and their behaviour have to be researched and discussed in a more systematic and scientific way. For instance, during the past few years some researchers have investigated the aggregate shape effects on ballast tamping and railroad track stability, as well as modelled and validated railroad ballast settlement (Tutumluer et al., 2006; Tutumluer et al., 2007; Tutumluer et al., 2011).

The CSIR in South Africa recently embarked on extensive research and development in the use of a modern three-dimensional (3D) laser scanning and numerical modelling techniques to improve measurements of the shape properties of aggregates and ballast materials (Anochie-Boateng et al., 2013; Mvelase et al., 2012; Anochie-Boateng et al., 2012). The overall goal was to link the shape parameters of aggregates and ballast obtained from the laser system to engineering properties and performance. The laser device has been evaluated for accuracy and precision, and calibrated to determine basic shape properties of aggregates and ballast materials used in roads and railways (Anochie-Boateng et al., 2011; Anochie-Boateng et al., 2011; Anochie-Boateng et al., 2010).

#### **2.4.1 Parameters of ballast particle shape**

Form is a first order property that reflects variations in the overall shape of a particle (Barrett, 1980). Almost all parameters of particle form measures the relation between the three principal axes of the particle. The physical dimensions, surface area and volume have been used to compute index parameters commonly used to describe the shape properties of aggregate/ballast (Anochie-Boateng et al., 2013). Although there are some differences in their precise definitions, the long, intermediate, and short diameters of a particle are frequently used to summarise its shape. These three diameters are sometimes referred to as the  $L$ ,  $I$ , and  $S$  diameters respectively.  $L$ ,  $S$  and  $I$  can be obtained accurately from three dimensional scanned models as shown in Figure 2.7. It is possible to measure these dimensions manually using callipers, although this is time consuming and any set of measurements may be subjected to user variation.



**Figure 2.7: Principal dimensions of ballast particle scanned at CSIR**

Kuo et al. (1998) defined two fundamental parameters to describe the shape of a rock aggregate as elongation and flatness ratios. Flatness ratio is defined as the ratio of the particle intermediate to the longest dimension, perpendicular to the long and short dimension (Equation 2.1: Sneed & Folk, 1958). Elongation ratio is defined as the ratio of the particle longest dimension in the plane perpendicular to the intermediate dimension (Equation 2.2: Sames, 1966). The shape factor of an aggregate particle can be related to flatness and elongation characteristics (Equation 2.3: Aschenbrenner, 1956). The intercept working sphericity in Equation 2.4 was described by Aschenbrenner (1956).

$$\text{Flatness } (F) = \frac{S}{I} \quad (2.1)$$

$$\text{Elongation } (E) = \frac{I}{L} \quad (2.2)$$

$$\text{Shape factor } (SF) = \frac{SL}{I^2} \quad (2.3)$$

$$\psi = 12.8(F^2 E)^{1/3} / \{1 + F(1 + E) + 6(1 + F^2(1 + E^2))\} \quad (2.4)$$



Where,

$L$  = longest dimension of a particle

$I$  = intermediate dimension of a particle

$S$  = shortest dimension of a particle

$\Psi$  = working sphericity

Furthermore, Zingg (1935) proposed a classification for shapes and established a terminology that separates flat, cubic, ellipsoid and elongated shapes with a value of 0.67 (see Figure 2.8). This chart is a graphical approach to relate particle dimensions. Lines of equal sphericity based on Equation 2.4 are added to the Zingg diagram.

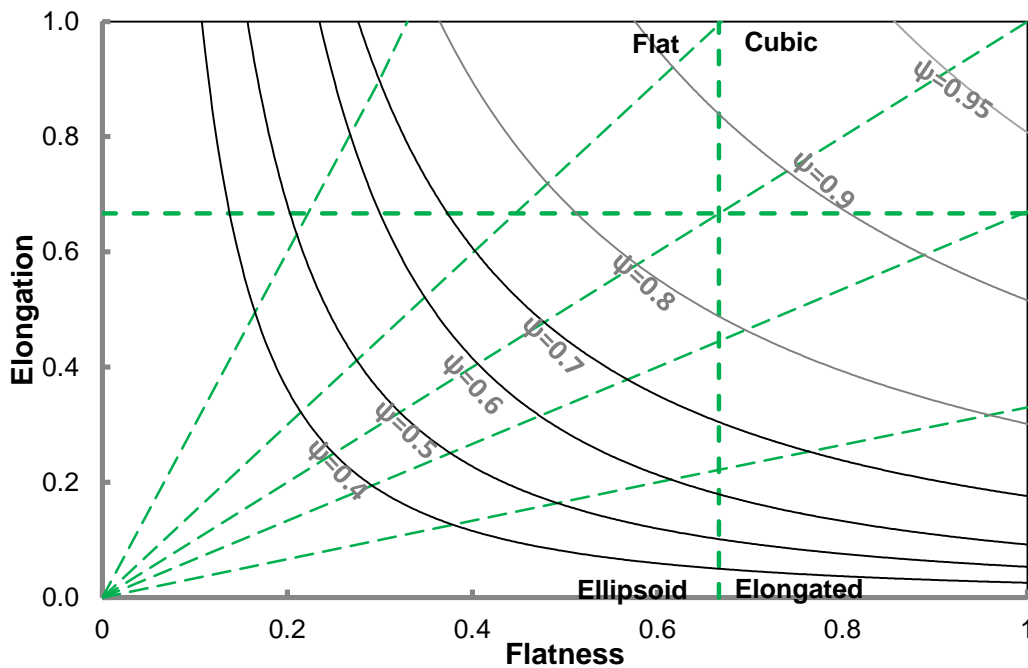


Figure 2.8: Chart to characterise particle shape (redrawn from Zingg, 1935)

### 2.4.2 Sphericity in 2D

Sphericity is a measure of how much the shape of a particle deviates from a sphere. A perfect sphere has a sphericity of one. Masad (2003) developed AIMS to measure aggregate shape properties and proposed computation of sphericity to describe aggregate form using Equation 2.5.

$$Sphericity = \sqrt[3]{\frac{SI}{L^2}} \quad (2.5)$$

Where,

$L$  = longest dimension of a particle

$I$  = intermediate dimension of a particle

$S$  = shortest dimension of a particle

### 2.4.3 Sphericity in three dimensional

Lin et al. (2005) and Hayakawa et al. (2005) quantified sphericity based on the surface area and volume properties of the aggregate. Thus, an accurate measurement of the surface area and volume has direct influence on the sphericity of the aggregate particle. Ballast aggregates have irregular and non-ideal shapes. It is therefore difficult to obtain a direct measurement of the surface area and volume properties using the traditional methods for quantifying the shape properties of aggregates. Advanced techniques, such as the laser scanning method, allow for accurate measurement of surface area and volume. The sphericity of an aggregate particle is quantified based on the surface area and volume properties of the aggregate in Equation 2.6.

$$sphericity = \frac{\sqrt[3]{36 V^2}}{A} \quad (2.6)$$

Where,

$A$  = surface area

$V$  = volume

### 2.4.4 Current approach to derive ballast roundness using 2D images

Roundness, or its inverse, i.e. angularity, represents the curvature of particles' corners. Wadell (1933) defines roundness as the ratio of the average radius of curvature of the corners to the radius of the largest inscribed circle. The definition that is presented in Equation 2.7 has been universally adopted as an ideal one.

$$Roundness = \frac{1}{N} \sum_{i=1}^N \left( \frac{r_i}{R} \right) \quad (2.7)$$

Where  $r_i$  is the individual corner radius,  $R$  is the radius of a circle inscribed about the particle, and  $N$  is the number of corners on the particle. A projected two-dimensional (2D) image of the particle is used to obtain roundness in Equation 2.8. The average roundness for the total sample is defined by Equation 2.7.

$$Roundness_a = \frac{1}{N_t} \sum_{i=1}^{N_t} n_i m_i \quad (2.8)$$

Where  $n_i$  is the number of particles in group  $i$ ,  $m_i$  is the mid-point roundness of group  $i$ , and  $N_t$  is the total number of particles. Krumbein (1941) also produced a chart for a visual assessment of particle roundness in two dimensions. Folk (1955) concluded that when charts are used for classification, the risk of obtaining errors is negligible for sphericity but large for roundness. Equation 2.9 shows how the roundness index was determined by (Folk, 1955).

$$Roundness = \frac{4\pi A}{P^2} \quad (2.9)$$

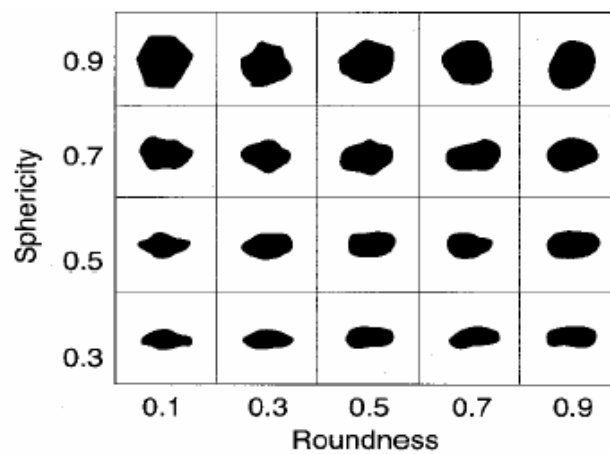
Where  $A$  is the area of the particle image and  $P$  is a perimeter of the particle 2D image. These methods discussed above are traditional methods of characterising the shape properties of ballast. The results of such methods are affected by human errors and are very subjective (Janoo, 1998). These researchers proposed roundness values that range between 0 and 1, where the value of 1 is an indication of a more rounded particle. It is important to highlight that charts such as those developed by Krumbein (1941) have a high degree of subjectivity. It is believed that the introduction of automation such as imaging and laser techniques in ballast shape measurements will be an improvement in these traditional methods (Tolppanen et al., 1999).

Figure 2.9 suggested by Quiroga and Fowler (2003) can provide two comparable charts for such a visual assessment of particle shapes. This type of visual assessments of particles only gives an idea of the particle shape, but does not indicate the fine surface characteristics. It is important to highlight that any comparing chart to describe particle properties has a high degree of subjectivity. Folk (1955) concludes that when charts are used for classification, the risk of sphericity errors is negligible but large for roundness.

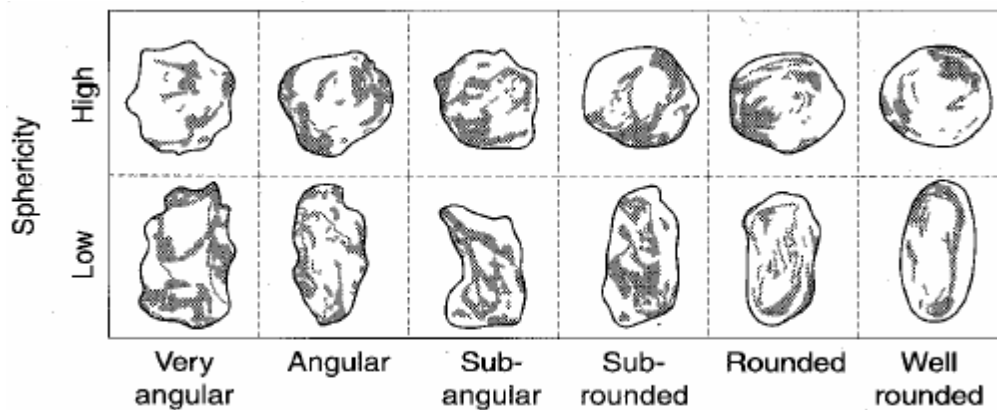
Bowman et al. (2001) noted that sphericity and roundness differ, as they are two measurements of very different morphological properties because sphericity is sensitive to elongation and roundness is related to angularity and texture. However, Rosoussillion et al. (2009) computed

roundness of the pebbles using a digital imagery procedure that allows replacing the easy-to-collect indices such as the Krumbein visual classes with more precise roundness parameters.

Most of the methods discussed above are called traditional methods of characterising the physical properties of ballast. The results of such methods are mostly affected by human errors and are time-consuming. Leonardo et al. (2009) suggested that the use of a three dimensional-laser scanning technique to study ballast material by developing a geometrical evaluation method of scanned images, produced both reliable and repeatable results.



a) Derived from measurements of sphericity and roundness



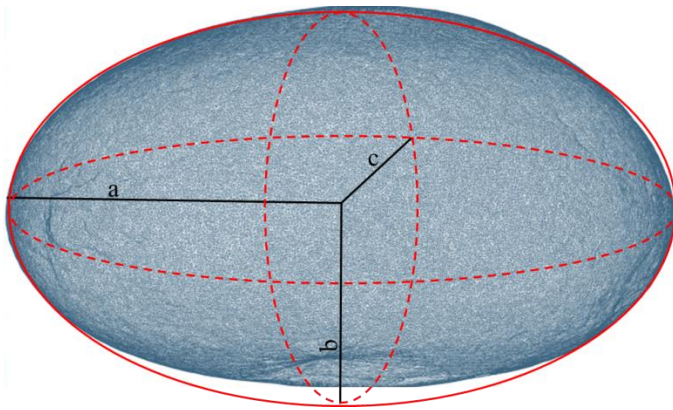
b) Based upon particle observations

**Figure 2.9: Visual assessment of particle shape (Quiroga & Fowler, 2003)**

### 2.4.5 Current approach to derive ballast roundness using 3D models

Hayakawa and Oguchi (2005) defined particle roundness as an approximation ratio of surface area of an ellipsoid ( $SA_e$ ) to the surface area of the particle ( $SA_p$ ) described by the longest ( $a$ ), intermediate ( $b$ ) and shortest ( $c$ ) dimensions in Figure 2.10. In this case, it is assumed that each ballast particle has the shape of a symmetrical ellipsoid in which the dimensions correspond to the principal axes. The standard equation of the quadric surface (ellipsoid) presented in Equation 2.10 can be used to derive the surface area of a ballast particle.

$$\frac{x^2}{a^2} + \frac{y^2}{b^2} + \frac{z^2}{c^2} = 1 \quad (2.10)$$

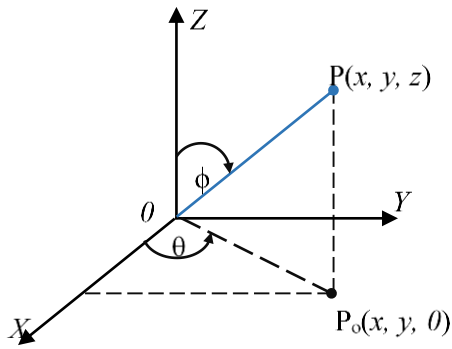


**Figure 2.10: A well-rounded pebble approximated by an ellipsoid with semi-axis**

The parametric equations of an ellipsoid can be written as follows in Equation 2.11:

$$\begin{cases} x = a \sin \phi \sin \theta \\ y = b \sin \phi \cos \theta \\ z = c \cos \phi \end{cases} \quad (2.11)$$

Where  $a \geq b \geq c$  are ellipsoid principal radii, and,  $(\theta, \phi)$ , are the surface parameters shown in Figure 2.12.



**Figure 2.11: Spherical coordinates**

for  $0 \leq \theta \leq 2\pi$  and  $0 \leq \phi \leq \pi$

Surface area (S) of an ellipsoid can be obtained from Equation 2.12:

$$SA_e = \int_0^\pi \int_0^{2\pi} \sin \phi \sqrt{a^2 b^2 \cos^2 \phi + c^2 (a^2 \sin^2 \theta + b^2 \cos^2 \theta)} \sin^2 \phi \, d\theta d\phi \quad (2.12)$$

The double integral presented in Equation 2.13 cannot be evaluated by elementary means. In this study, numerical integration was therefore done by using MATLAB software to derive and calculate surface area from the measured values of the bounding box of the scanned particles. Equation 2.13 can also be used to quantify roundness from scanned data as defined by Hayakawa and Oguchi (2005).

$$\rho = \frac{SA_e}{SA_p} \quad (2.13)$$

Where,

$\rho$  = individual particle roundness

$SA_e$  = surface area of an ellipsoid

$SA_p$  = surface area of ballast particle

The University of Illinois Aggregate Image Analyzer (UIAIA) system is based on capturing three projections of aggregate particles while moving on a conveyor belt. The projections are then used to reconstruct a three dimensional presentation of aggregate particles. The system provides information on gradation, form/shape, angularity, texture, as well as surface area and

volume using measured dimensions directly without any assumptions or idealisation of the particle shape (Rao et al., 2002). The longest and shortest dimensions are determined using the three views of an aggregate particle. After a number of particles are tested, the flat and elongation ratio are averaged for a certain aggregate sample (Tutumluer et al., 2000).

Among the form indices described above, the two sphericity parameters, two roundness parameters and the flat, elongation and shape factor can be computed directly using the data obtained using the 3D-laser scanning device used in this study. Therefore, these indices will further be investigated in this study.

#### **2.4.6 Current standard test to determine the flakiness index**

Raymond (1985) reported that most specifications restrict the percentage of flaky particles whose aspect ratio exceeds three (3) and exclude particles with an aspect ratio exceeding 10. Flaky particles cannot be used as ballast given their long and very thin dimensions that can align and form planes of weakness in both vertical and lateral directions. The use of increased flakiness appears to increase abrasion and breakage, increase permanent strain accumulation under repeated load and decrease stiffness (Selig & Waters, 1994).

Flakiness index test-procedures are contained in Technical Methods for Highways (TMH 1) Method B3 (TMH 1, 1986). Under the new South African National Standards (SANS), the method will be replaced by SANS 3001-AG4 (SANS, 2009). The test procedure starts with performing grading analysis on the aggregate sample to be tested. Each aggregate particle retained on a specific sieve size is then passed through a corresponding rectangular slot of a flakiness gauge. The particles passing the slots are regarded as flaky, whereas particles that do not pass are considered non-flaky. Flakiness index (%) is calculated by dividing the mass of aggregates passing the slots by the total mass of the sample. The test provides an indication of the flatness of aggregate particles.

In the TFR specification, flakiness index is defined as the ratio of the total mass passing bar sieve slots, which are 0.5 of the sieve size, to the total mass of aggregate retained on three specific sieve sizes. Figure 2.12 shows a photograph of the flakiness gauge apparatus.



**Figure 2.12: Current test method using a flat gauge (Courtesy of TFR)**

Mathematically, the flakiness index (FI) of a ballast material can be represented in Equation 2.14 as follows:

$$FI = \left( \frac{M_p}{M_T} \right) \times 100 \quad (2.14)$$

Where,

$M_p$  = total mass of aggregate passing a bar sieve slots

$M_T$  = total mass of aggregate retained on a specific sieve size (grading analysis)



#### 2.4.7 Current standard test to determine flat and elongated ratio

The form of aggregate particles can also be evaluated by using the flat and elongated particle test. Similar to the flakiness index test, the flat and elongated particle test provides an indication of the flatness and elongation of aggregates. The method is recommended in Superpave for evaluation of aggregate form (Asphalt Institute, 1996). The test procedures are contained in the American Society of Testing and Materials (ASTM) standard procedure ASTM D 4791 (ASTM D 4791, 2010). In this method, a proportional calliper device set at a pre-defined ratio is used to measure the ratios of the longest to the shortest dimensions of an aggregate particle. The Superpave recommends a ratio of 5:1 to be used for determining the flat and elongated ratio. The flat and elongation ratio is calculated by dividing the mass of flat and elongated particles to the total mass of the sample, and expressed as a percentage. Table 2.3 shows Superpave's specifications for flat and elongated particles for asphalt mixes (Asphalt Institute, 1996). Figure 2.13 shows a photograph of a proportional calliper device used for testing flat and elongated particles. This method has not been adopted by the rail industry.

**Table 2. 3: Specifications for flat and elongated particles (Asphalt Institute, 1996)**

Traffic (Million ESALs)	Maximum flat and elongated particles (%)
< 0.3	-
< 1	-
< 3	10
< 10	10
< 30	10
< 100	10
≥ 100	10



**Figure 2.13: Proportional calliper device**

#### **2.4.8 Laser-based determination of flakiness index**

A new flakiness index equation that is based on the 3D-laser scanning technique was proposed to determine the flakiness of aggregate particles used in road construction (Anochie-Boateng et al., 2011b). The equation uses the volume ratio instead of the mass ratio presented in TMH 1 to compute the flakiness index of the aggregate particle (see Equation 2.15). The 3D-laser scanning device is used to directly obtain the volume parameters of the aggregate particle to compute the flakiness index. Table 2.4 shows the slots specified for the different sieve sizes.

**Table 2. 4: Slots of specified width with appropriate sieve size (TMH1 & SANS 3001)**

Sieve Retained (mm)	SANS 3001-AG4		TMH 1	
	Min Length of slot (mm)	Width of slot (mm)	Min Length of slot (mm)	Width of slot (mm)
63.0	150.0	37.5	150.0	37.5
53.0	100.0	25.0	126.0	31.5
37.5	75.0	18.7	106.0	26.5
26.5	50.0	14.0	75.0	18.8
19.0	40.0	10.0	53.0	13.3
13.2	27.0	7.0	38.0	9.5
9.8	20.0	5.0	26.4	6.6
6.7	15.0	3.5	19.0	4.8
4.8			13.4	3.4

$$FI_v = \left( \frac{V_p}{V_T} \right) \times 100 \quad (2.15)$$

Where,

$FI_v$  = flakiness index based on volume

$V_p$  = total volume of flaky aggregates scanned

$V_T$  = total volume of the aggregate sample

## 2.5 PROPERTIES OF BALLAST MATERIAL

The key functions of ballast are distributing load from sleepers, damping of dynamic loads, developing lateral resistance and providing free draining conditions. A major concern relating to the performance of ballast is its ability to withstand both vertical ( $\sigma_1$ ) and lateral forces ( $\sigma_3$ ). According to Indraratna et al. (2006), in the design and analysis of railway track structures, tests on scaled down aggregates cannot be relied upon for the prediction of deformation parameters. Therefore, large scale testing is imperative, wherein the sample must be prepared according to the field grading and tested under stresses representative of the field situation.

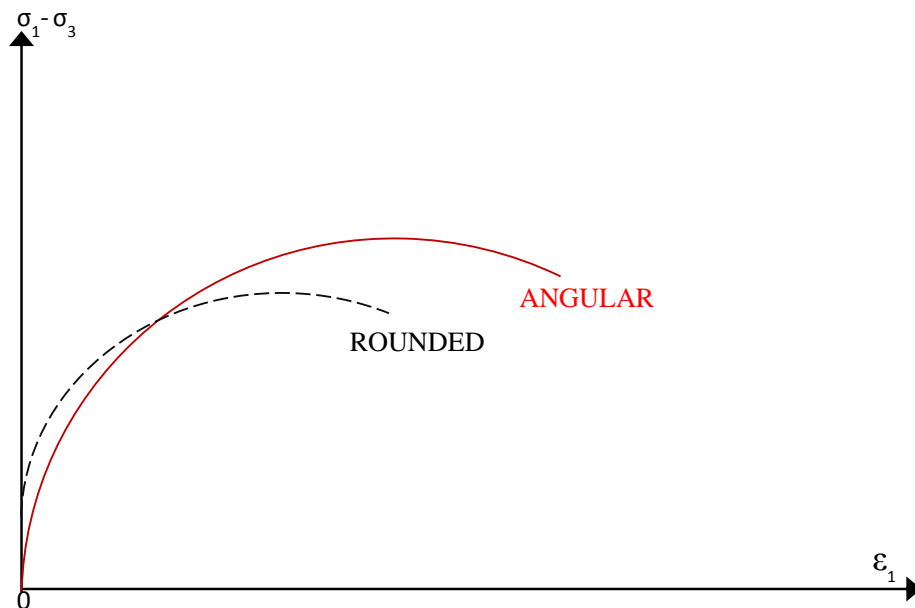
Physical properties of ballast are largely responsible for successful ballast performance in the field environment as noted by Indraratna et al. (2004). The physical properties of ballast can be divided into two categories. The first group is concerned with the properties of individual particles, including durability, shape and surface examination, before being declared suitable. The second category considers the physical properties of ballast particles that are in contact with each other, but not influencing deformation. These properties are permeability, void ratio, bulk density and specific gravity.

Individual particles are tested for toughness, wearing by attrition, resistance to crushing under static loading and resistance to sudden shock loading. Ballast that satisfies the durability requirements is then subjected to further examination that evaluates shape and surface characteristics, gradation, defects and the existence of impurities. These tests are concerned with establishing a quantitative estimate of the resistance to in-track instability and degradation under loading. Tests include flakiness, elongation, sphericity, angularity or roundness, fractured particles, surface texture, grain size, particle size distribution and fine particle content. Three

important aspects of mechanical properties of ballast, namely shear strength, settlement and degradation are described in the following sections.

### 2.5.1 Ballast shear strength

In general, angularity increases frictional interlock between grains, which increases shear strength. Holz and Gibbs (1956) concluded that shear strength of highly angular quarried materials is higher than that of relatively sub-angular or sub-rounded river gravels (Figure 2.14). The ballast stone must be angular with as many sides as possible to facilitate interlocking between the stones and in so doing, increase the shear strength of the ballast bed, something that would not be possible with rounded ballast. Selig and Waters (1994) reported that increasing angularity of sands significantly increased the shear strength, but also increased the strain at failure and decreased the stiffness.



**Figure 2.14: Effect of particle shape on stress strain characteristics (Modified after Holz & Gibbs, 1956)**

Jeffs and Marich (1987) reported that angular aggregates settle less than rounded aggregates. According to Jeffs and Tew (1991), the shape of ballast grains depends on the production process and nature of deposits. If the effects of particle orientation on strength, and the effects of

shape on track stability that were indicated in this chapter for rounded ballast are to be avoided, then an even more restrictive definition of shape would be required.

### 2.5.2 Ballast settlement

Settlement of ballast may not be a problem if it is occurring uniformly along the length of the track (Selig & Waters, 1994). In fact, differential track settlement is more important than the total track settlement. According to Selig and Waters (1994), ballast contributes most of the substructure settlement even though one of the functions of ballast is to restrain track geometry. Given that ballast is responsible for nearly all the track settlement, every effort to reduce settlement is focused on ballast layer.

Total settlement caused by repeated loading is equal to the sum of the compressions of the layers down to depth of negligible traffic effect. The ballast settlement,  $S_B$ , is:

$$S_B = \varepsilon_B H_B \quad (2.16)$$

Where,

$\varepsilon_B$  = plastic ballast strain

$H_B$  = ballast layer thickness

The sub-ballast settlement,  $S_S$ , is likewise:

$$S_{BS} = \varepsilon_S H_S \quad (2.17)$$

Where,

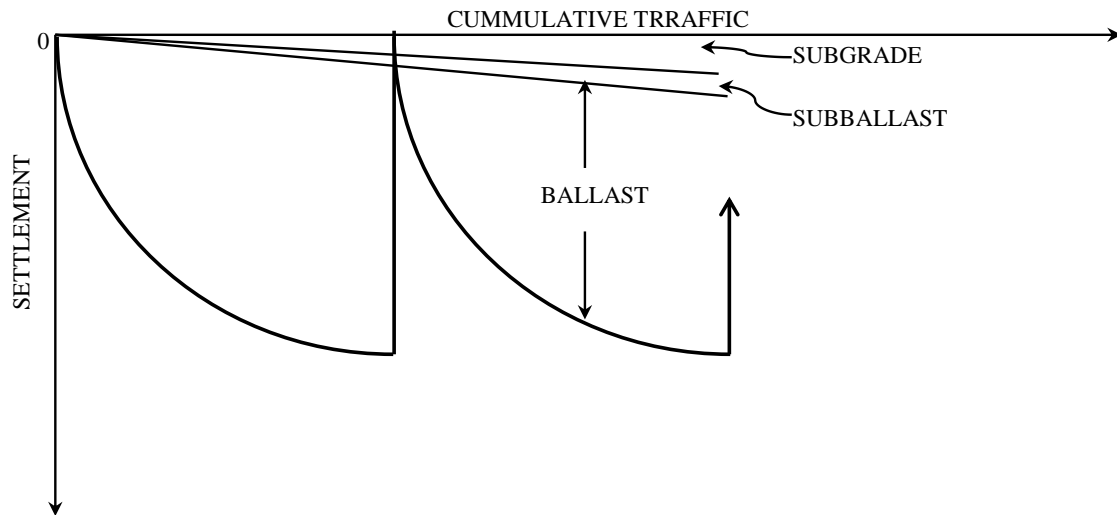
$\varepsilon_S$  = plastic sub-ballast strain

$H_S$  = sub-ballast layer thickness

Finally, the subgrade layer compression is  $S_G$ . Each of these three components is plotted in Figure 2.15. The total settlement,  $S_L$ , is then:

$$S_L = S_B + S_S + S_G$$

More than half of the total settlement is contributed by ballast, but  $S_S$  and  $S_G$  are still significant.



**Figure 2.15: Ballast, sub-ballast and subgrade contributions to total settlement (modified from Selig & Waters, 1994)**

Railway ballast deforms and degrades progressively under heavy train (repeated) loadings. The track progressively moves vertically and laterally from the desired geometry. This deviation is irregular and riding quality decreases as dynamic loading increases. Excessive settlement can reduce riding quality, cause speed restrictions, and potential derailment. Ballast tamping is used to correct geometry. Tamping is the process of lifting and laterally adjusting the track to the desired geometry, while rearranging the upper portion of the ballast layer to fill resulting voids under the sleeper. During tamping the sleeper is lifted and aligned. The dynamic track stabilising machine is introduced directly behind the tamping machine after tamping to compact ballast.

The rail track settlement is usually related to the number of load cycles by a semi-logarithmic relationship in Equation 2.18.

$$S_N = a(1 + k \log N) \quad (2.18)$$

Where,

$S_N$  = settlement of ballast

$N$  = load cycles

$a$  = settlement at first cycle

$k$  = empirical constant

Indraratna et al. (2000) conducted several tests to investigate the effect of load cycles and axle loads on settlement. They employed Equation 2.19 to model the ballast settlement.

$$S_N = aN^b \quad (2.19)$$

Where  $b$  is an empirical coefficient determined from nonlinear regression analysis. In this study, the settlement behaviour of ballast with different shape properties will be investigated under cyclic loading using triaxial equipment.

## 2.6 LOSS OF CANT HOLDING ON CURVES

Cant is the difference between the vertical height of the inner and outer rail crowns at a corresponding point to assist steering around curves. Figure 2.16 shows how the track is super elevated to provide the necessary cant to steer the train. The ballast should resist vertical, lateral and longitudinal forces applied to the sleeper in order to retain the track in its required position.

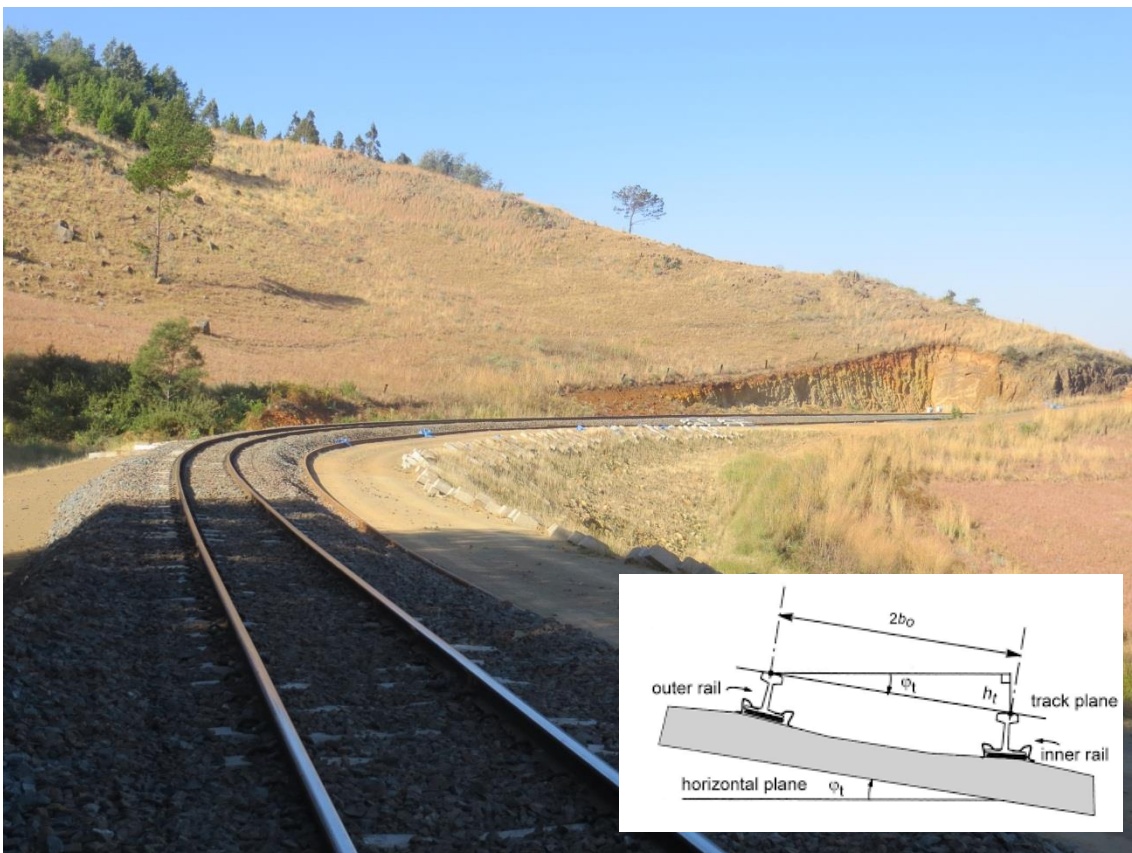


Figure 2.16: Cant visible of track around curve

Therefore, ballast allows correction of the vertical and horizontal defects of the track (track geometry) through the process of lifting, levelling, aligning and tamping. A good ballast stone should have as many sides as possible. This will ensure that different ballast stones can interlock and remain in that stable position. Good ballast performance is required to ensure the proper track cant is maintained.

## **2.7 EFFECTS OF PARTICLE CHARACTERISTICS ON TRACK PERFORMANCE**

The effects of some of the particle characteristics on mechanical behaviour of granular materials, including ballast, have been examined by means of laboratory tests. Little information is available from field tests because of the large expense involved and the difficulty of controlling the variables. Conventionally, the shear strength of granular material is assumed to vary linearly with the applied stress, and the Mohr-Coulomb theory is used to describe the conventional shear behaviour. However, the Mohr-Coulomb envelop is generally non-linear, especially at the high stresses in track. In this study the linear approach was used.

Selig and Waters (1994) reported that Holts and Gibbs (1956) conducted triaxial tests on sub-angular to sub-rounded gravel and on sharp, angular crushed quartz rock, both with similar grading curves. As expected, the angular material had a higher strength. Huang (2010) simulated by discrete element modelling (DEM) shear box, the effect of ballast angularity and surface texture on aggregate assembly strength. It has been proven by Huang (2010) that angular ballast particles perform better than rounded particles in term of both strength and stability. Surface texture was found to play a predominant role in controlling strength. Hai (2010) found that the internal frictional angle of rough and angular, and smooth and round ballast were 35° and 15°, respectively. According to Tutumluer et al. (2006), surface texture may even be more important than aggregate angularity since angular particles with smooth surfaces have lower strength properties than rounded particles with rough surfaces.

In order to design an even more efficient track structure and minimise maintenance cost, ballast degradation and plastic track deformation must be examined and studied in detail. In this study, static triaxial tests were used solely for the determination of the strength parameters  $c$  (apparent cohesion) and  $\phi$  (angle of internal friction). Dynamic triaxial tests (repeated load) were used for plastic deformation or permanent deformation tests.



### **3 METHODOLOGY**

#### **3.1 INTRODUCTION**

A typical track consists of superstructure (rails, fastenings and sleepers) and sub-structure (ballast, sub-ballast and formation, including subgrade). The function of the ballast is to transfer the load from the superstructure to the subgrade. Performance of the track system depends on the effectiveness of the ballast in providing drainage, stability, flexibility, uniform support to the superstructure, and distribution of the track loading to the subgrade and facilitating maintenance. Increase in axle loads and traffic density increase the rate of settlement of the track. To keep this within permissible limits, stresses in the subgrade should be reduced suitably to ensure stability of track.

Ballast is usually composed of blasted rocks originating from high quality igneous metamorphic or well-cemented sedimentary rock quarries. Crushed angular hard stones and rocks having a uniform gradation and free of dust have been considered as acceptable ballast materials. For quality assessment, and in order to relate the results of laser scanning and triaxial tests to the material type, standard tests were performed. The objective of this chapter is to present the methodology followed during the study. The methodology comprised of the following:

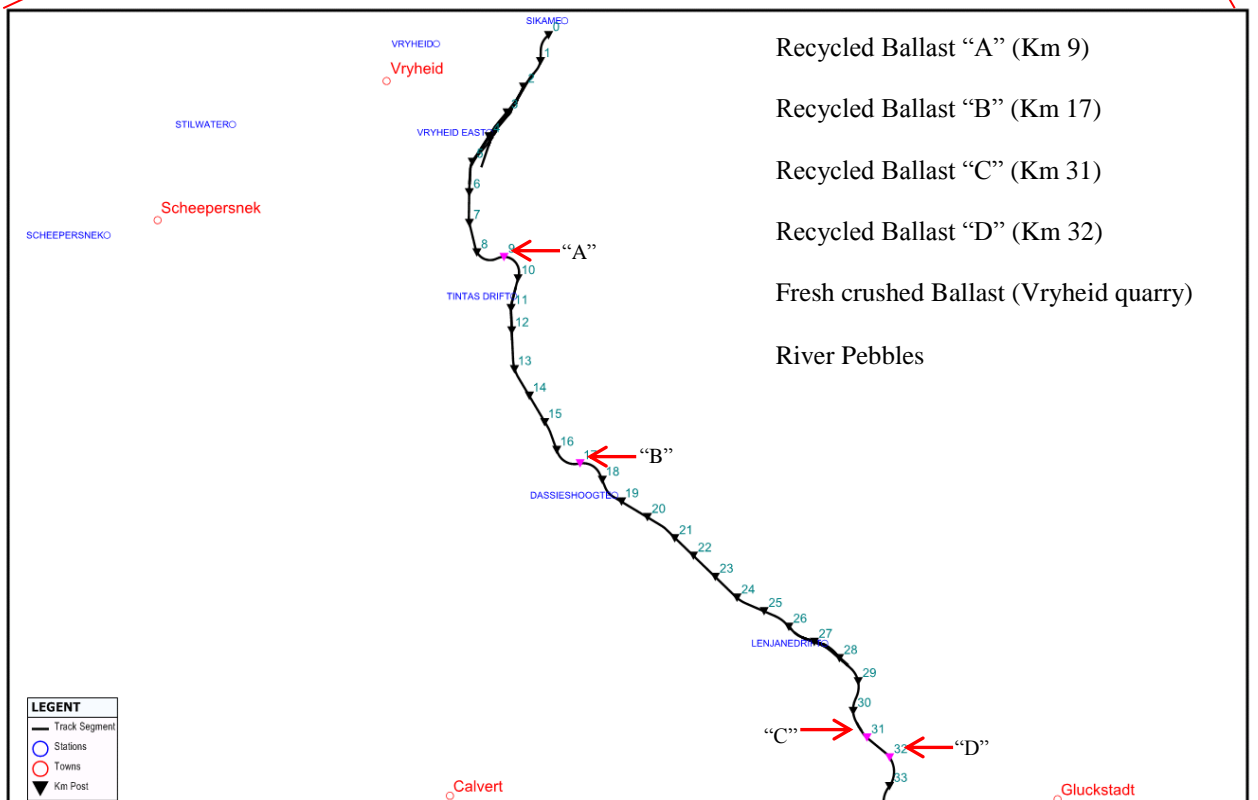
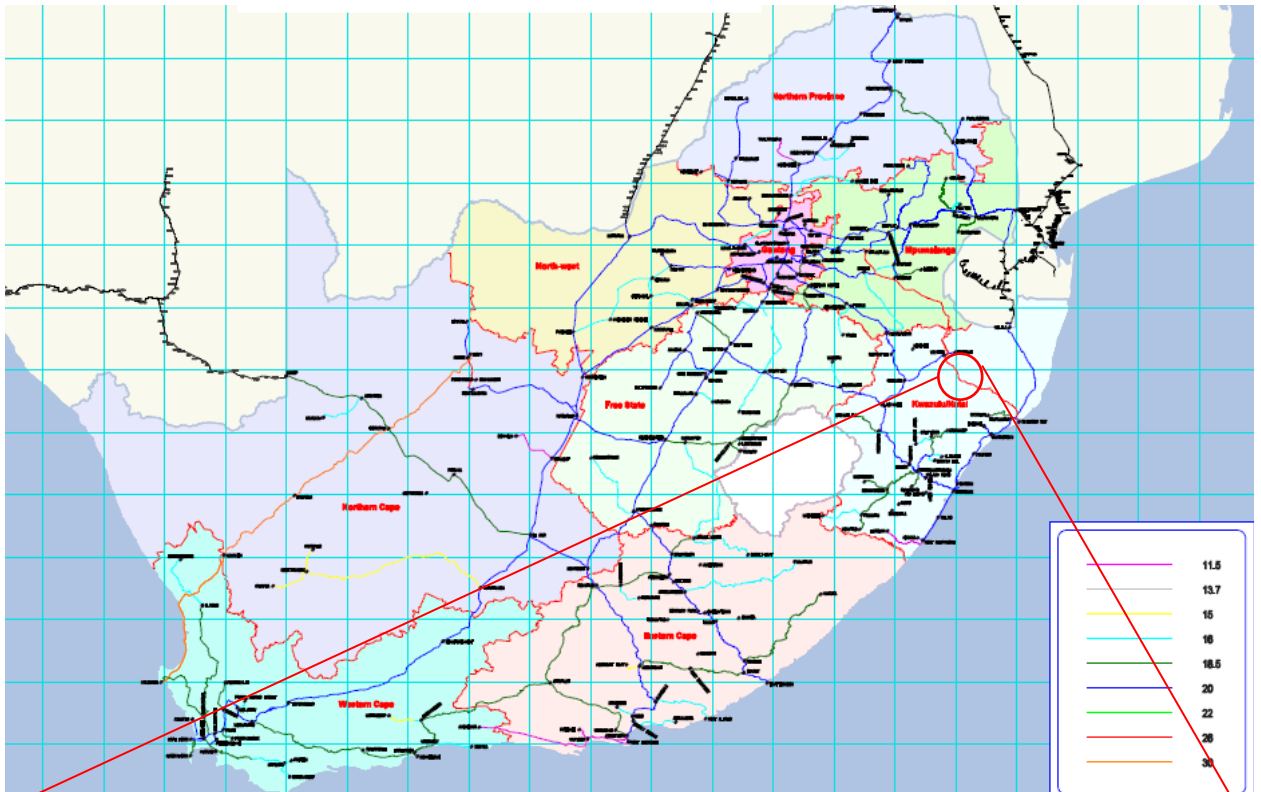
- Sampling and sample description
- Physical properties of track ballast
- Laser-based method to quantify ballast shape properties
- Triaxial testing

#### **3.2 SAMPLING AND SAMPLE DESCRIPTION**

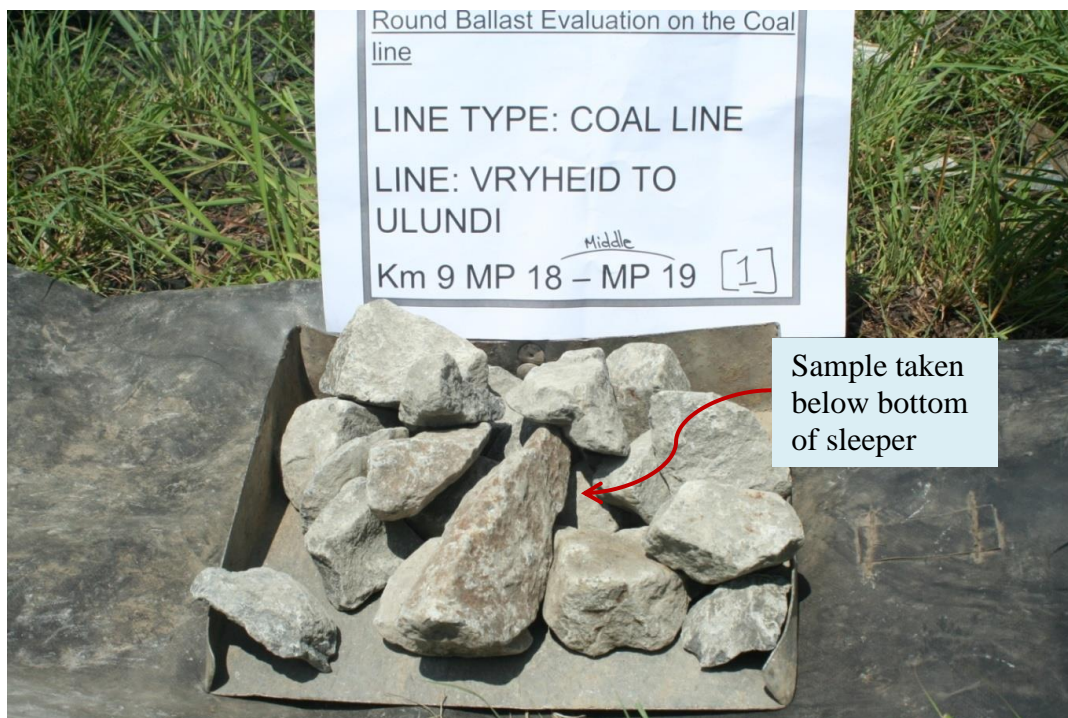
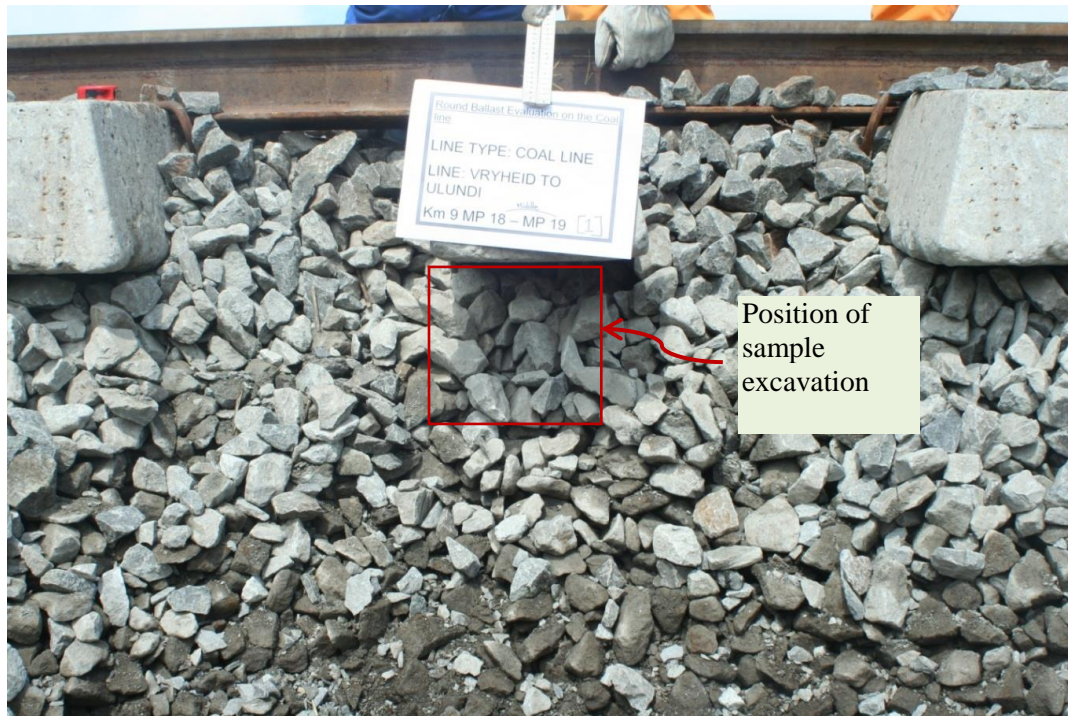
One fresh ballast sample from a quarry, and four recycled ballast from a heavy haul coal line in South Africa was selected for this study. A typical pebble material was also included in the study to act as a reference material for determining the roundness of the ballast materials. Recycled ballast refers to the reclaimed material returned to track during the track formation rehabilitation. The parent rock of recycled ballast remains mostly the same as that of fresh crushed ballast. Because dolerite is the most commonly used ballast type in the heavy haul line, preliminary testing for the reproducibility of tests was conducted using a dolerite obtained from a quarry in South Africa. The same dolerite was used in the main testing program. The field materials were selected from the line section, maintenance depot of Transnet Freight

Rail (TFR), which noted repetitive ballast tamping, track geometry (cant loss on curves) and ballast roundness.

Figure 3.1 shows the ballast sampling points on the coal line route and sources of the other ballast material for this study. The recycled ballast was subjected to a traffic volume of 2 738 million gross tons (MGT). Samples were taken below the sleeper and around said point (Figure 3.2) with special focus on collecting rounded particles for the laboratory analyses. The visual examination indicated that about 90% of recycled ballast comprised of semi-angular crushed rock fragments, while the remaining 10% consisted of semi-rounded river gravels. These materials were chosen so that a comparison of their physical characteristics could be made. Figure 3.3 gives a visual picture of the field samples, quarry stockpile and pebbles used in this study.



**Figure 3.1: Ballast sampling positions along the heavy haul coal export route and sources of other sample materials**



**Figure 3.2: Illustration of sample position in the ballast layer**





**Recycled Ballast Sample "A" at Km 9**



**Recycled Ballast Sample "B" at Km 17**



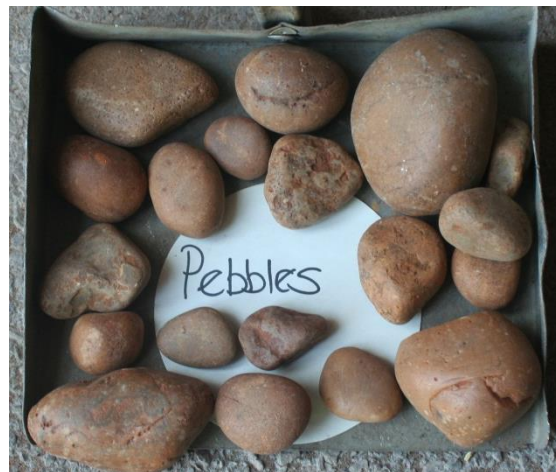
**Recycled Ballast Sample "C" at Km 31**



**Recycled Ballast Sample "D" at Km 32**



**Fresh Crushed Ballast Sample from quarry stockpile**



**Pebbles**

**Figure 3.3: View of undisturbed recycled samples at different positions on the coal line, fresh ballast and river pebbles**

### 3.3 PHYSICAL PROPERTIES OF BALLAST MATERIALS

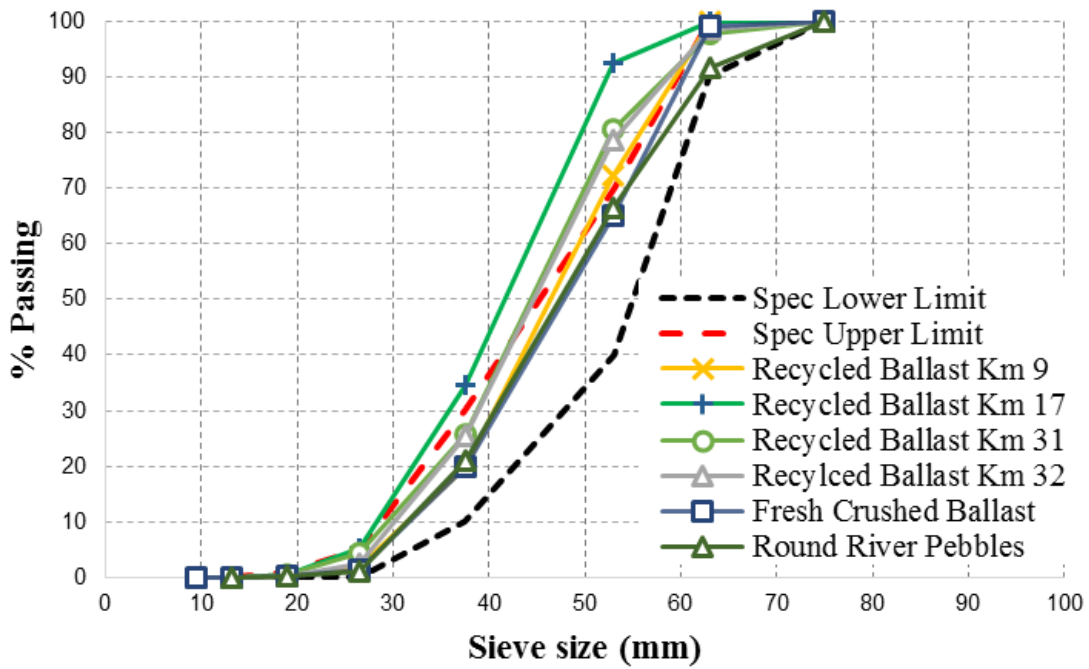
In general, ballast that satisfies the Los Angeles Abrasion test is subjected to further tests that evaluate shape, surface characteristics, grading and unit mass. For the purpose of this study, physical tests were performed on the quarry sample using the TFR S406 ballast specification. The physical tests were conducted to determine whether material studied were suitable for use as railway ballast. The tests were done in the geotechnical engineering laboratory of the Track Testing Centre at Transnet. Table 3.1 summarises the physical properties of ballast material used in the study, as evaluated by the standard ballast tests. These tests provide basic guidelines for accepting or rejecting a given material as potential railway ballast. Therefore, this sample was suitable for use as ballast material in heavy haul lines.

**Table 3.1: Physical characteristics of fresh crushed dolerite ballast**

<b>Physical Characteristic Test Result</b>	<b>South African Standard Recommendation</b>	<b>Test Value</b>
Void Content	> 40	43
Relative Density	> 2.5	2.7
Grading	Pass or Fail	Pass
Flakiness Index	< 30	8
Los Angeles	< 22	12
Mill Abrasion	< 7	6
Absorption	< 1	0.6
Weathering	< 5	1.2

### 3.4 GRADING ANALYSIS

Sieve analysis (grading) tests were conducted on all samples to determine particle size distribution in accordance to the specification (Arangie, 2011). Figure 3.4 presents the particle size distribution of the six materials and compares the four recycled ballast, fresh crushed ballast and river pebbles to TFR recommended specification for heavy haul tracks. All recycled ballast material failed to meet specification limits. The five ballast materials were composed of particles ranging from 19 mm to 63 mm. The aim of the grading was to obtain samples for laser scanning.



**Figure 3.4: Grading analysis result of the six materials compared to TFR specs**

Table 3.2 presents a summary of grain size with a uniformity coefficient  $C_u$  and coefficient of curvature  $C_c$ .  $D_{50}$  is the mean particle size, the particle size corresponding to 50% of particles passing by weight. Therefore, heavy haul standard grading limits contain more than 50% of particles with sizes between 26.5 mm and 37.5 mm. For comparative analysis, representative particle samples were assembled from graded material, and used for laser scanning.

**Table 3.2: Summary of grain size characteristics of ballast and pebble material**

Material description	Recycled ballast				Fresh Crushed ballast	River pebbles	Limits of percent passing each sieve (recommended ballast grading)
Material source	Coal line Km 9	Coal line Km 17	Coal line Km 31	Coal line Km 32	Lancaster quarry	Kimberly mine	
Sieve size (mm)	Sieve analysis (Percentage passing)						
73.0	100	100	100	100	100	100	100
63.0	100	93	98	99	99	92	90-100
53.0	72	35	81	78	65	67	40-70
37.5	20	5	26	26	20	21	10-30
26.5	2	0	4	3	1	1	0-5
19.0	0	0	1	0	0	0	0-1
13.2	0	0	0	0	0	0	0
9.5	0	0	0	0	0	0	0
Particle size characteristics							
$d_{max}$ (mm)	53	53	63	63	63	63	
$d_{min}$ (mm)	9.5	9.5	9.5	9.5	19	13.2	
$d_{10}$ (mm)	31.47	28.32	29.41	30.06	31.68	42.41	
$d_{30}$ (mm)	40.52	36.25	38.72	38.81	40.98	38.38	
$d_{50}$ (mm)	46.43	44.28	44.37	44.66	47.83	46.38	
$d_{60}$ (mm)	49.38	44.28	47.19	47.59	51.26	50.39	
$C_u$	1.57	1.56	1.6	1.58	1.62	1.19	
$C_c$	1.06	1.05	1.08	1.05	1.03	0.69	

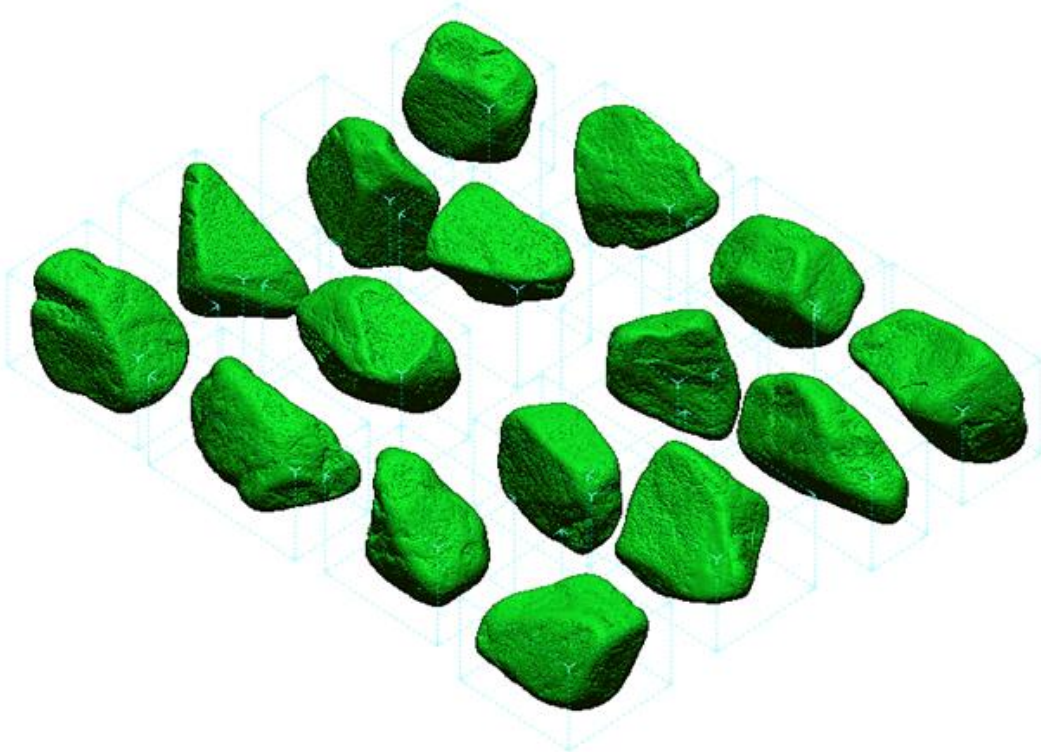
### 3.5 REPRESENTATIVE SAMPLE SIZE

All the ballast particles used for this study were scanned in accordance with the CSIR guideline for scanning of aggregates and ballast particles (Anochie-Boateng, 2014). In order to obtain a statistical representative scanned sample, a quartering approach was used to scale-down the samples for laser scanning (Table 3.3). A total of 356 particles (as presented in Table 3.3) from six material sources were scanned to evaluate their shapes. This approach makes use of particle dimensions (height, width and length) and surface area to compute an index describing ballast roundness. The total number of particles with their corresponding sieve size is presented in Table 3.3. After the scanning was completed, the software of the laser device system was used to model the ballast particles in three-dimensions, as shown in Figure 3.5.



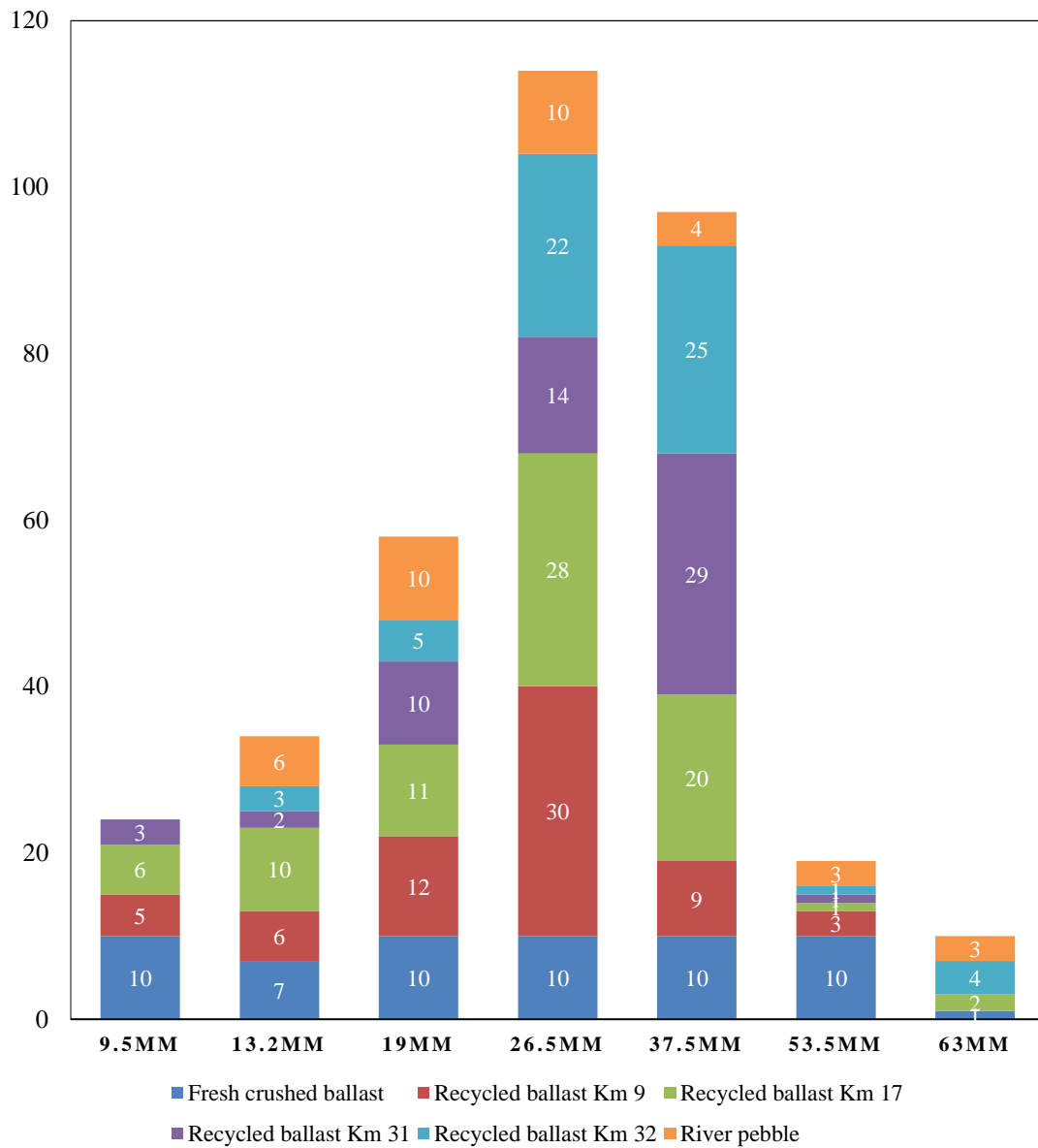
**Table 3.3: Statistical representative samples of ballast and pebble**

Sieve Size	Fresh Ballast	Recycled Ballast				Pebbles	Total
		Km 9	Km 17	Km 31	Km 32		
9.5 mm	10	5	6	3	-	-	24
13.2 mm	7	6	10	2	3	6	34
19.0 mm	10	12	11	10	5	10	58
26.5 mm	10	30	28	14	22	10	114
37.5 mm	10	9	20	29	25	4	97
53.5 mm	10	3	1	1	1	3	19
63.0 mm	1	-	2	-	4	3	10
Scanned	58	65	78	59	60	36	356



**Figure 3.5: three dimensional modelled recycled ballast particles**

Sample data were collected using a simple random sampling method. Sample groups are independent from each other and each sample follows a normal distribution, as presented in Figure 3.6. This type of distribution will allow the analysis of variance (ANOVA) to be conducted.



**Figure 3.6: Normal distribution of the sample size to be scanned**

Representative samples of particles of fresh crushed dolerite ballast, recycled dolerite ballast and natural round pebbles that were used in scanning are presented in Figure 3.7 to Figure 3.12. The following figures also included the mass of the reduced sample.

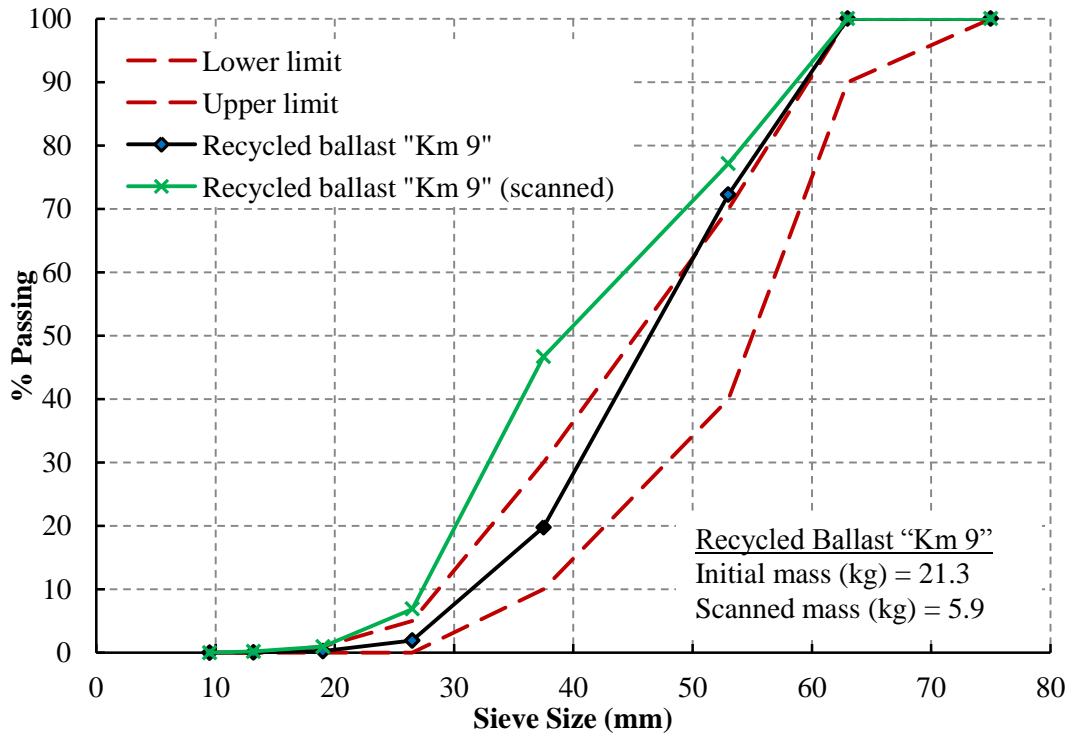


Figure 3.7: Grading analysis of recycled ballast (Km 9) to be scanned

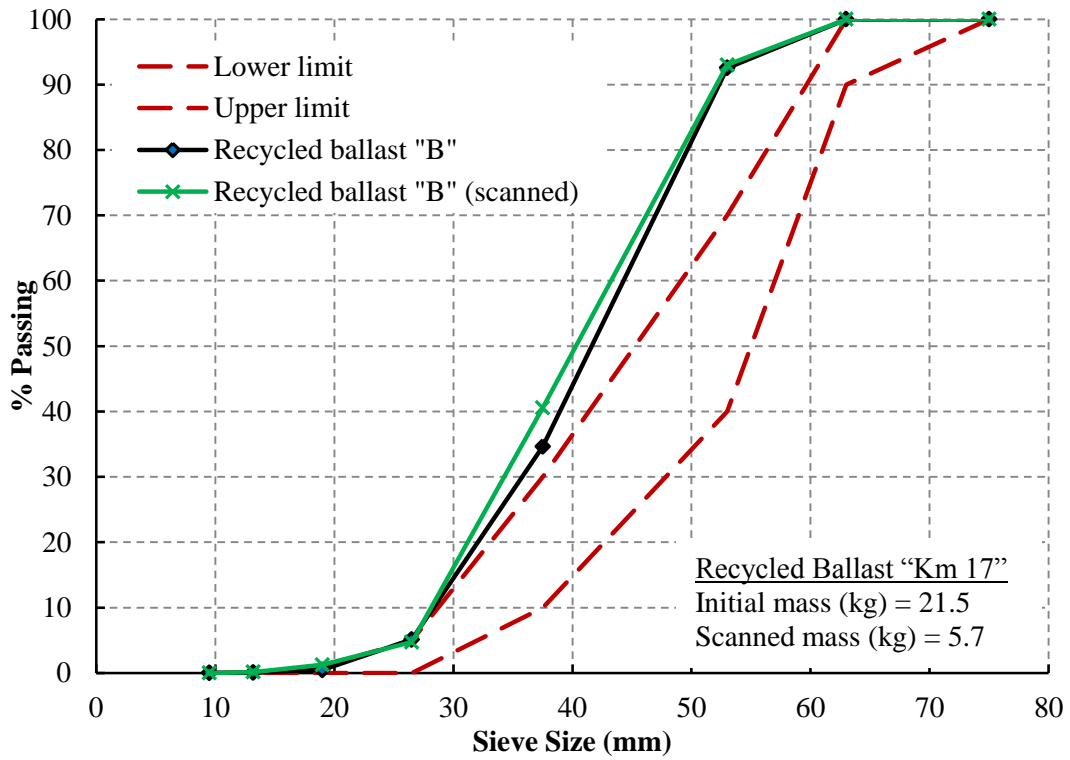


Figure 3.8: Grading analysis of recycled ballast (Km 17) to be scanned

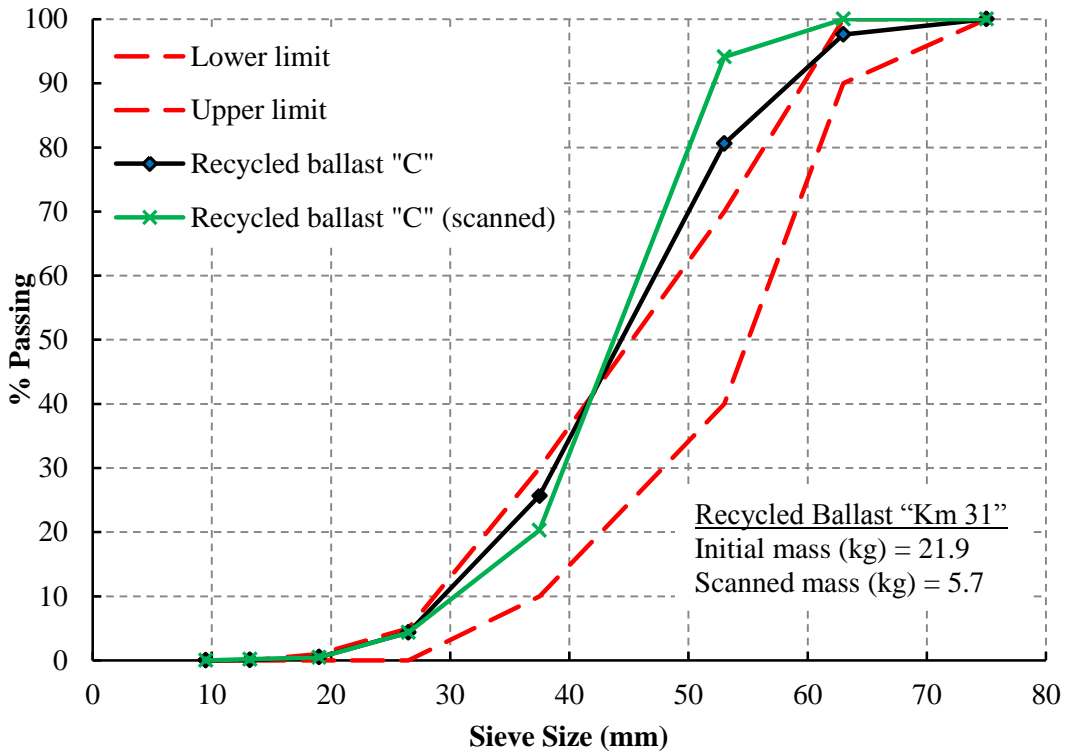


Figure 3.9: Grading analysis of recycled ballast (Km 31) to be scanned

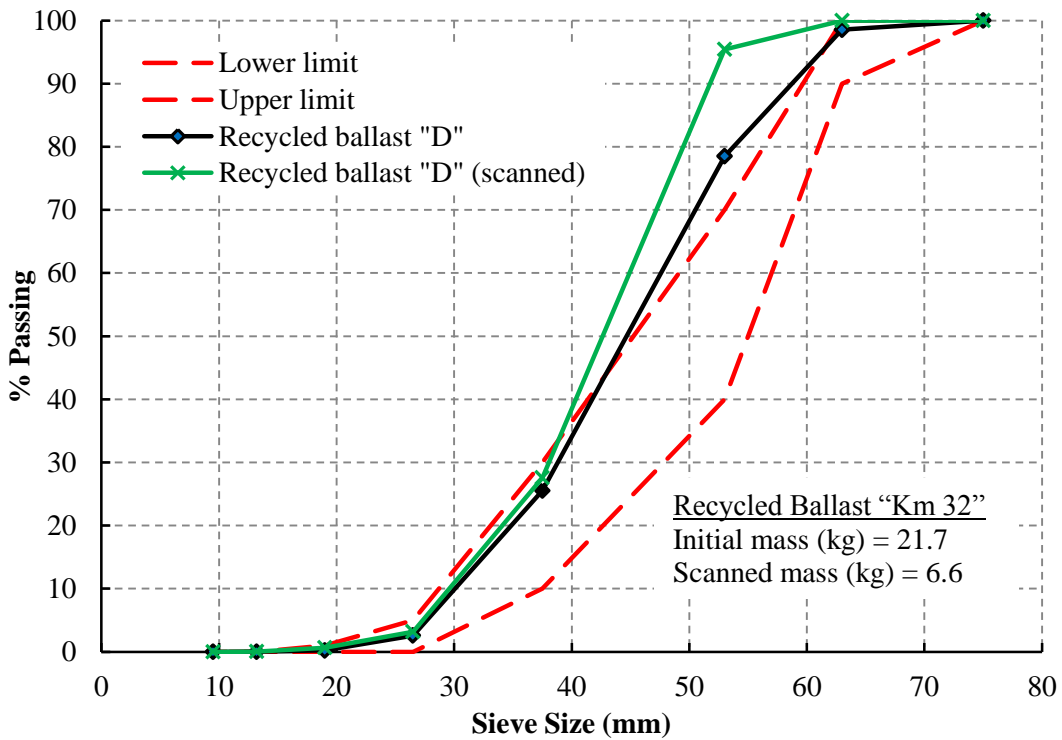


Figure 3.10: Grading analysis of recycled ballast (Km 32) to be scanned

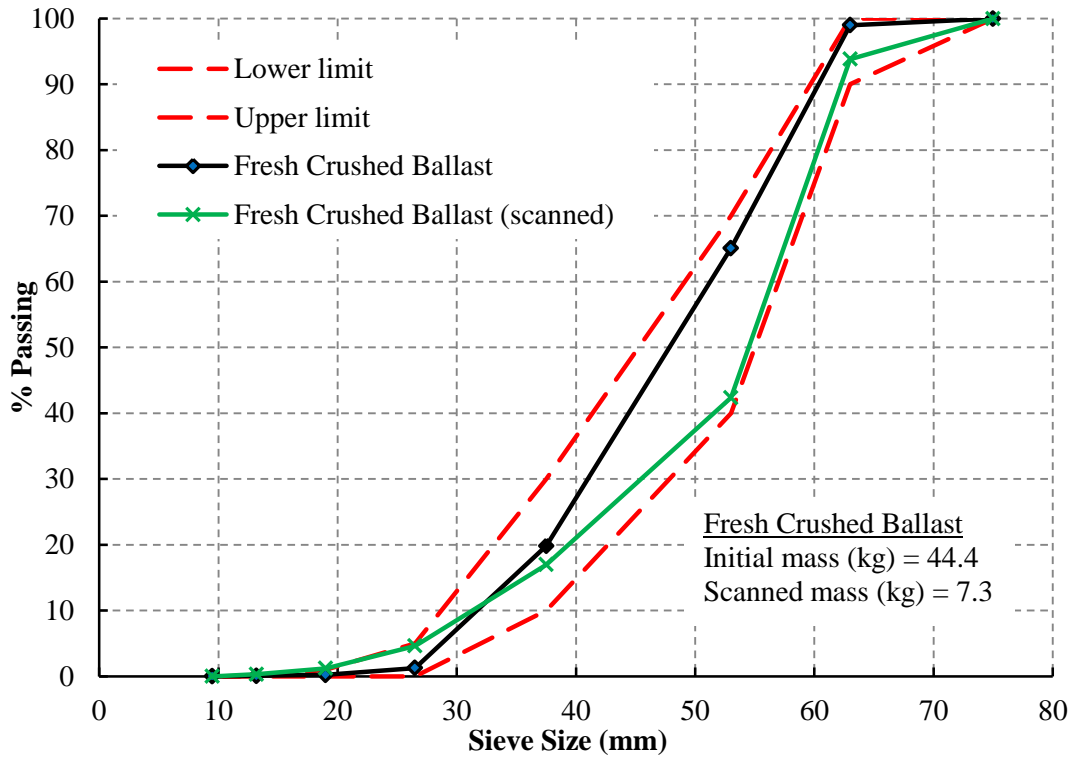


Figure 3.11: Grading analysis of fresh crushed ballast to be scanned

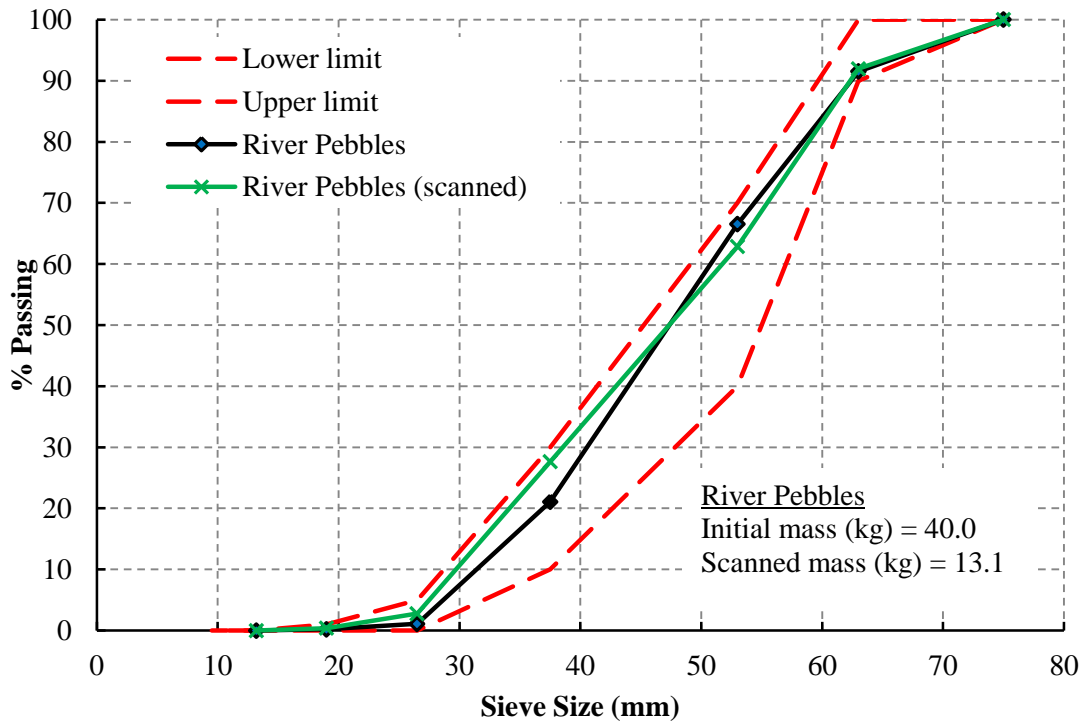
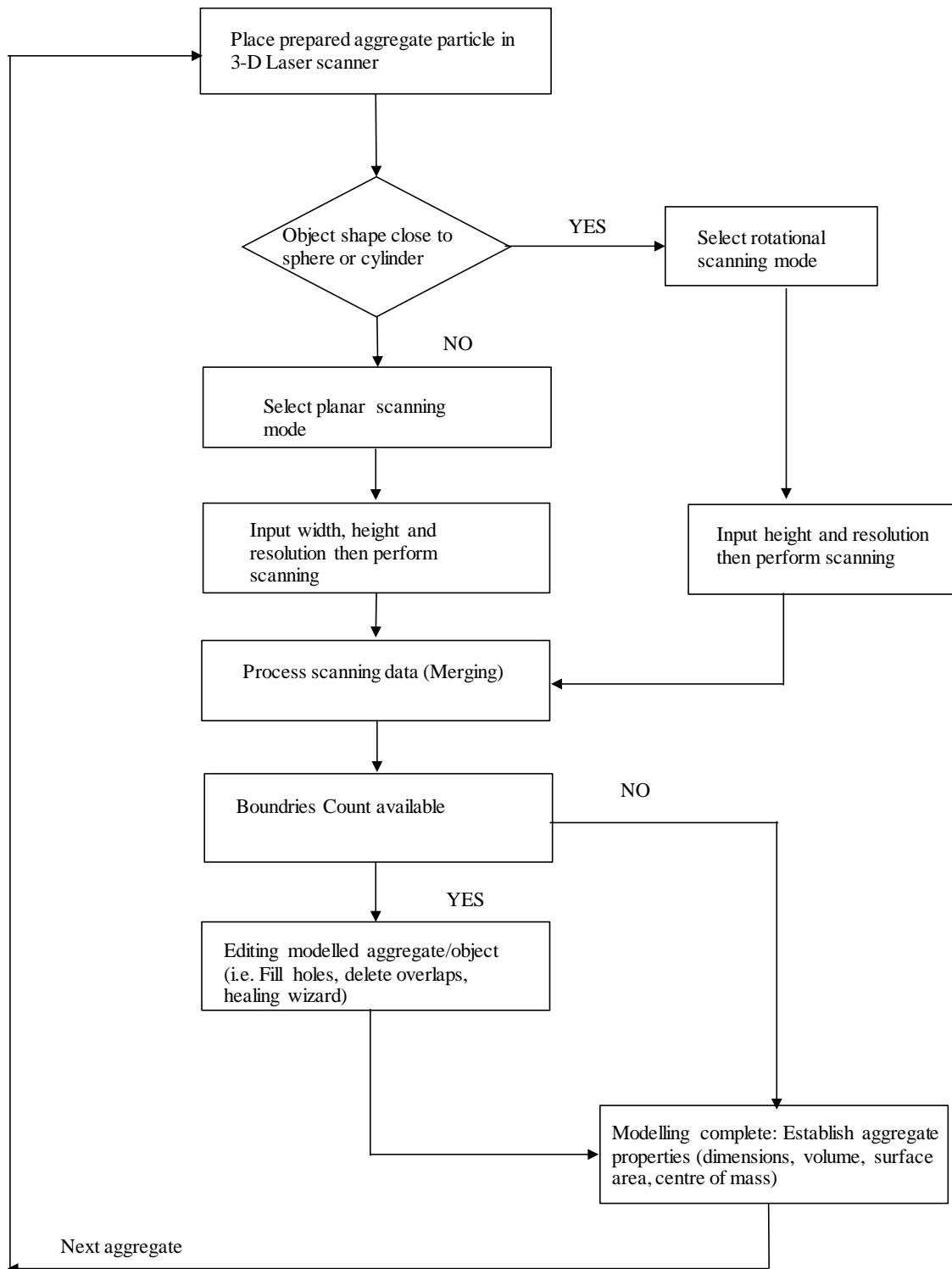


Figure 3.12: Grading analysis of river pebbles to be scanned

### **3.6 LASER APPROACH TO DETERMINE SHAPE PROPERTIES**

The quantification of ballast shape properties by using the laser-scanning technique was used to compare with triaxial test results. Two different approaches were used to analyse ballast scan data to determine their shape properties. The first approach makes use of the ballast dimensions (longest dimension, intermediate dimension and shortest dimension), surface area and volume, to compute indices describing ballast form.

The second approach was a developed surface area model of laser scan data to quantify the roundness of the ballast. Figure 3.13 shows schematic procedures used for the scanning of aggregate and ballast particles. All the ballast particles used for this study were scanned in accordance with the CSIR guideline for scanning of aggregates and ballast particles (Anochie-Boateng et al., 2014). Individual ballast particles were scanned in the laser device as a three-dimensional solid element (object) with six plane faces.



**Figure 3.13: Aggregate and ballast scanning process (Anochie-Boateng et al., 2014)**

### **3.6.1 Description of samples for scanning process**

To establish whether the scanning technique would lead to a reasonable prediction of ballast characteristics, a quartering sampling approach was used. Representative samples of particles from samples of fresh crushed dolerite ballast, recycled dolerite ballast and natural round pebble material that were used in the accompanying triaxial testing program were assembled.

Figure 3.14 shows a schematic of the process used for the scanning of the 3D-models. Particles were taken from a randomly selected sample as discussed before. These samples were then quartered, and re-quartered as needed, to obtain a number of particles that was suitable for the shape assessment study. The samples were dry-sieved using a 465 mm diameter sieve set of 63, 53, 37.5, 26.5, 19, 13.2 and 9.5 mm. The reduced samples were also washed and oven dried for scanning purposes.



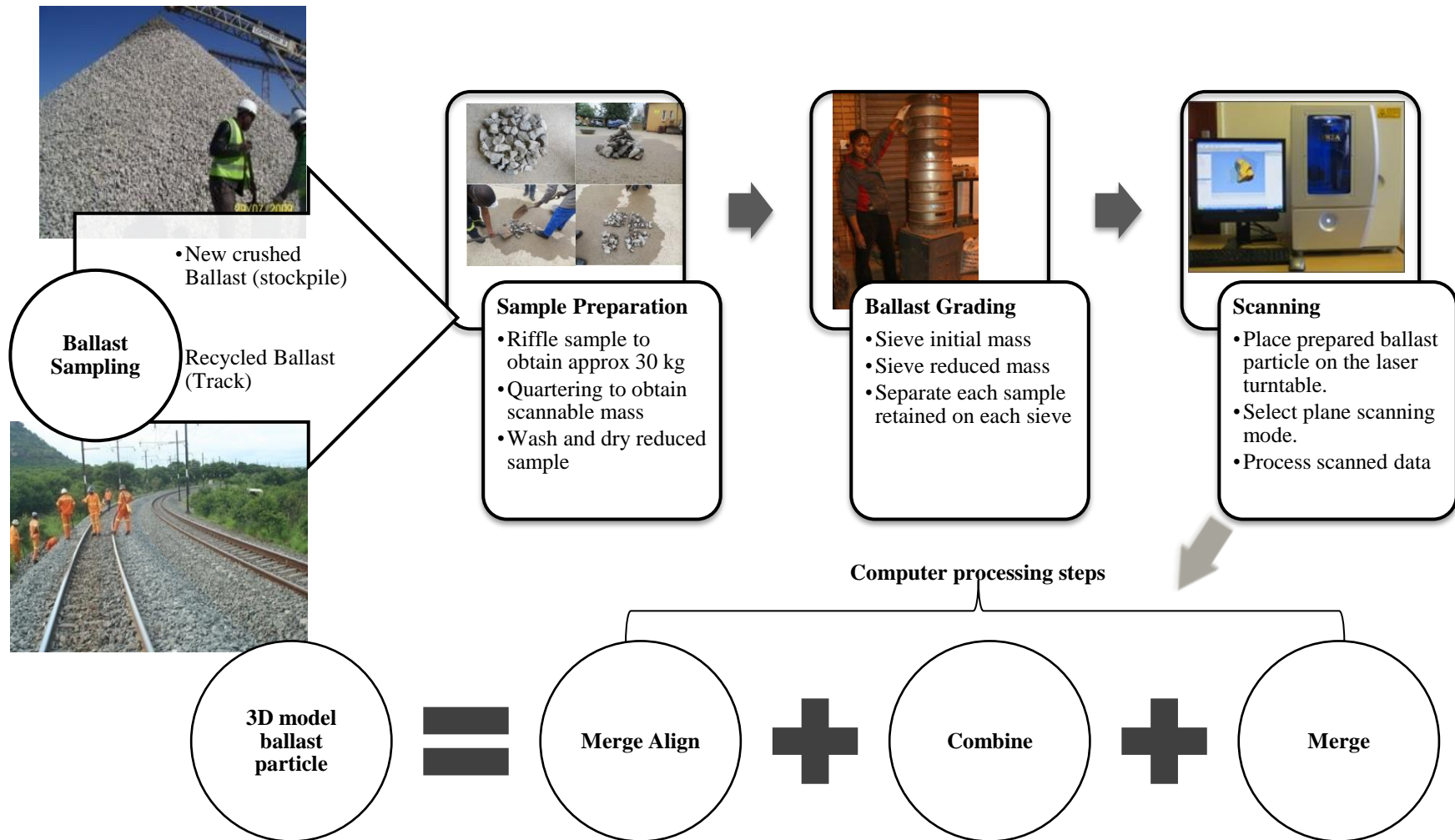


Figure 3.14: Process used for 3D laser-based measurements of ballast particles

### 3.6.2 Laser scanning mode

Based on the shape of ballast particles, the planer scanning mode option in the software was selected for scanning. Since a scan only captures one side of each particle, it must be turned over and rescanned to capture the hidden side. Using this mode of scanning, four planes (representing four side surfaces) of the particle were first scanned, followed by two planes (representing top and bottom surfaces) to complete the six faces for each particle. To register the two surfaces in a common reference frame, at least three point correspondences are required. Figure 3.15 shows the four side faces and two side faces of a typical ballast stone. Four surfaces are scanned and then followed by two surfaces to complete the scanning of a ballast particle. These are determined by gluing three ball bearings to each particle. The centre points of the balls are identified and used as reference points.

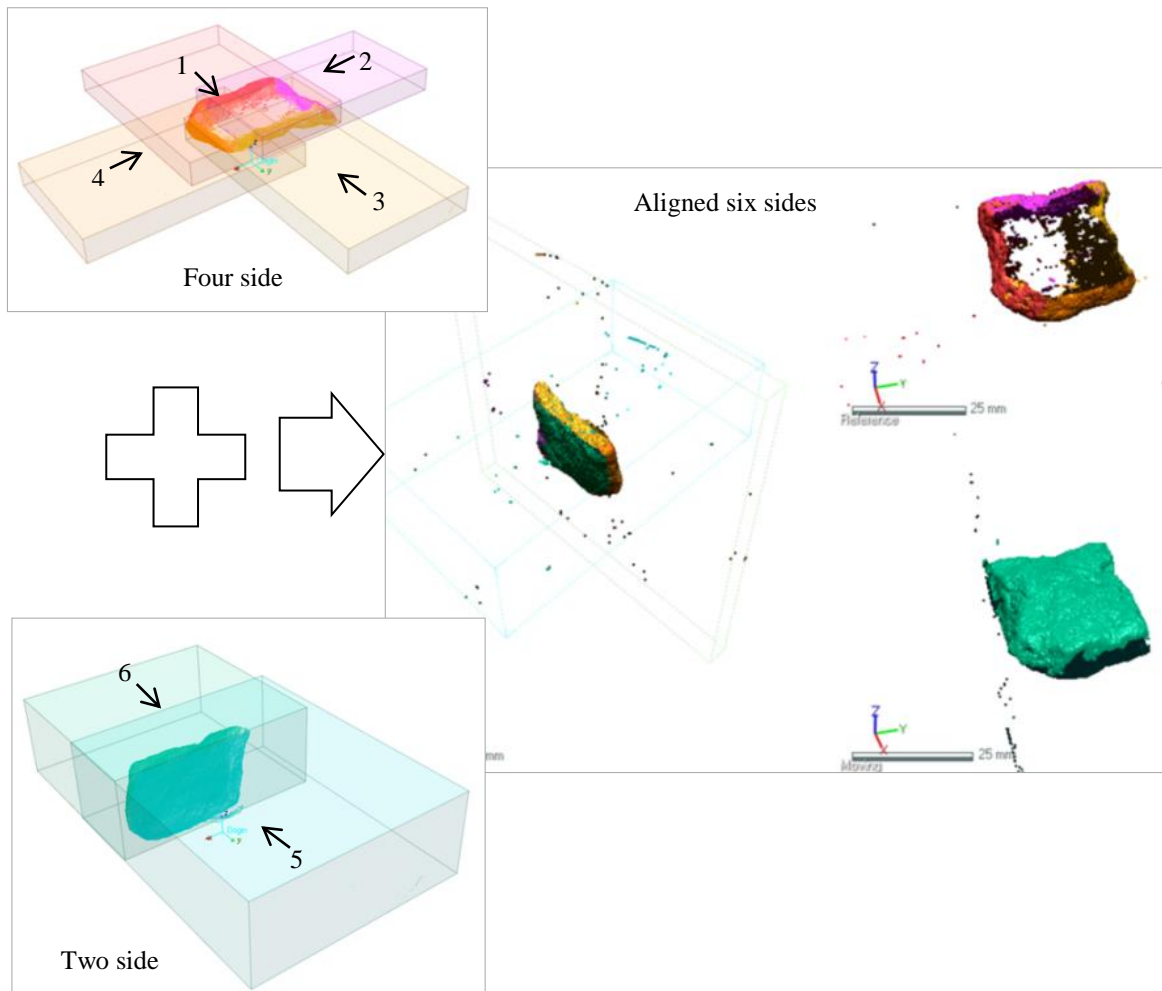


Figure 3.15: Typical planer scanning mode of the four- and two-side faces

After the scanning was completed, the laser scanning software was used to integrate and merge the scanned surfaces to obtain the dimensions of the ballast particle. The surface area and volume of the ballast particle were also obtained directly from the software by post-processing.

The time taken for the scanning process depended on the resolution and size of the aggregate particle. High resolution and large particle size implied a long scanning time. On the average, the total time for pre-processing and post-processing of a ballast particle was 50 minutes. In this study, the highest resolution of 0.1 mm (100  $\mu$ m) was used to scan all the particles. During the processing, different tools including the align, combine and merge tools available in the software were applied to firstly bring scanned surfaces together, and secondly to remove any irregularities, fill holes and merge the scanned surfaces to obtain a complete three dimensional model.

### **3.7 TRIAXIAL TESTING OF BALLAST SAMPLES**

These aspects are further investigated during the triaxial testing. In the field of geotechnical engineering, the repeated load triaxial testing method has proved to be most reliable (Knutson, 1976; Allen, 1973). It has therefore been selected as the test method in this study. A proper evaluation of the behaviour of railway ballast requires that the specimens be prepared to the particle size representative to the field conditions. Both fresh and recycled ballast were subjected to the same testing program to enable a valid comparison. Besides shear strength and deformation characteristics of railway ballast, the particle shape is an important aspect of ballast behaviour.

The testing program was selected to provide enough information to enable proper definition of ballast shape properties, shear strength and deformation characteristics of railway ballast. It is important to evaluate the effect of particle shape on the overall behaviour of the ballast layer.

#### **3.7.1 Experimental set-up and procedure**

A 210 mm diameter and 380 mm tall triaxial specimen yields a volume of 0.013 m<sup>3</sup>. The grading of the specimen was important, therefore sieving and mixing of each sample before triaxial testing was performed. Sieving was performed using a shaker with 465 mm diameter  $\times$  110 mm high sieve. The sieve system was capable of taking approximately 25 kg of material at a time. Detailed steps of triaxial testing are presented in Appendix A.

### **3.7.2 Triaxial shear strength testing of ballast samples**

Static triaxial tests were used for the determination of the shear strength properties  $c$  (apparent cohesion) and  $\phi$  (angle of internal friction) of the samples. The test was conducted in accordance with the TFR in-house triaxial testing protocol developed for granular material (Arangie, 1995). The specimen dimensions, i.e. a height ( $H$ ) of 385 mm and a diameter ( $D$ ) of 210 mm, corresponding to an acceptable  $H/D$  ratio of 1.85, were used for the triaxial tests.

During testing, three different confining pressures of 70 kPa, 90 kPa and 120 kPa were first applied to the samples before an axial monotonic load was gradually applied and increased to shear the samples (i.e. when peak shear stress was attained). Test conditions were selected based on a computer program called GEOTRACK and modelled to coal line conditions (Arangie, 1995). A strain rate of 1 mm/min was applied on the samples in a universal testing machine with loading capacity of 100 kN. The loading frame was operated using the 10% of full load capacity setting, yielding a full capacity of the system, allowing satisfactory control at the relatively small loads needed on the samples. After the sample was placed on the loading plate, the confining vacuum was maintained at all times to prevent sample collapse. All tests were performed under consolidated-drained conditions. As expected, increasing confining pressure resulted in increased deviator stress at failure. Figure 3.16 shows the ballast specimen before testing.



**Figure 3. 16: Ballast particles of samples and triaxial specimen**

### **3.7.3 Repeated load triaxial testing**

Repeated load triaxial testing was performed on the six samples. This test closely resembles the load environment and failure mechanisms of ballast in track. All tests were conducted at the CSIR pavement materials testing laboratory. The confined repeated axial load test was conducted by using an in-house permanent deformation testing method. During testing, a repeated haversine load of 0.1 seconds followed by a 0.9-second rest period is applied to the ballast sample. The repeated axial load test can be conducted up to 100,000 load-cycles.

Permanent axial deformation is recorded throughout and used to calculate plastic strains. In this study, a deviator stress of 101 at a confining pressure of kPa 90 kPa was used to determine the permanent deformation of the ballast samples studied. The cell pressures of 70, 90, 120 kPa are representative of field conditions on the Coal line selected for this study. These values were obtained by Arangie (1995) using a Geotrack software to represent axle loads of 26 ton (~94kPa) and 34 ton (~121kPa) to current and the predicted axle load due to increasing coal exporting market. The 30 ton (~107kPa) represents the locomotive axle load. The entire rail network ranges The 70 kPa was included to expand the range of cell pressures for the testing, and also cover the lower tonnage rail network that are less than 26 ton.

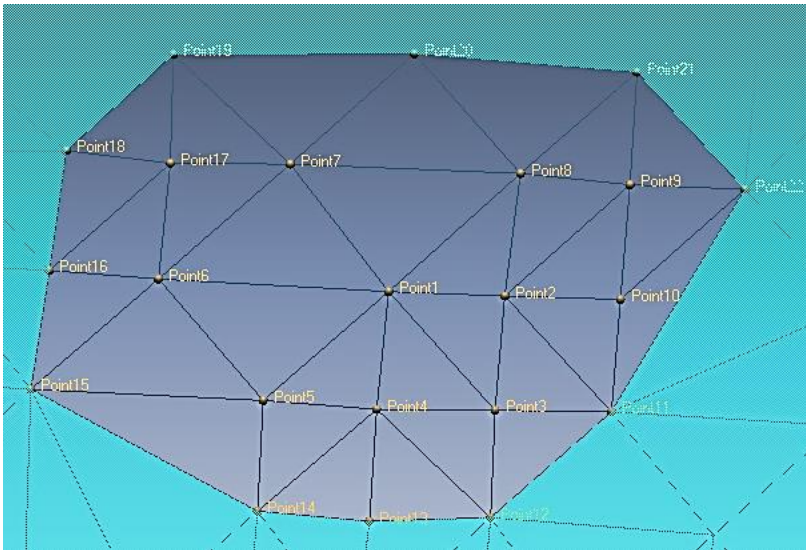
## 4 DATA ANALYSIS AND DISCUSSION OF LASER SCANNING RESULTS

### 4.1 INTRODUCTION

The objectives of this chapter are to conduct data analysis and discussions of the results obtained during the study. The analysis of the laser scan data is performed using physical dimensions. Numerical computations were used to verify the surface area and volume data obtained from scanning. The Mill Abrasion test method was used to verify the shape properties determined from the 3D-laser scanning technique for all ballast samples investigated. Detailed discussions on the test methods were provided in the literature survey conducted for this study in Chapter 2.

### 4.2 SURFACE AREA, VOLUME AND DIMENSIONS

The surface area, volume and principal dimensions of the ballast particles were obtained directly from the laser scanning software after post-processing of the scanned data. In numerical analysis, three dimensional shapes are commonly approximated by a polygonal mesh of irregular tetrahedral in the process of setting up equations for finite element analysis. Figure 4.1 was used to calculate the surface area for validation purposes.



**Figure 4.1: Wire frame with surface triangles obtained from the laser scanner**

Numerical computations were used to verify the surface area and volume data obtained from scanning. In three dimensions, the area of a triangle with vertices  $A = (x_A, y_A, z_A)$ ;  $B = (x_B, y_B, z_B)$ ;  $C = (x_C, y_C, z_C)$  is the Pythagorean sum of the areas of the respective projections on three principal planes ( $x = 0, y = 0$  and  $z = 0$ ), and computed as follows:

The equation of the plane from the  $xyz$  coordinates of three points is given by:

$$\begin{vmatrix} x_A & y_A & z_A & 1 \\ x_B & y_B & z_B & 1 \\ x_C & y_C & z_C & 1 \end{vmatrix} = 0. \quad (4.1)$$

Equation 4.1 is expanded to Equation 4.2 by the Pythagorean sum to obtain the area of the first triangle. The area is equal to the sum of all areas of the projected principal planes.

$$A_1 = \frac{1}{2} \sqrt{\left| \det \begin{pmatrix} x_A & y_A & 1 \\ x_B & y_B & 1 \\ x_C & y_C & 1 \end{pmatrix} \right|^2 + \left| \det \begin{pmatrix} y_A & z_A & 1 \\ y_B & z_B & 1 \\ y_C & z_C & 1 \end{pmatrix} \right|^2 + \left| \det \begin{pmatrix} z_A & x_A & 1 \\ z_B & x_B & 1 \\ z_C & x_C & 1 \end{pmatrix} \right|^2} \quad (4.2)$$

The following equations can be used to calculate the area of the first triangle:

1. The area of a planer triangle specified by its vertices  $v_i=(x_i, y_i)$  for  $i = A, B, C$  is given by:

$$Area_{xy} = \frac{1}{2} \left| \det \begin{pmatrix} x_A & y_A & 1 \\ x_B & y_B & 1 \\ x_C & y_C & 1 \end{pmatrix} \right| = \frac{1}{2} |x_A y_B - x_A y_C + x_B y_C - x_B y_A + x_C y_A - x_C y_B| \quad (4.3)$$

2. The area of a planer triangle specified by its vertices  $v_i=(y_i, z_i)$  for  $i = A, B, C$  is given by:

$$Area_{yz} = \frac{1}{2} \left| \det \begin{pmatrix} y_A & z_A & 1 \\ y_B & z_B & 1 \\ y_C & z_C & 1 \end{pmatrix} \right| = \frac{1}{2} |y_A z_B - y_A z_C + y_B z_C - y_B z_A + y_C z_A - y_C z_B| \quad (4.4)$$

3. The area of a planer triangle specified by its vertices  $v_i=(z_i, x_i)$  for  $i = A, B, C$  is given by:

$$Area_{zx} = \frac{1}{2} \left| \det \begin{pmatrix} z_A & x_A & 1 \\ z_B & x_B & 1 \\ z_C & x_C & 1 \end{pmatrix} \right| = \frac{1}{2} |z_A x_B - z_A x_C + z_B x_C - z_B x_A + z_C x_A - z_C x_B| \quad (4.5)$$



The determinant of the matrix in Equation 4.5 can be obtained by using the MDETERM function in Excel. For  $N$  triangles, the total surface area ( $SA_T$ ) of the scanned ballast particles can be computed by summing the surface areas of all poly-faces that make up the particle (Equation 4.6).

$$SA_{tot} = \sum_{N=1}^{\infty} A_N = A_1 + A_2 + A_3 + A_4 + \dots + A_N + \dots \quad (4.6)$$

The volume of a given tetrahedron with vertices  $\{A = (x_A, y_A, z_A), B = (x_B, y_B, z_B), C = (x_C, y_C, z_C)$  and  $D = (x_D, y_D, z_D)\}$  is  $(1/6) \cdot |\det(A-B, B-C, C-D)|$ . This can be rewritten using a dot product and cross product, yielding in Equation 4.7.

$$V_1 = \frac{|(A-D) \cdot ((B-D) \times (C-D))|}{6} \quad (4.7)$$

Similarly, the total volume ( $V_{tot}$ ) of  $N$  tetrahedral can be expressed as Equation 4.8.

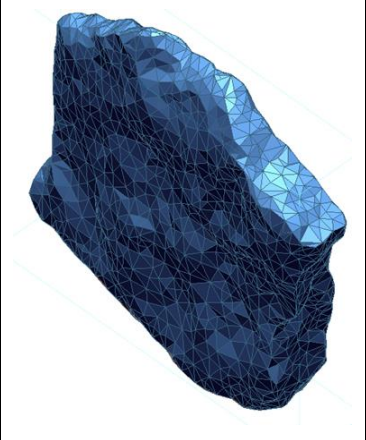
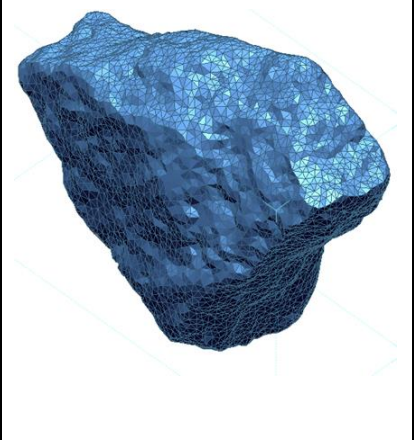
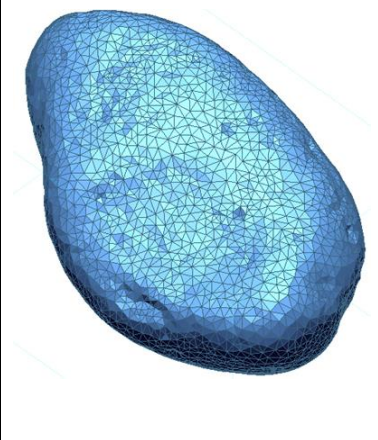
$$V_{tot} = \sum_{N=1}^{\infty} V_N = V_1 + V_2 + V_3 + V_4 + \dots + V_N + \dots \quad (4.8)$$

In the three dimensional laser scanner, the surface area of the ballast particles is determined using the triangulation method from the matrix of mesh points of triangular elements. The laser software divides the surface mesh of scanned aggregate/ballast particles into triangular sub-surfaces called poly-faces that make up the particle. The total surface area is computed based on the sum of the surface areas of all poly-faces, and the total volume is equal to the sum of the sub-volume of all voxelised (tetrahedral) meshes. Table 4.1 presents the laser scanning results of five (5) poly-faces (triangles), which were used as an example for verification by the Pythagorean computation theory. The results confirm that the surface areas obtained directly from the three dimensional laser software agree with the theoretical Pythagorean computations (Equation 4.2).

**Table 4.1: Area verification of the laser results**

Reference		Coordinates			Poly-face Area		
Poly-face No.	Point No.	Position X	Position Y	Position Z	Pythagorean Area (mm <sup>2</sup> )	Laser Area (mm <sup>2</sup> )	% Difference in Area
1	Point1	-12.038	0.890	8.925	0.00524	0.00520	0.76
	Point2	-12.141	0.884	8.924			
	Point3	-12.130	0.783	8.924			
2	Point1	-12.038	0.890	8.925	0.00549	0.00550	-0.18
	Point3	-12.130	0.783	8.924			
	Point4	-12.025	0.786	8.926			
3	Point1	-12.038	0.890	8.925	0.00531	0.00530	0.19
	Point4	-12.025	0.786	8.926			
	Point5	-11.925	0.796	8.933			
4	Point1	-12.038	0.890	8.925	0.01051	0.01050	0.10
	Point5	-11.925	0.796	8.933			
	Point6	-11.834	0.906	8.929			
5	Point10	-12.243	0.878	8.929	0.00517	0.00520	-0.58
	Point22	-12.356	0.973	8.934			
	Point11	-12.233	0.779	8.936			

Figure 4.2 illustrates three types of scanned particles showing details of the poly-faces with the resulting surface area and volume parameters. The software integrated in the 3D-laser scanning device was programmed to directly compute both the surface area and volume of processed ballast particles. The surface area of an individual particle was calculated from the surface mesh of the scanned particle.

		
Freshly crushed ballast No. of poly-faces = 3 466 Surface area = 1 885 mm <sup>2</sup> Volume = 3 180 mm <sup>3</sup>	Recycled ballast No. of poly-faces = 10 080 Surface area = 2 367 mm <sup>2</sup> Volume = 7 035 mm <sup>3</sup>	River pebble No. of poly-faces = 7 764 Surface area = 3 489 mm <sup>2</sup> Volume = 15 959 mm <sup>3</sup>

**Figure 4.2: Mesh of poly-faces to determine surface area and volume**

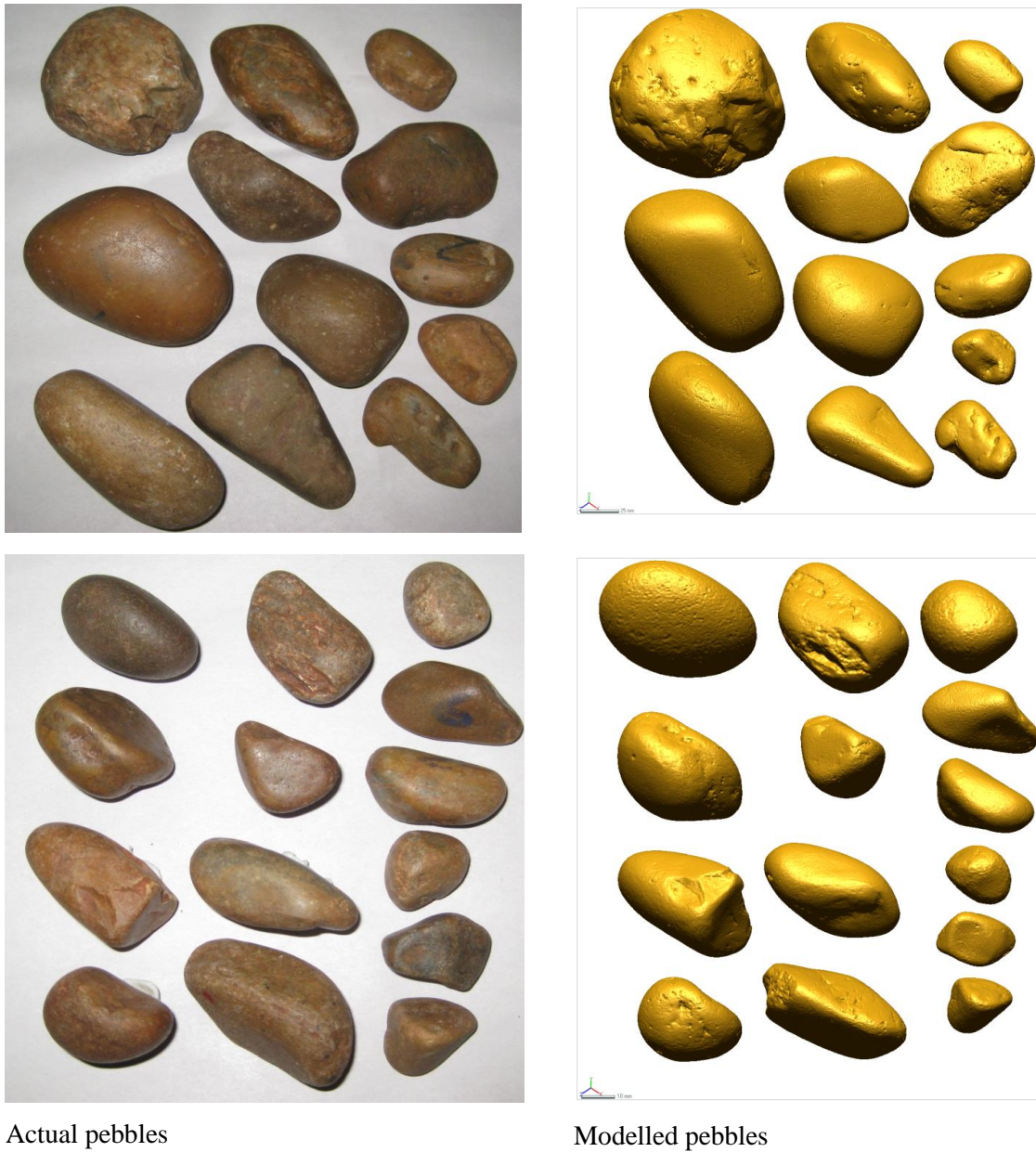
### 4.3 PROCESSING LASER SCANNED DATA

Once the processing of the scan results was completed, dimensions, volume and surface area of the aggregates were obtained directly from the post-processing data. The “box principle” uses the principle of fitting a three dimensional bounding box around the aggregate and recording the size of the box in terms of longest, intermediate and shortest dimensions. Laser scanned models were taken in order to assess particle shape of the materials used in this study. These models were then analysed for shape parameters using MATLAB. The developed MATLAB code is presented in Appendix B. This computer code was designed to assess both the length ratio and ellipsoid surface area to compute the roundness index of 356 scanned ballast particles.

### 4.4 RESULTS OF SCANNED BALLAST PARTICLES

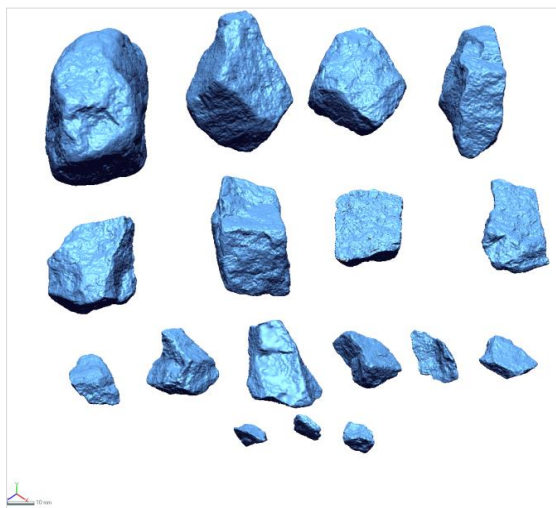
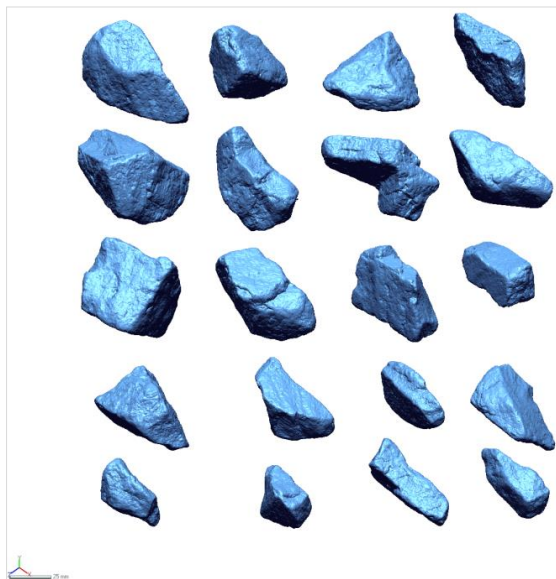
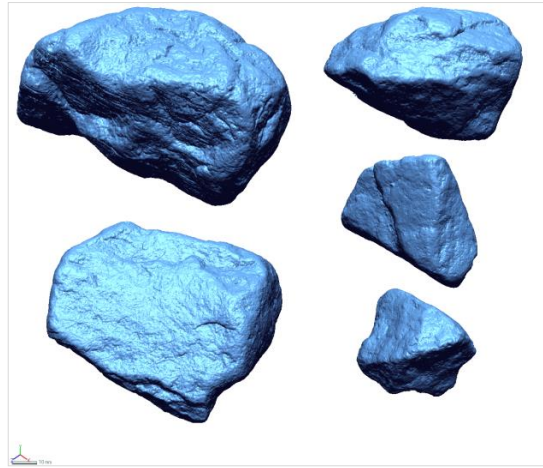
The results presented in this section were used to determine the ballast shape properties. Figure 4.3 shows photos of actual pebbles and models of the scanned pebbles. Similar samples for recycled dolerite ballast are shown in Figure 4.4. For each material type, the figures show representative particles ranging from sub-angular to well-rounded particles. From the figures, it is clear that the laser scanning technique is capable of producing models that are similar to the actual material. It is therefore reliable to analyse the ballast stones to obtain an indication of the shape properties of the actual ballast.

Laser scanned models were used to assess the particle shape of the materials used in this study. The computer code was designed to assess both the length ratio and ellipsoid surface area to compute roundness index of 356 scanned ballast particles.



**Figure 4.3: Actual images versus modelled river pebbles**





Actual recycled ballast

Modelled recycled ballast

**Figure 4. 4: Actual ballast particles versus modelled recycled ballast**

Various algorithms exist that may be implemented using 2D digital images or three dimensional data clouds. After processing the data of the scanned ballast particles, the dimensions (width, height and depth), surface area, volume and coordinates of the centre were obtained directly by using Rapidform software. Other information that can be obtained after processing the scanned ballast particles is surface points (vertices) in terms of x, y, z Cartesian coordinates and triangular surfaces known as poly-faces.

The x, y, z Cartesian coordinates can be exported to other data processing software such as Microsoft Excel<sup>TM</sup> and MATLAB<sup>TM</sup> for further analysis. In this study, the MATLAB<sup>TM</sup> program was used. The length to width ratio, sphericity, shape factor and roundness was calculated for each particle and then averaged for each sieve retained (see Appendix C for results).

#### **4.5 DETERMINATION OF BALLAST SHAPE INDICES BY USING PHYSICAL PROPERTIES**

The literature survey conducted during the study revealed that aggregate parameters measured using the laser scanning technique could be used to compute indices to describe ballast shape properties. The approach makes use of the ballast dimensions (longest dimension, intermediate dimension and shortest dimension), surface area and volume to compute indices describing ballast shape. Ballast physical parameters measured by the laser-scanning device used in this study included the dimensions (width, height and depth), surface area and volume. It is important to emphasise that the evaluation of the capability and accuracy of the laser scanning device to measure these parameters has been accomplished in previous studies, and was not repeated in this study (Anochie-Boateng et al., 2010; Anochie-Boateng et al., 2011a).

The following steps were followed to compute flatness and elongation ratios from the laser scanning technique. Dimensions (longest, intermediate, and shortest) of the individual ballast particles were obtained directly from the three dimensional bounding box.

- The flatness ratio ( $F$ ) of an individual ballast particle was computed by dividing the shortest dimension by the intermediate dimension (Equation 2.1).
- The elongation ratio ( $E$ ) of an individual ballast particle was computed by dividing the longest dimension in the plane perpendicular to the intermediate dimension (Equation 2.2).
- Furthermore, Zingg (1935) proposed a classification for shapes and established a quadrant that separates the terms with a value of 0.67 to each other.
- Shape factor ( $SF$ ) is computed by the ration of flatness and elongation in Equation 2.3.
- Working sphericity using elongation and flatness is shown in Equation 2.4.

- Finally, computed data were plotted on the  $x$ -axis (flatness ratio) versus  $y$ -axis (elongation ratio), called the shape classification chart.

Three different shape indices computed by using the aggregate's physical properties were selected for further investigation in this study. These selected form indices are:

- sphericity computed using orthogonal dimensions of an aggregate particle as defined by Equation 2.5;
- sphericity computed using the surface area and volume as defined by Equation 2.6; and
- roundness computed using surface area of the particle and surface area of the ellipsoid by Equation 4.11.

#### **4.5.1 Flat and elongated particles**

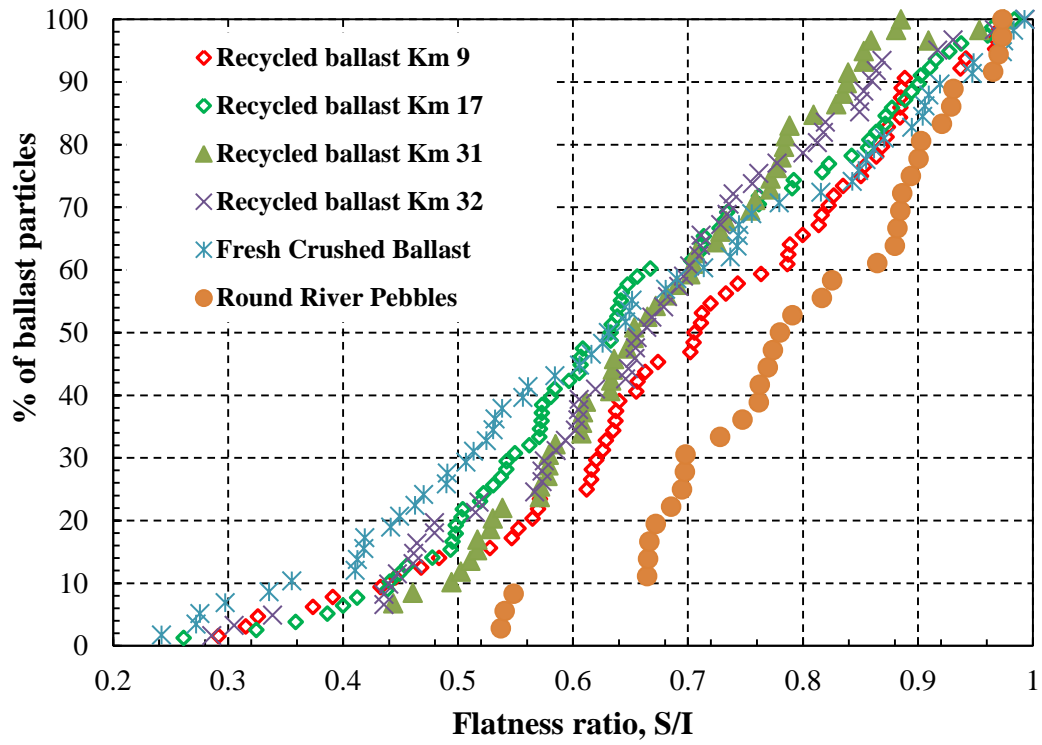
The longest, intermediate and shortest dimensions of the ballast particles were used to compute flat and elongation ratio using Equation 2.1 and Equation 2.2. This means the river pebble sample was expected to have higher flatness ratio values, greater than 0.66, as compared to other types of ballast studied.

For equal dimensional ballast particles, the flat and elongation ratio approaches a minimum value of 1. The flat and elongation ratio statistical parameters for the six types of ballast studied were presented in Table 4.2 and 4.3. As expected, the average flatness ratio of river pebble was the highest, followed by recycled Km 9. The averages of the flatness ratio values of crushed and recycled ballast are similar. The average flatness ratio of freshly crushed ballast was the lowest, followed by recycled Km 17, Km 31 and Km 32. The average elongation ratio of freshly crushed ballast was the lowest, followed by round river pebble, recycled Km 9, Km 17, Km 32 and Km 31.

The distribution of the flatness ratio and elongation ratio of all studied ballast and river pebble were plotted in Figure 4.5 and Figure 4.6, respectively. The results indicate that most particles were slightly elongated and moderately flat.

**Table 4. 2: Statistical parameters for flatness ratio**

Sample description	Average	Standard deviation
Round River Pebble	0.79	0.13
Recycled Ballast Km 9	0.70	0.18
Recycled Ballast Km 32	0.66	0.16
Recycled Ballast Km 31	0.69	0.13
Recycled Ballast Km 17	0.66	0.17
Freshly Crushed Ballast	0.65	0.21

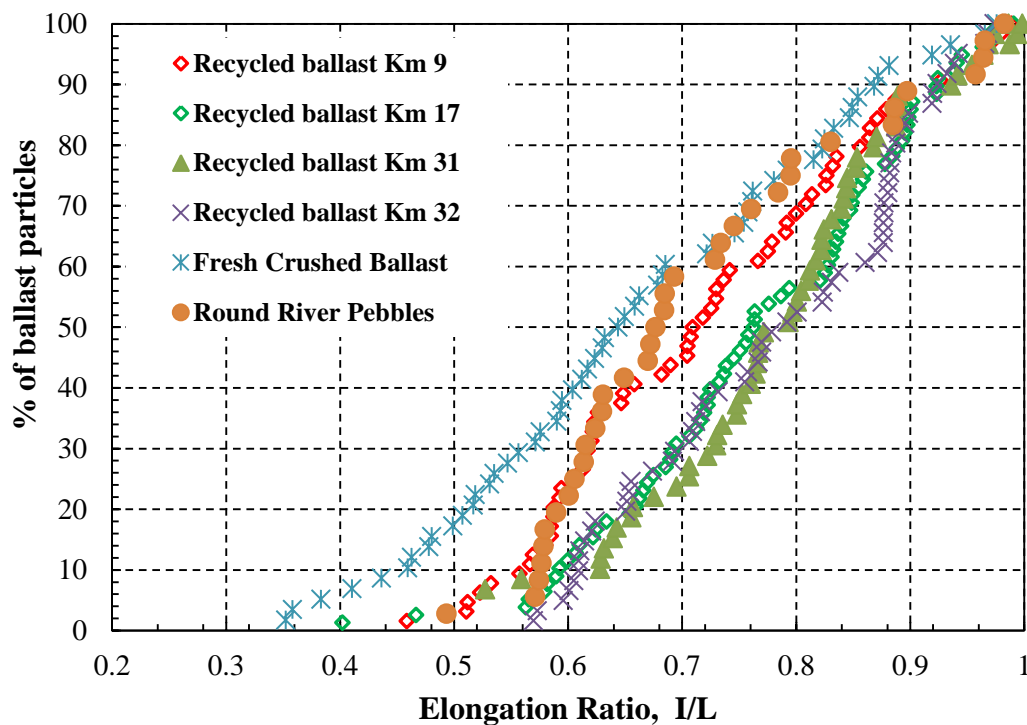


**Figure 4. 5: Distributions of flatness ratio**



**Table 4. 3: Statistical parameters for elongation ratio**

Sample description	Average	Standard deviation
Recycled Ballast Km 31	0.80	0.11
Recycled Ballast Km 32	0.78	0.12
Recycled Ballast Km 17	0.77	0.13
Recycled Ballast Km 9	0.72	0.14
Round River pebble	0.71	0.13
Freshly Crushed Ballast	0.66	0.16

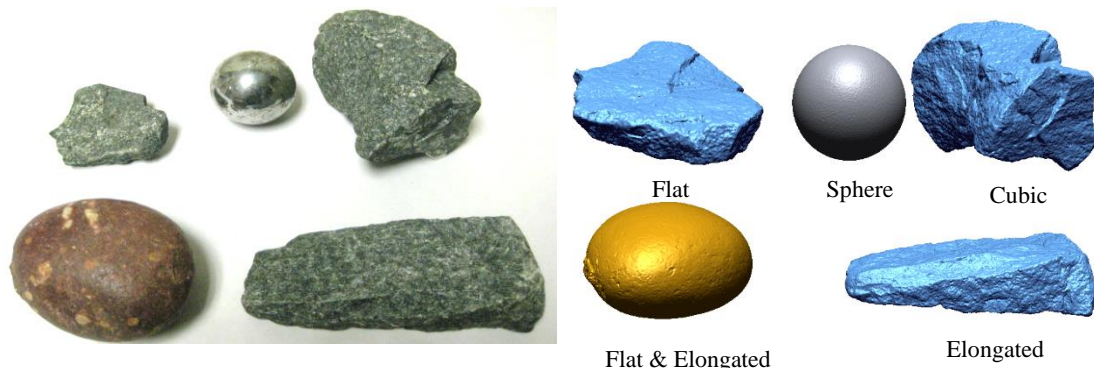


**Figure 4. 6: Distributions of elongation ratio**

#### 4.5.2 Development of shape chart classification

Scanned particles were visually classified as cubic, flaky, elongated, and flat & elongated, which are shown in Figure 4.7. In this picture, although each particle can be viewed, they are not very easy to evaluate. One can more easily evaluate the shapes of particles by plotting the ratios of dimensions, elongation ratio and flatness ratio. These do not present the size of the particles but purely the shape relationship of each individual particle. The number of particles

that fall into the four different quadrants namely cubic, flaky, elongated and flat & elongated differs with sample type.



**Figure 4. 7: Actual vs scanned particles for shape classification**

Figure 4.8 presents a plot of the flatness ratio against the flatness of the 356 scanned particles. The chart included shape factor ( $SF$ ) and working sphericity. The typical exponential growth of flatness regarding the elongation of the particles, the power function was found to be most suitable curve fits to model the relationship between the two ratios. As a result, four regression power models were developed to represent the working sphericity ( $\psi$ ) of the ballast shapes (i.e. ranging between  $\psi = 0.5$  and  $\psi = 1$ ). When all the 365 scanned particles from the four shapes were combined, grouped samples have the highest cubic particles of 144 in number, followed by the flaky particles of 127, elongated 71 and flat & elongated 44.

For ease of comparison, the results were plotted in Figure 4.8. The shaded polygon represents recommended ballast shape with limit of  $SF$  ranging between 0.67 and 1.5 and sphericity between 0.8 and 0.9. Therefore, the recommended average ballast shape should be scattered within the shaded polygon. Any particle scattered below the shaded polygon were not recommended because they are too flaky, and flat & elongated. While any particle scattered above the shaded polygon were too spherical.

As expected, the average sample shape of freshly crushed ballast and recycled ballast Km 9 were lying on top of  $SF$  value of 1.0 meaning these samples were dominated with cubic particles. The average of the sample shape of other recycled samples was similar with  $SF$  less than one (1), meaning the samples are flakier in shape. The average of pebble shapes was

scattered above the shaded polygon with high spherical particles. Table 4.4 presents a summary of the average parameters obtained for different ballast materials. As expected, the sample with the highest spherical particles was round river pebbles, followed by recycled ballast Km 31, recycled ballast Km 9, recycled ballast Km 17, recycled ballast Km 32 and freshly crushed ballast.

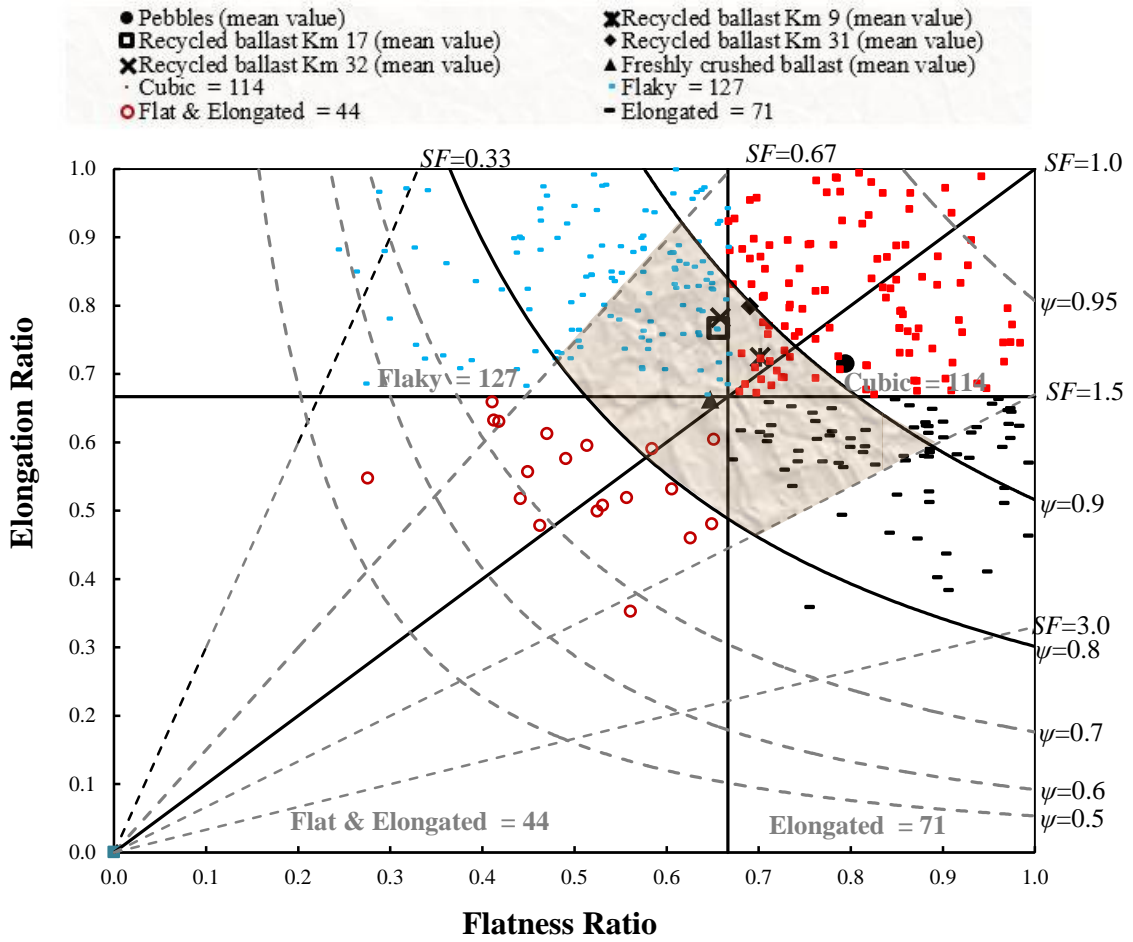


Figure 4.8: A shape chart classification for all scanned particles

**Table 4.4: Average parameters for shape chart**

Shape parameters	Equation references	Recycled ballast Km 9	Recycled ballast Km 17	Recycled ballast Km 31	Recycled ballast Km 32	Freshly Crushed ballast	River pebbles
Flatness Ratio (F)	Eqn. (2.1)	0.79	0.66	0.69	0.66	0.65	0.79
Elongation Ratio (E)	Eqn. (2.2)	0.72	0.77	0.80	0.78	0.66	0.71
Shape Factor (SF)	Eqn. (2.3)	0.97	0.89	0.87	0.87	0.98	1.11
Sphericity ( $\psi$ )	Eqn (2.4)	0.87	0.87	0.89	0.87	0.82	0.91

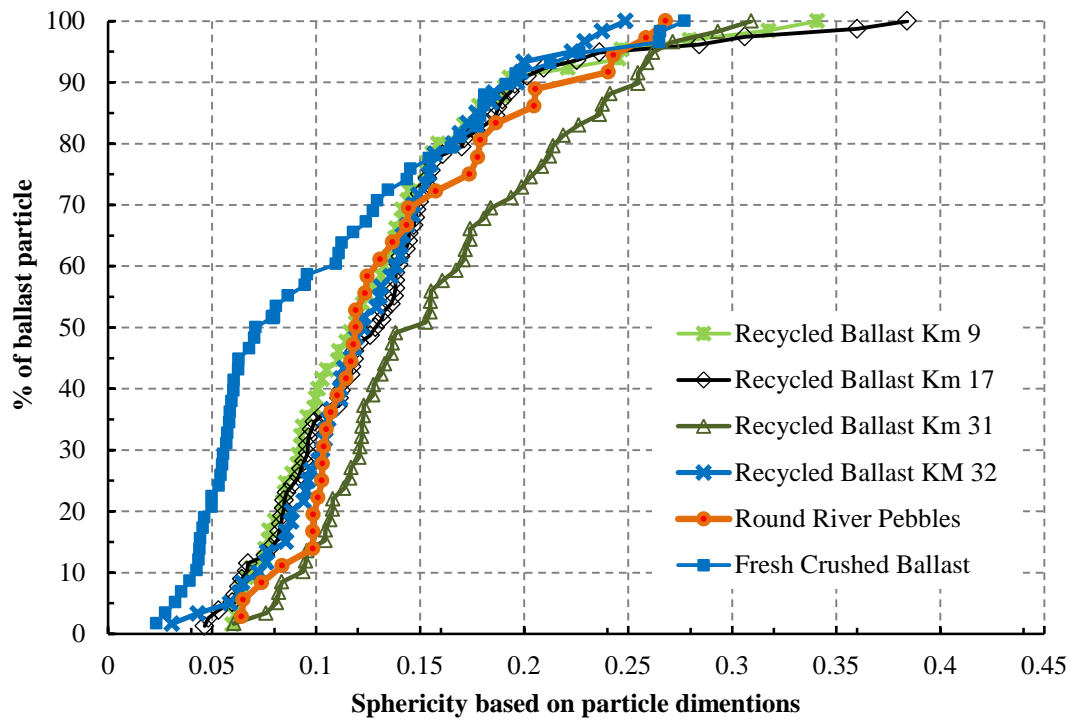
### 4.5.3 Sphericity computed using principal dimensions

The principal dimensions of individual ballast particles were used to compute another sphericity parameter that was defined using Equation 2.5. For equal dimensional particles such as round stone, the computed sphericity approaches a maximum value of one (1). Consequently, the river pebble sample was expected to have higher sphericity values. Table 4.5 shows sphericity statistical parameters for the studied samples. Unexpectedly, the average sphericity of recycled ballast Km 31 was the highest, followed by that of river pebble, recycled ballast Km 32, recycled ballast Km 17, recycled ballast Km 9 and freshly crushed.

Figure 4.9 shows plots of the distributions of sphericity computed using principal dimensions. For sphericity values smaller than 0.4, the distributions of sphericity was for all scanned samples. Freshly crushed ballast' has lower sphericity values followed by recycled ballast Km 31; recycled ballast Km 9, river pebble, and recycled ballast Km 17. The results of 14 spherical objects are also plotted in Figure 4.9. All the spherical objects have a sphericity value of one (1), which was expected.

**Table 4. 5: Statistical parameters for sphericity computed using principal dimensions**

Sample description	Average	Standard deviation
Freshly crushed ballast	0.10	0.07
Recycled ballast Km 9	0.13	0.06
Recycled ballast Km 17	0.14	0.06
Recycled ballast Km 32	0.16	0.06
Recycled ballast Km 31	0.13	0.05
Pebble	0.14	0.05



**Figure 4.9: Distributions of sphericity computed using principal dimensions**

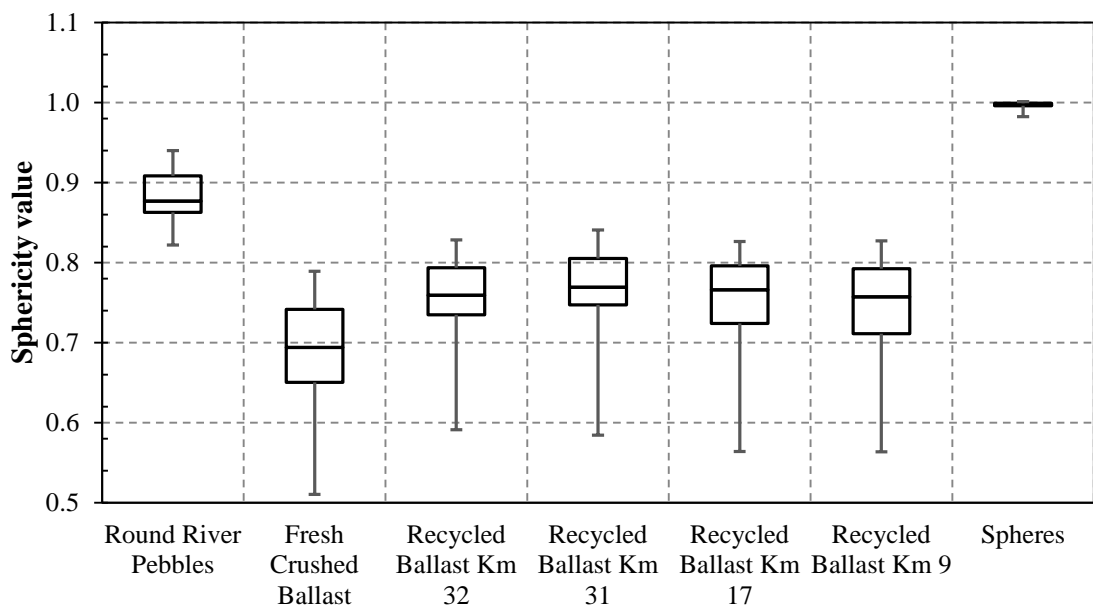
#### 4.5.4 Sphericity computed using surface area and volume

The surface area and volume of individual stone particles were used to compute a sphericity parameter that describes the form of ballast, using Equation 2.6. The sphericity computed by using Equation 2.6 approaches a maximum value of one (1) for round shaped aggregate particles. Therefore, for the types of aggregates used in this study, the river pebble sample was expected to yield higher sphericity values. Figure 4.10 presents a box and whisker plot of the sphericity for materials studied. As expected, the average sphericity of freshly crushed ballast was the lowest, followed by that of recycled ballast Km 31.

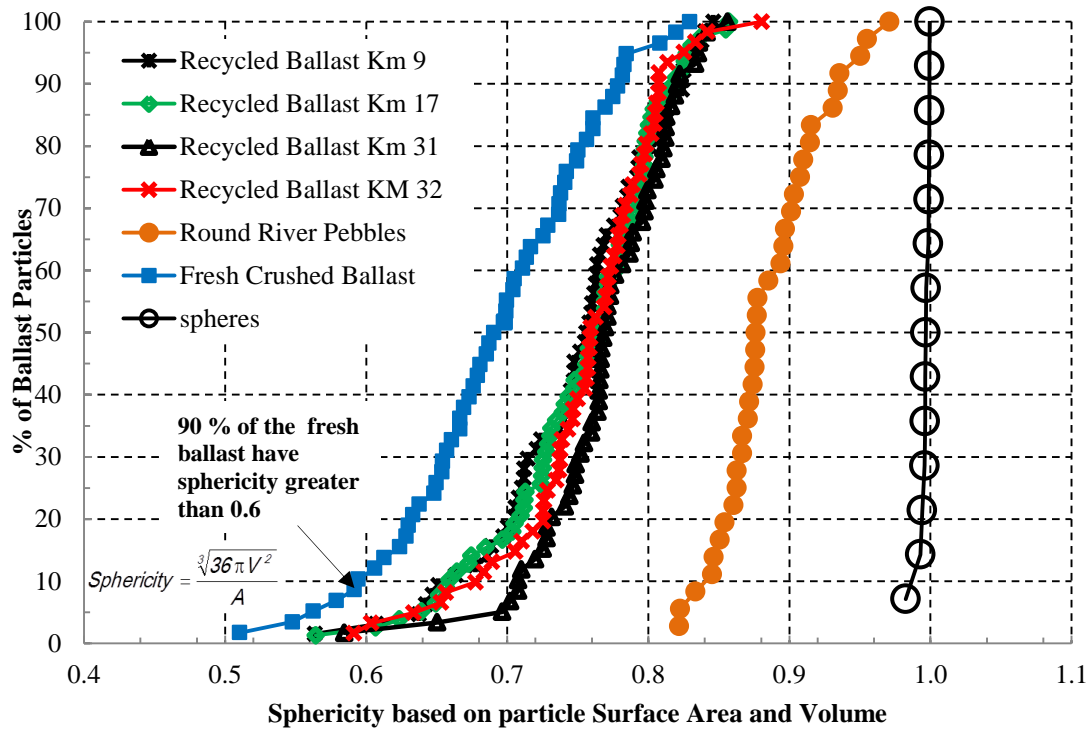
Figure 4.11 shows the distributions of the sphericity computed using surface area and volume. The sphericity distributions are plotted for 365 particles scanned. Included in the figure are sphericity values of 14 spherical objects. The spherical objects had different sizes and were manufactured using different types of material (steel, ceramic, rubber and plastic). As expected, all the spherical objects plotted closer to a value of one (1). River pebbles has higher sphericity values with a distribution ranging from 0.82 to 0.97, followed by freshly crushed ballast with a distribution ranging from 0.51 to 0.83. Overall, the sphericity distributions of recycled ballast

did not differ significantly. Recycled ballast Km 32 has relatively higher sphericity values, followed by recycled ballast Km 31, recycled ballast Km 9 and recycled ballast Km 17.

It was also observed that the distribution of sphericity values for different samples may differ significantly; despite their average values being closer to each other. Therefore, a single property such as flakiness index cannot accurately differentiate shape properties of the ballast samples. The use of laser scanning technique provided more information required to distinguish the shapes of different samples used in this study.



**Figure 4.10: Box and whisker plot for the sphericity values of six samples scanned**



**Figure 4.11: Distributions of sphericity computed using surface area and volume**

The distribution of sphericity indices computed by using surface area and volume, distinguished the form properties of the studied material clearer than other form indices. This may be because the indices were computed using volume and surface area, which represent the overall 3D-shape of ballast. On the other hand, the sphericity computed by using principal dimensions was based on bounding box, which does not necessarily represent the overall three dimensional form of aggregates.

#### 4.6 DEVELOPMENT OF BALLAST SURFACE AREA MODEL

Figure 4.12 presents a plot of the surface area against the volume of the 356 scanned particles. Various mathematical functions, i.e. linear, nonlinear, logarithmic, and hyperbolic were investigated using non-linear regression analyses. Considering the typical exponential growth of surface area regarding the volume of the particles, the power or logarithmic functions were found to be most suitable curve fits to model the relationship between the two properties. As a result, four regression power models were developed to represent the surface area of the ballast shapes (i.e. elongated, flat and elongated, flaky and cubic).

The power model, expressed by  $SA=aV^b$ , was used to evaluate the relationship between the surface area and volume of the scanned ballast materials. Statistical regression analyses were performed using this power model to obtain the model parameters  $a$  and  $b$ . Table 4.6 presents a summary of the model parameters obtained for individual shape parameters for the ballast materials. The power model adequately predicts the volume from individual shapes as observed from the generally high correlation coefficients ( $R^2$  values) also given in Table 4.6.

When the entire test data from the four shapes were combined, a unified surface area model was successfully developed to account for the volume of ballast particles (see Equation 4.9). It can be seen that the laser device provided accurate surface area model for the ballast materials. This is observed from the high coefficient of correlation value ( $R^2 > 0.98$ ) of the surface area model. Theoretical surface area of a cube is given in Equation 4.9, which is closer to the cubic ballast used in this study (Table 4.6). Based on the surface area, regression model developed, if the volume of the particle is known, the surface area of a particle model can be determined using Equation 4.10.

$$SA_c=6\times V^{\frac{2}{3}} \quad (4.9)$$

$$SA_{pm}=8.1974 \times V^{0.6417} \quad (4.10a)$$

$$SA_{pm}\approx 8\times V^{\frac{2}{3}} \quad (4.10b)$$

Where,

$SA_c$  = surface area of cube

$V$ = volume of the ballast

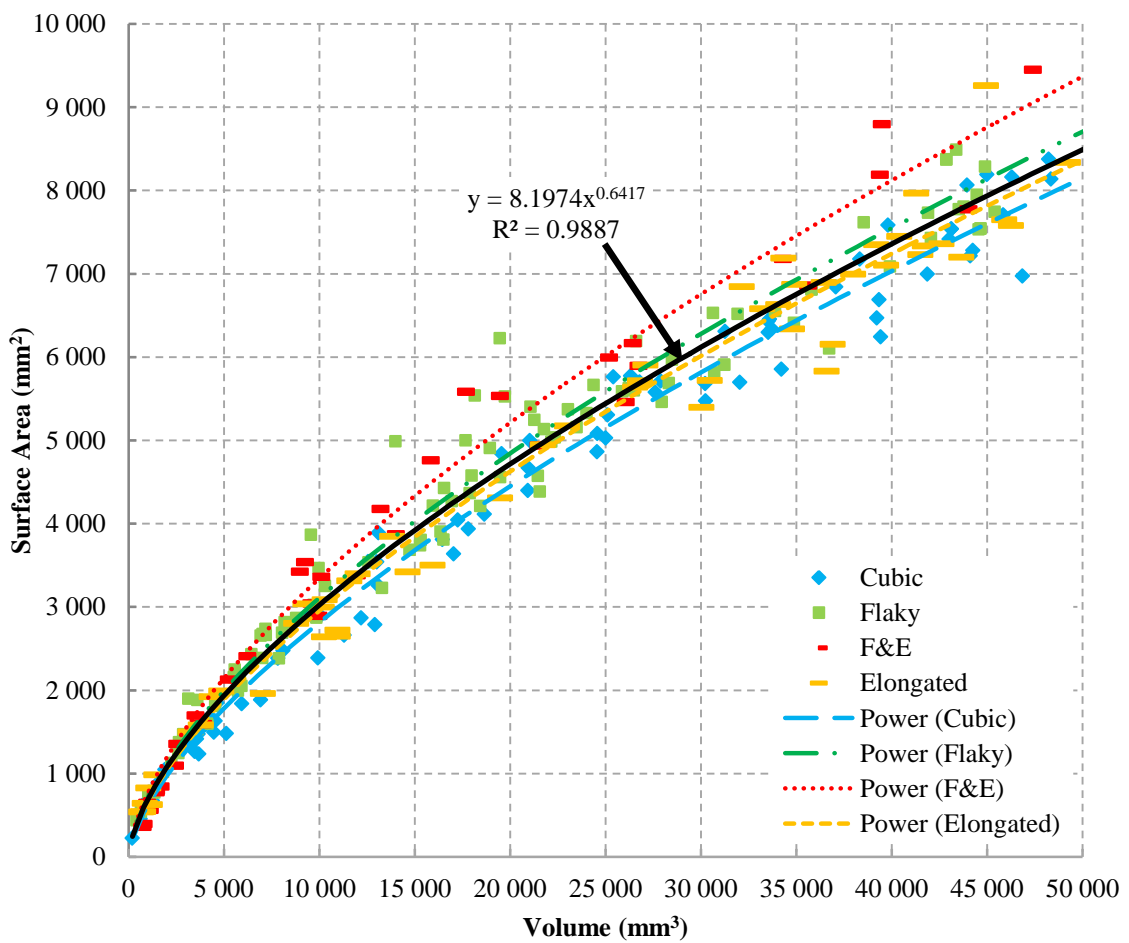
$SA_{pm}$  = surface area of a particle model

Crushers are likely to produce particles that are elongated, flat and elongated, flaky and cubic in shape. The result shows that flat and elongated particles have higher surface area than cubic particles. This could be a reason why cubic particles are most preferred over flaky and elongated particles, which tend to break under load. Li et al. (2015) preferred cubical particles for stable and strong ballast, whereas elongated, flaky, rounded, or smooth shapes should be avoided.



**Table 4. 6: Ballast surface area model parameter**

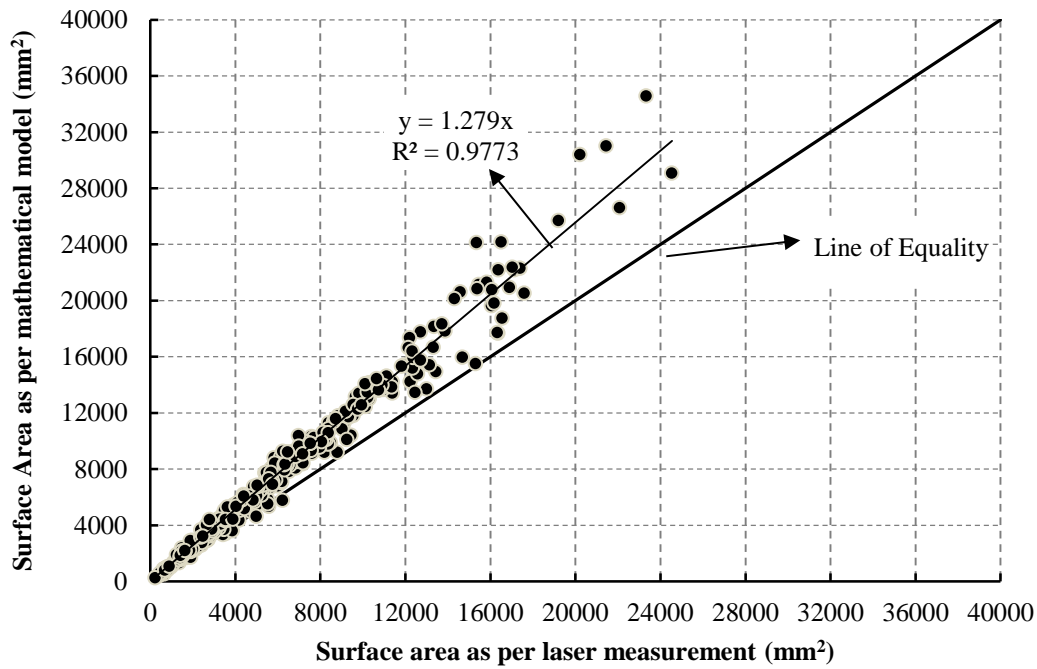
Shape category	Multiplicative factor $a$	Power $b$	$R^2$
Elongated	7.6818	0.6463	0.9921
F&E	9.1828	0.6403	0.9943
Flaky	8.5499	0.6401	0.9881
Cubic	6.4164	0.6605	0.9942



**Figure 4. 12: Plots of surface area versus volume results of scanned particles**

Figure 4.13 shows a comparison between the surface areas computed from the three dimensional laser and the developed surface area model. The data points were above the line of equality, indicating higher surface area from mathematical model as compared to laser

measurement. It can be seen that there is an excellent correlation ( $R^2 = 0.98$ ) between the scanned surface area and the modelled surface area of the samples. Therefore, it is expected that the model would be suitable for all crushed aggregates, ballast and natural gravel. The model can be used to estimate the particle surface area when the mass of and the specific gravity are known and used to compute the volume.



**Figure 4.13: Relationship between mathematical model and scanned surface area**

#### **4.7 ROUNDNESS COMPUTED USING SURFACE AREAS**

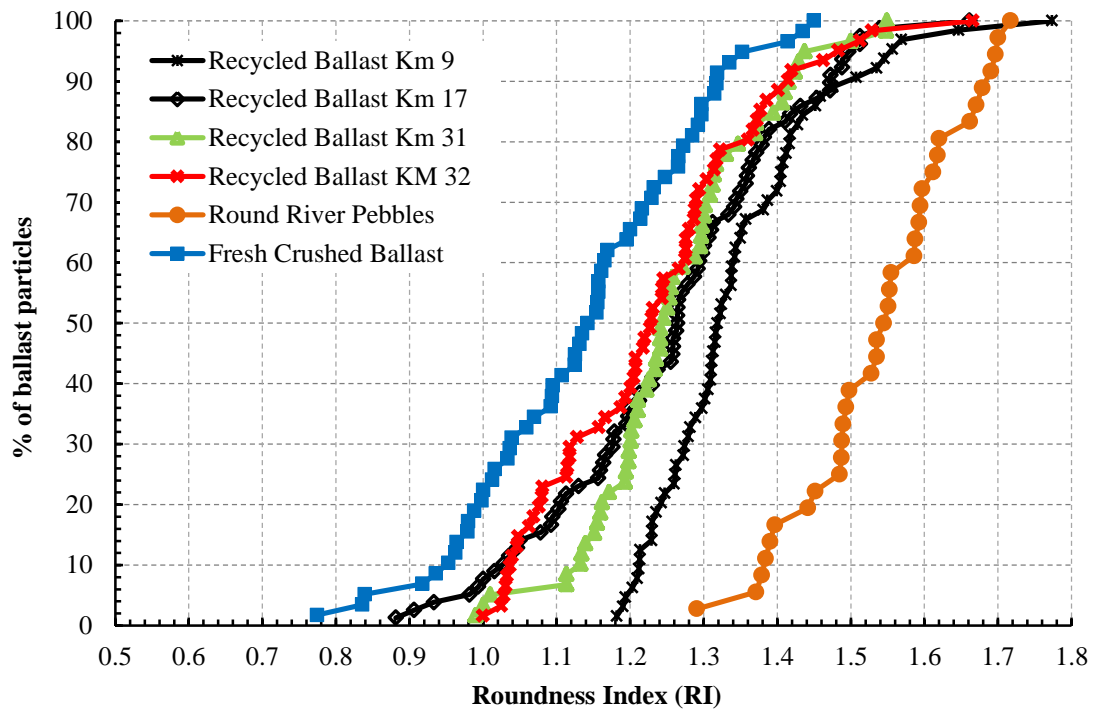
The definition and meaning of the roundness presented in the literature by Hayakawa, and Oguchi (2005) is probably wrong as it was verified to be angularity. The double integral presented in Equation 2.12 (Surface area of an ellipsoid) cannot be evaluated by elementary means. In this study, numerical integration was therefore done by using MATLAB software to derive and calculate surface area from the measured values of the bounding box of the scanned particles.

Equation 4.11 (inverse of Equation 2.13) was used to determine the roundness of the six ballast materials. This equation allows the use of three dimensional measurements of the particle as the actual shape of ballast is in three-dimensions.

$$\text{Roundness} = \frac{SA_{pm}}{SA_e} \quad (4.11)$$

Where,  $SA_e$  is the surface area of an ellipsoid and  $SA_{pm}$  is the surface area of the particle model.

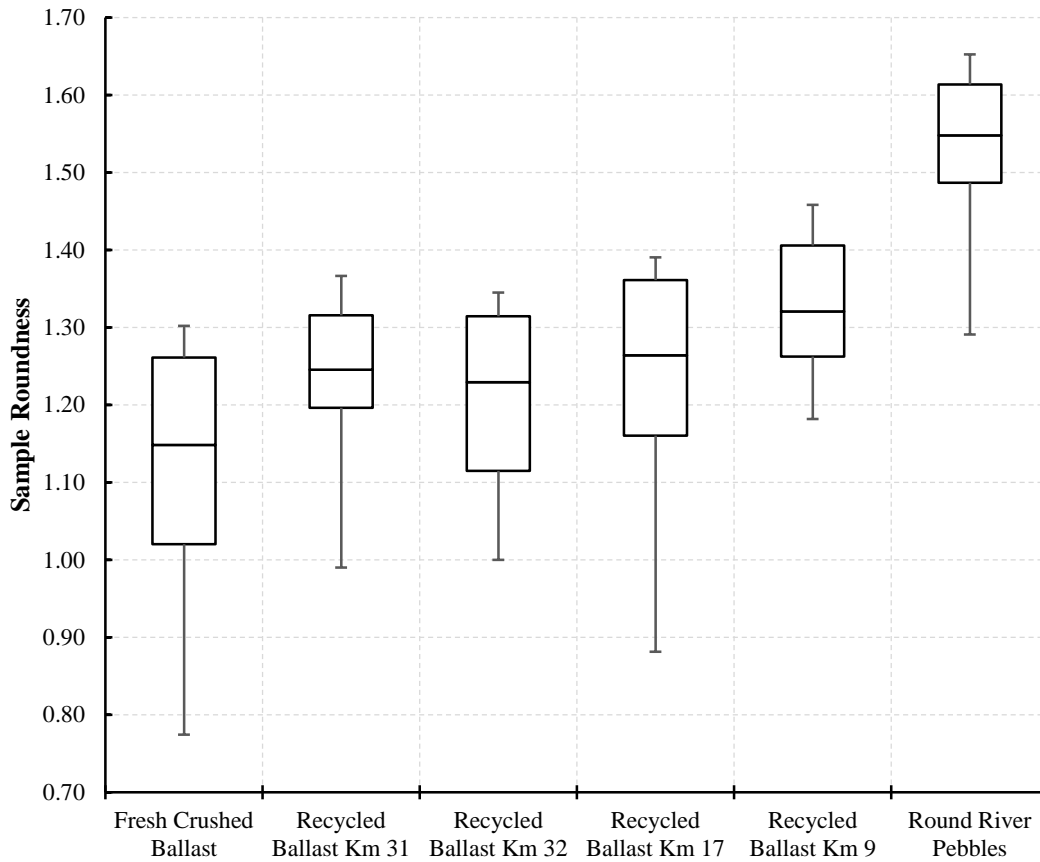
Figure 4.14 shows roundness results of the six samples where 90% of fresh crushed ballast particles have roundness values greater than 0.95 whereas the 90% of pebbles have roundness values between 1.3 and 1.7. It can be seen that recycled ballast samples are degrading from the shape (i.e. angular) of fresh crushed ballast toward the shape of a pebble (i.e. rounded). In comparison, the recycled ballast from Km 9 is more rounded than the recycled samples from Km 17, Km 31 and km 32.



**Figure 4.14: Distributions of ballast roundness index**

Roundness results were statistically analysed for five railway ballast and river pebbles. The Median of all the values is used as a representative of the entire data set because of the presence of outliers. Figure 4.15 presents a box and whisker plot of variation between scanned particles from each sample. As expected the highest roundness was found in river pebbles sample,

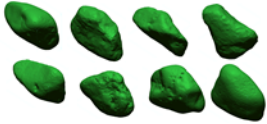
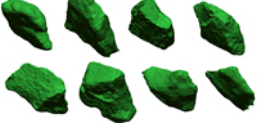
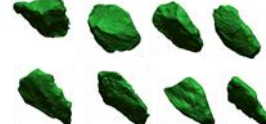

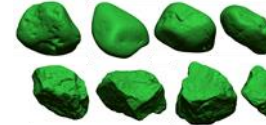


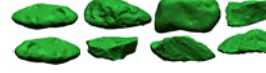
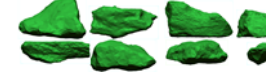



followed by the recycled ballast Km 9, recycled ballast Km 17, recycled ballast Km 32, recycled ballast Km 31 and the freshly crushed ballast.



**Figure 4. 15: Box and whisker plot for the roundness values of six samples scanned**

Table 4.7 provides comparable charts for visual assessment of the roundness of six, selected particles of the materials investigated. The results show that the roundness value between 1.7 and 1.4 is typical for excessive rounded particles, while particles with low roundness have values between 1.3 and 0.8. Consequently, the river pebble sample is expected to have higher roundness values than fresh crushed ballast.

**Table 4.7: Ballast roundness chart developed using three dimensional laser models**

Particle Shape	Degree of roundness		
	High (1.7-1.4)	Medium (1.4-1.3)	Low (1.3-0.8)
Flaky			
Cubic			
Elongated			
Flat & Elongated			

#### 4.8 CORRELATION OF FLAKINESS INDEX WITH BALLAST SHAPE INDICES

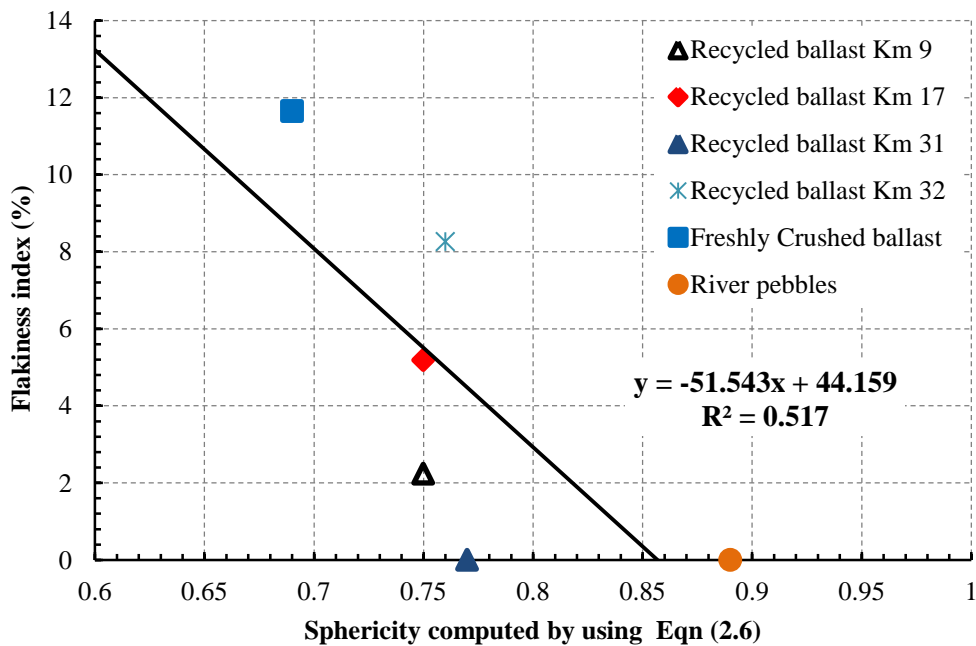
The correlation of ballast shape indices with the results of flakiness index (laser-based) is the current standard test methods (TMH1 B3) used to characterise shape properties of ballast in South African railway. Detailed discussion on the test method was provided in the literature survey conducted for this study (Chapter 2, Section 2.4.8). Using the laser-based method for determination of flakiness index, a single flakiness index parameter is normally computed to represent the whole sample. The flakiness index results for each of the six samples studied are in Table 4.8. The flakiness index values were correlated with the average ballast shape indices presented in Tables 4.4, Table 4.5 and Table 4.8.

**Table 4. 8: Ballast shape indices computed from laser results**

Indices	Recycled ballast Km 9	Recycled ballast Km 17	Recycled ballast Km 31	Recycled ballast Km 32	Freshly Crushed ballast	River pebbles
<b>Flakiness Index (%)</b>	2.24	5.19	0.00	8.26	11.65	0.00
<b>Sphericity Average</b>	0.75	0.75	0.77	0.76	0.69	0.89
<b>Roundness Average</b>	1.25	1.23	1.25	1.20	1.11	1.54

Figures 4.16 to 5.19 show correlations of flakiness index with the sphericity computed by using the aggregate surface area and volume, the sphericity computed by using the aggregate orthogonal dimensions, flat and elongation ratio and roundness index respectively. Overall, good correlations were observed. The trends of the plots agree with theory underlying each of the shape indices. The highest correlation was found between the sphericity computed using the principal dimensions ( $R^2$  equal 0.546), followed by the flakiness index with the roundness computed using the surface area ( $R^2$  equal 0.533), the sphericity computed by using ballast surface area and volume ( $R^2$  equal 0.517) and the flatness ratio ( $R^2$  equal 0.501).

On the other hand, the distribution plots of various laser-based shape indices presented earlier, clearly indicated that the river pebble sample differs in terms of its shape properties. Therefore, the suitability of the ballast laser scanning technique to determine ballast shape properties is strengthened.



**Figure 4.16: Flakiness index versus sphericity computed by using volume and surface area**

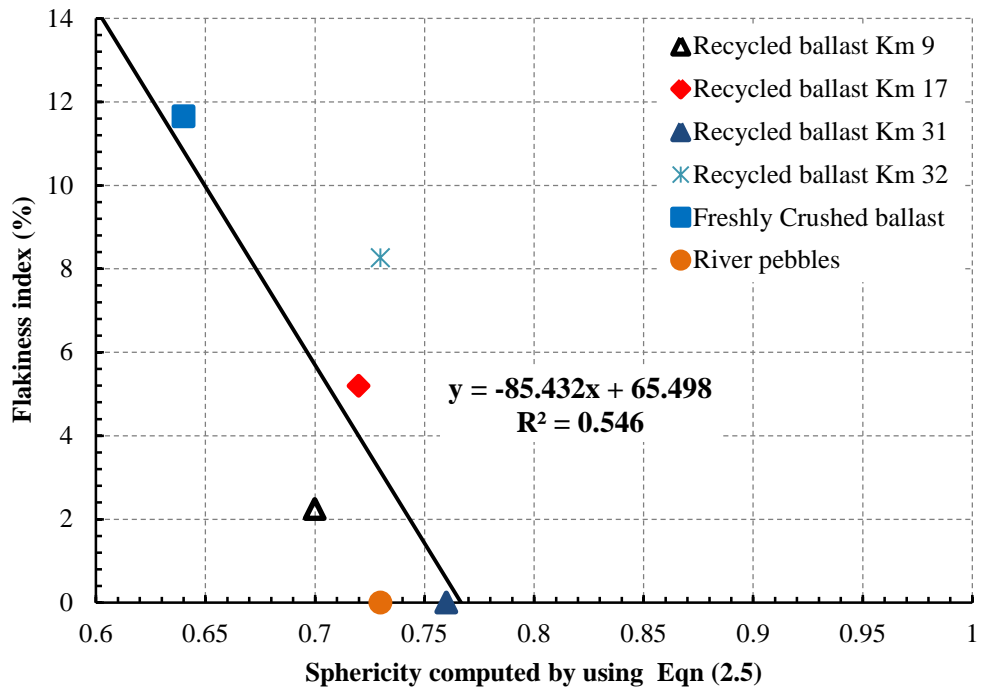


Figure 4.17: Flakiness index versus sphericity computed by using principal dimensions

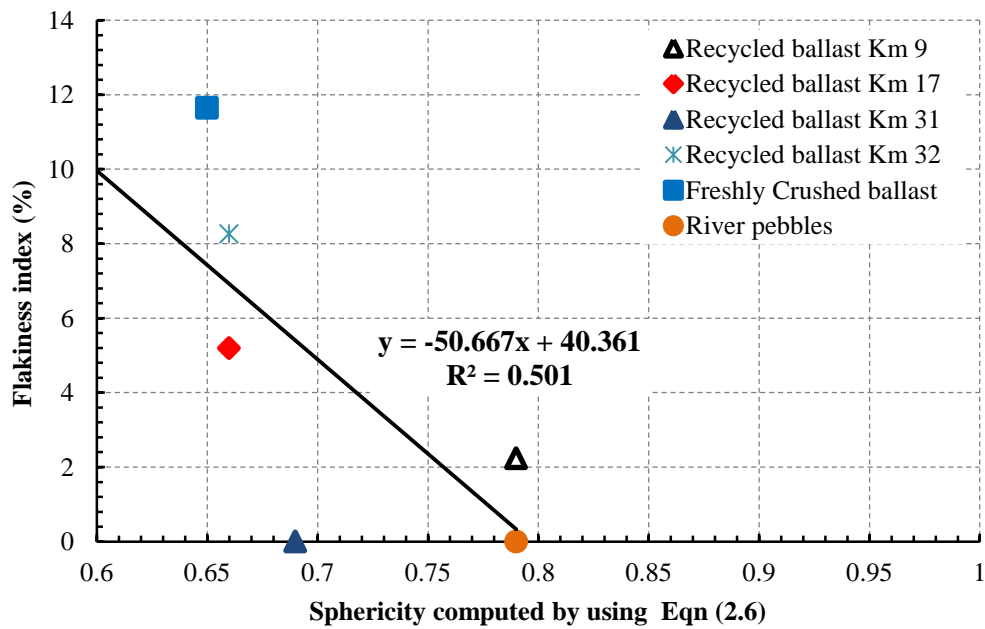
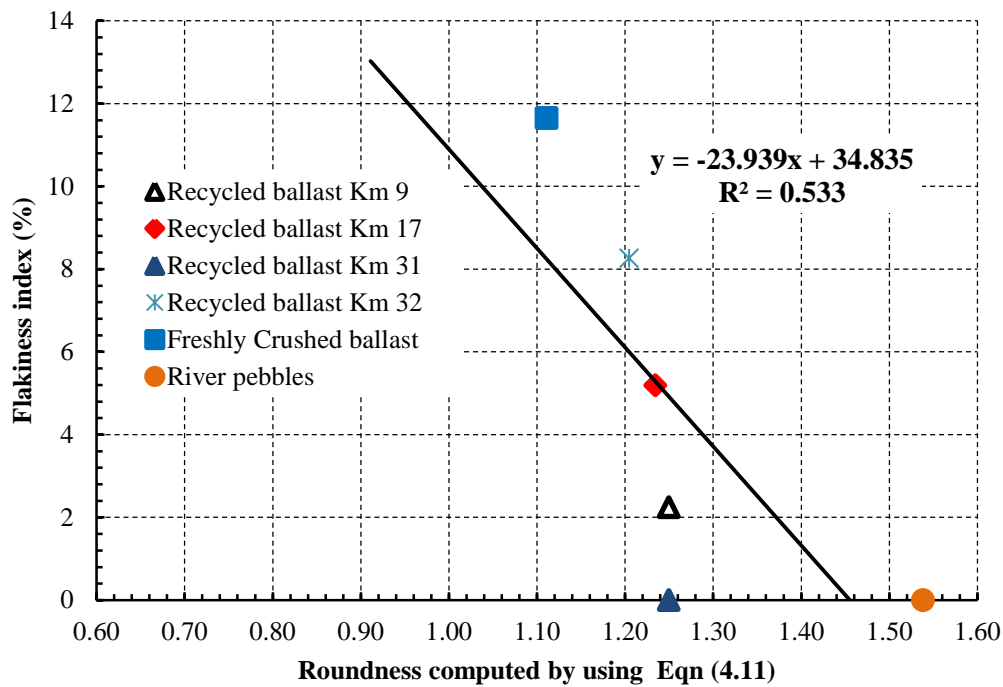


Figure 4. 18: Flakiness index versus flatness ratio



**Figure 4. 19: Flakiness index versus roundness index**

#### **4.9 BALLAST SHAPE STATISTICAL ANALYSIS**

The laser scanner results were statistically analysed for five railway ballast samples, river pebbles and perfect spheres. Analysis of variance (ANOVA) was performed on six group samples to determine the variability in the scanned analysis results. The single factor analysis of variance allows comparison of several groups of observations, all of which are independent and possibly with a different mean for each group. A test of great importance is whether all means are equal.

The ANOVA test is used to compare sphericity, roundness, flatness and elongation of all the scanned particles, pebbles, recycled and crushed ballast to confirm which recycled ballast fall in the same range. The ANOVA test can only inform whether there is a difference between the groups. The ANOVA test was done in Microsoft Excel. Data was checked for normal distribution in Figure 3.6 before performing the ANOVA tests.



#### 4.9.1 ANOVA test results of ballast shape

The objective of this analysis was to determine the variability in different ballast samples based on the laser analysis results. The ANOVA was done on the six types of samples.

Hypotheses:

$H_0$  = there is no difference in the mean value of all groups

$H_1$  = there is a difference in the mean value of all groups

$\alpha = 0.05$ , so if p value  $< \alpha$ , reject  $H_0$ .

Testing at  $\alpha = 0.05$  significance level,  $H_0$  is rejected.

The results of the ANOVA analysis are presented in Table 4.9 to 4.12. Overall, testing at  $\alpha = 0.05$  significance level,  $H_0$  is rejected and the sphericity, roundness, flatness and elongation of all the scanned particles is different. By examining the results of ANOVA analysis, the highest  $F_{\text{value}}$  used to reject the  $H_0$  was found in sphericity results, followed by the roundness, elongation and flatness. A high  $P_{\text{value}}$  means values for the data were different and hence reject the hypothesis because there was a significance difference amongst the data. In this ANOVA results,  $F_{\text{critical}}$  values were smaller than the  $F_{\text{values}}$ , therefore, the null hypothesis was rejected, as the mean values of the data are not similar.

**Table 4.9: Analysis of variance for sphericity**

Source	Sum of Squares	Degrees of freedom	Mean Squares	$F_{\text{value}}$	$P_{\text{value}}$	$F_{\text{critical}}$	Significant at 5%
Between Groups	0.855	5	0.171	52.637	1.21E-40	2.240	Yes
Within Groups	1.137	350	0.003				
Total	1.992	355					

**Table 4.10: Analysis of variance ANOVA for Roundness**

Source	Sum of Squares	Degrees of freedom	Mean Squares	$F_{\text{value}}$	$P_{\text{value}}$	$F_{\text{critical}}$	Significant at 5%
Between Groups	4.090	5	0.818	42.605	3.076E-34	2.240	Yes
Within Groups	6.720	350	0.019				
Total	10.811	355					

**Table 4.11: Analysis of variance for Flatness**

Source	Sum of Squares	Degrees of freedom	Mean Squares	F <sub>value</sub>	P <sub>value</sub>	F <sub>critical</sub>	Significant at 5%
Between Groups	0.635	5	0.127	4.457	0.001	2.240	Yes
Within Groups	9.967	350	0.028				
Total	10.601	355					

**Table 4.12: Analysis of variance for Elongation**

Source	Sum of Squares	Degrees of freedom	Mean Squares	F <sub>value</sub>	P <sub>value</sub>	F <sub>critical</sub>	Significant at 5%
Between Groups	0.750	5	0.150	8.492	1.33E-07	2.240	Yes
Within Groups	6.184	350	0.018				
Total	6.934	355					

#### 4.10 VALIDATION OF LASER-BASED SHAPE PROPERTIES

To validate the capability of the laser-based shape indices, the Mill Abrasion (MA) test was used to simulate ballast resistance to abrasion/polishing. The ballast polishing was measured based on the following procedure:

- Two ballast samples were obtained from a selected source; each sample was 1.5 kg and retained the 19 mm and 26.5 mm sieve.
- The ballast particles were scanned with a three dimensional laser to obtain initial ballast shape properties before MA tests.
- The machine consists of a watertight steel cylinder, closed at one end, with internal dimensions of 250 mm diameter and 264 mm length.
- The MA drum in Figure 4.20 was filled with 3 kg of ballast materials.
- The drum was charged with 2 l of water and rotated through 10 000 revolutions and subjected to a target polishing time of 167 minutes.
- During rotation, the test material was lifted by a ridge on the inner side of the drum and thrown down.
- The sample was washed on top of the 9.5 mm sieve.
- The same sample was scanned and analysed after the MA test to trace the changes in shape properties.



**Figure 4.20: Typical Mill Abrasion test machine used for this study**

The mechanical stress on the rock is by both impact and attrition through the interactions of stones and drum wall. Figure 4.21 shows a ballast specimen before and after carrying out the test.



**Figure 4.21: Ballast sample before and after a Mill Abrasion test**

#### 4.10.1 Mill Abrasion results of sphericity and roundness validation

The test method provides a measure of the ability of the ballast stone to withstand degradation both during construction and under various track conditions. It also furnishes additional data pertaining to the quality of the material, as well as whether its index properties are likely to change in the track and be detrimental to its performance.

Figure 4.22 shows the distributions of the sphericity computed using surface area and volume. The sphericity distributions are plotted for scanned particles before and after MA test. Included in the figure are sphericity values of 14 spherical objects. As expected, particles results after the MA test has higher sphericity values with a distribution ranging from 0.72 to 0.90 and followed by before MA test with a distribution ranging from 0.63 to 0.86. The results indicate that most particles after polishing were becoming spherical. Similar comparison of roundness before and after is shown in Figure 4.23.

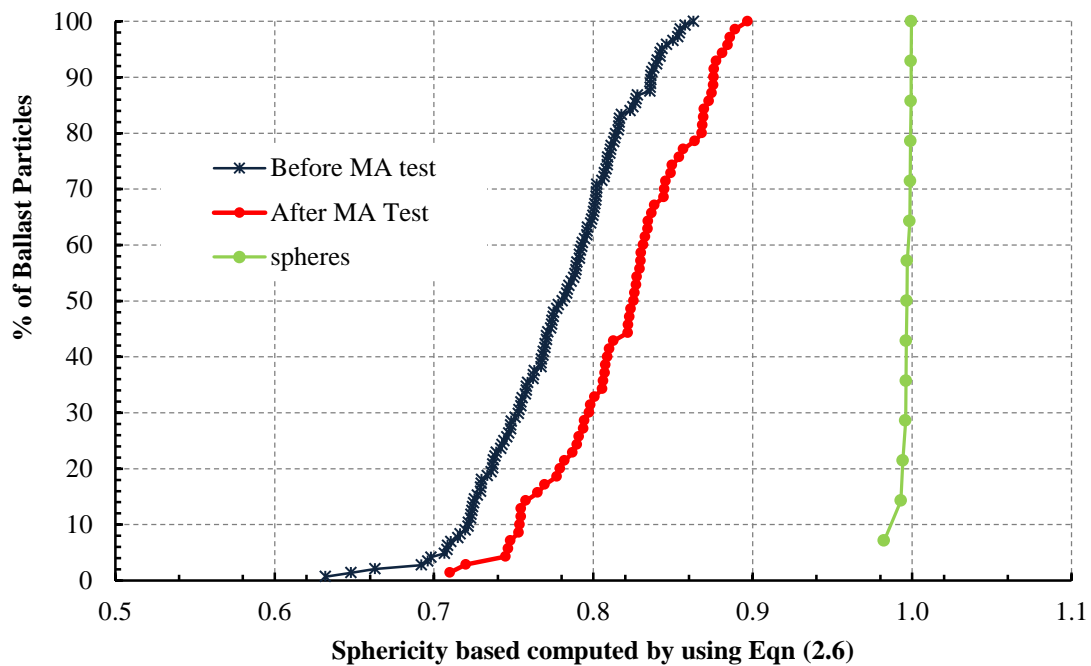
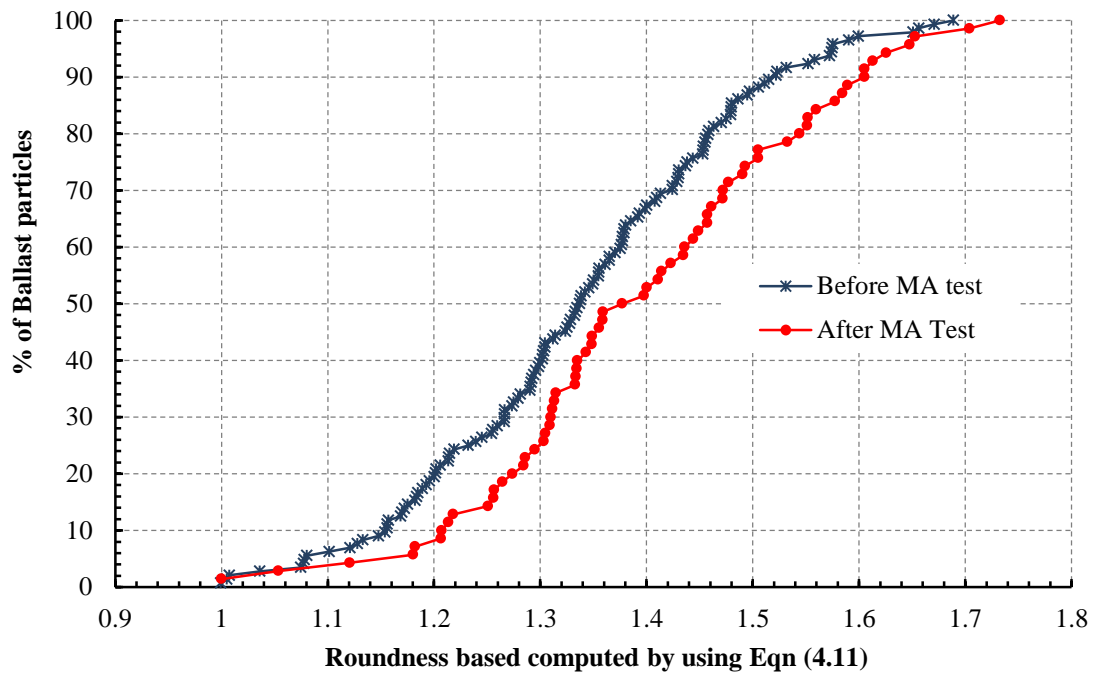


Figure 4.22: Sphericity validation results



**Figure 4.23: Roundness validation results**

The ANOVA results in Table 4.13 for  $F_{critical}$  values was smaller than the  $F_{values}$ , therefore the null hypothesis was rejected for sphericity, as the mean values of the data are not similar. Table 4.14 shows the  $F_{critical}$  values smaller than the  $F_{values}$ ; therefore, the null hypothesis for roundness was rejected, as the mean values of the data are not similar. By examining the results of ANOVA validation analysis, the highest  $F_{value}$  used to reject the  $H_0$  was found in sphericity results, followed by the roundness.

**Table 4.13: ANOVA sphericity validation**

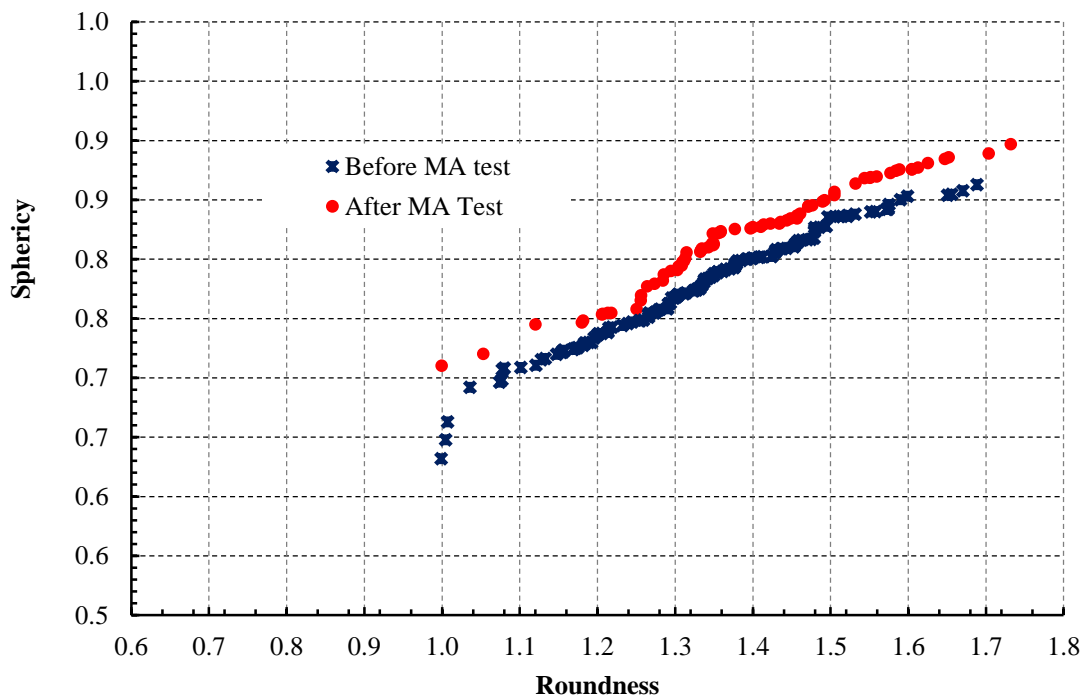
Source	Sum of Squares	Degrees of freedom	Mean Squares	$F_{value}$	$P_{value}$	$F_{critical}$
Between Groups	0.087	1	0.087	46.419	9.903E-11	3.886
Within Groups	0.394	210	0.002			
Total	0.481	211				

**Table 4.14: ANOVA roundness validation**

Source	Sum of Squares	Degrees of freedom	Mean Squares	F <sub>value</sub>	P <sub>value</sub>	F <sub>critical</sub>
Between Groups	0.187	1	0.187	8.962	0.003	3.886
Within Groups	4.386	210	0.021			
Total	4.573	211				

#### 4.10.2 Relationship of sphericity and roundness index

Figure 4.24 shows a plot of sphericity against roundness of the ballast sample before and after the MA test. As expected, all scanned particles after the MA test were more spherical than before the MA test, as it can also be seen in the actual photos presented in Figure 4.21. This sample has low sphericity and roundness, which validates the fact that crushed ballast should generally be less rounded than the polished sample after the MA test.



**Figure 4. 24: Relationship between roundness and sphericity**

These results clearly demonstrate the capability of the laser scanning technique to measure the effect of sphericity and roundness before and after the MA test. Ballast should have high wear

and abrasive qualities to withstand the impact of dynamic trainloads without excessive degradation. Li et al. (2015) noted that the type of parent rock from which the ballast is crushed, would affect the derived particle size, shape, and angularity of individual particles. Excessive polishing of the ballast will result in the reduction of particle size and loss of supporting strength of the ballast section. Ballast should be hard, durable and as far as possible, have angular edges or corners. Based on the three dimensional laser results, a general roundness index can be developed for ballast materials used on the coal line, which could be extended to other railway, ballast materials.

## 5 DATA ANALYSIS AND DISCUSSION OF TRIAXIAL TEST RESULTS

### 5.1 INTRODUCTION

The behaviour of railway ballast should be investigated in the real track under actual operating conditions. However, such field tests are very expensive, time consuming, and disrupt traffic. Therefore, laboratory experiments that can simulate field load and boundary conditions are usually carried out on ballast specimens. Fresh crushed ballast was used in cyclic loading to simulate the loading by train.

In order to test the effect of particle characteristics on shear strength and on settlement of railway ballast, a triaxial testing apparatus was used to test particle sizes typical of railway ballast. Railway ballast contains particles up to 53 mm in diameter. Heavy haul railway ballast is comprised of a ballast sized distribution curve with the largest particle passing the 63 mm sieve.

### 5.2 DISCUSSION OF TRIAXIAL TEST RESULTS

The popular Mohr-Coulomb model is a perfect elastic-plastic model commonly used for geotechnical calculations. The results from the triaxial tests provide parameters that are employed in the analysis of the strength of the tested materials. For this study, Mohr's circles were first constructed using the applied confining pressures and the corresponding maximum shear stresses at failure. The Mohr-Coulomb failure envelope was then constructed for determining the strength parameters of the materials. The Mohr-Coulomb failure envelope is defined by Equation 5.1.

$$\tau = c + \sigma \tan \phi \quad (5.1)$$

Where  $\tau$  is the shear strength of the material,  $\sigma$  is the applied normal stress;  $c$  is cohesion and  $\phi$  is the angle of internal friction of the material. The maximum shear stresses were used to construct Mohr's circles to represent the six samples. The peak strength was defined as the peak value of the deviator stress ( $\sigma_3$ ). Typical failure curves of applied load against displacement are shown in Figures 5.3, 5.5, 5.7, 5.9 and 5.11 at 70 kPa, 90 kPa and 120 kPa confining pressure. The peak strength was defined as the peak value of deviator stress. Failure occurs when the contribution of shear and normal stress is such that the Mohr Circle is tangent to the failure



envelope. It is expected that the cohesion parameter ( $c$ ) would be equal to zero for the ballast materials since there were no fines in the materials tested. Generally, higher shear strength was obtained for fresh crushed angular ballast. As expected, increasing confining pressure resulted in increased deviator stress at failure as shown in Figures 5.4, 5.6, 5.8, 5.10 and 5.12. In comparison, the fresh crushed ballast exhibits higher internal friction angle, followed by the recycled ballast, while the river pebble show a lower internal friction angle. It is believed that the relatively higher roundness of new crushed ballast contributes to better particle interlock.

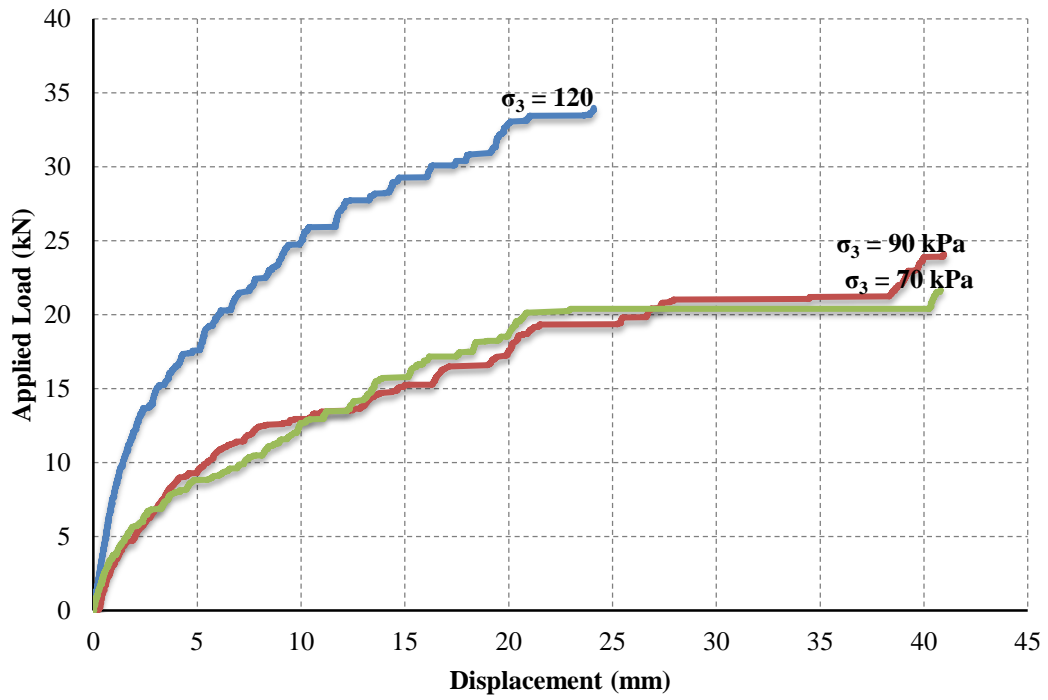


Figure 5.1: Shear test results for recycled ballast from Km 9

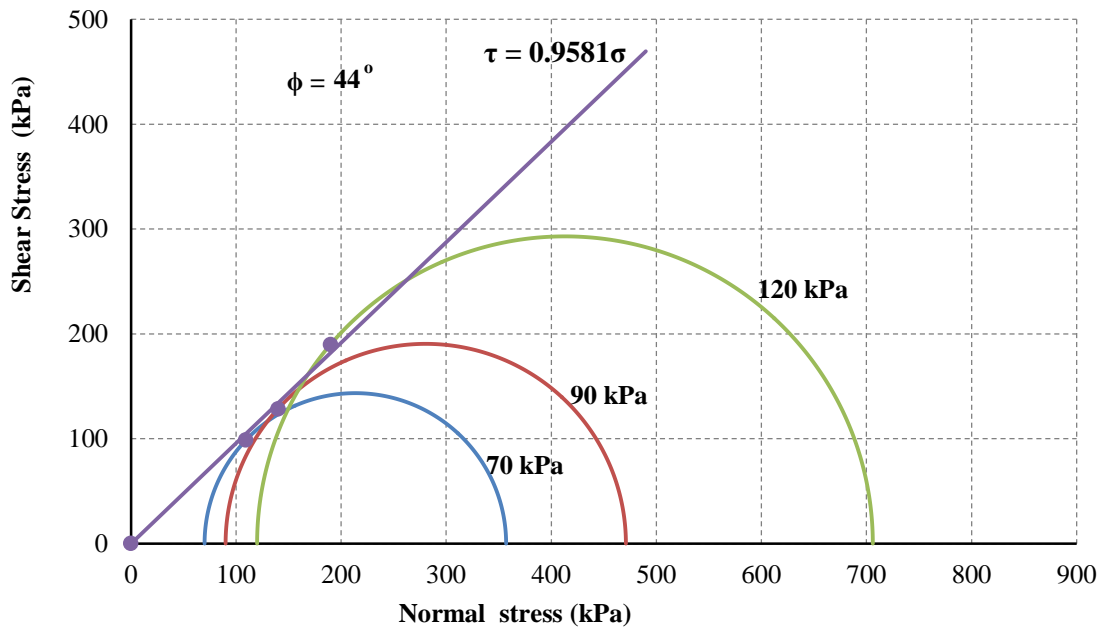


Figure 5.2: Mohr circles and failure envelop of recycled ballast from Km 9

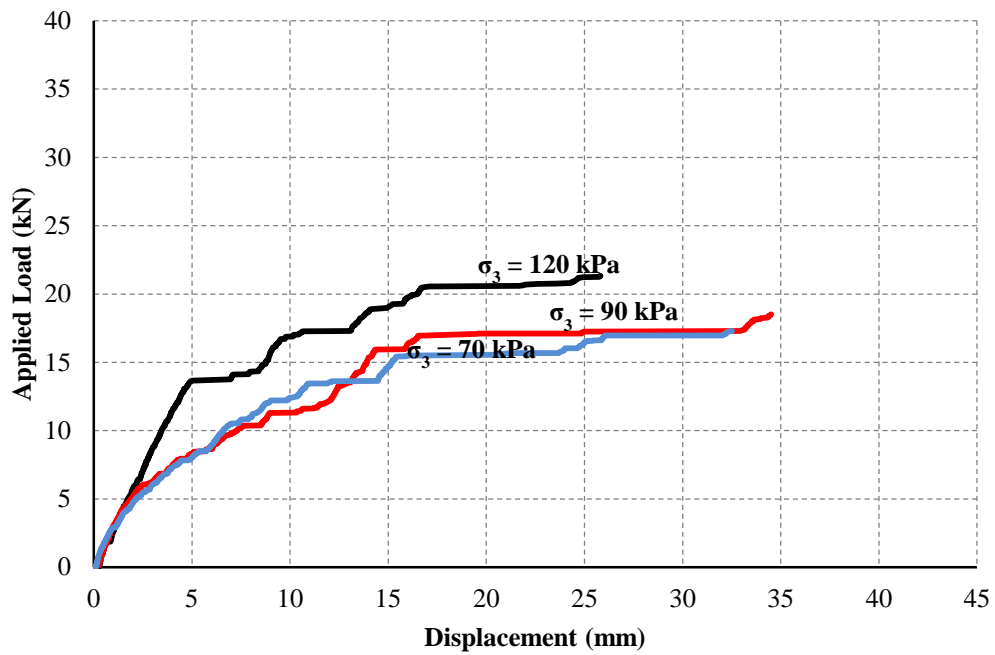


Figure 5.3: Shear test results for recycled ballast from Km 17

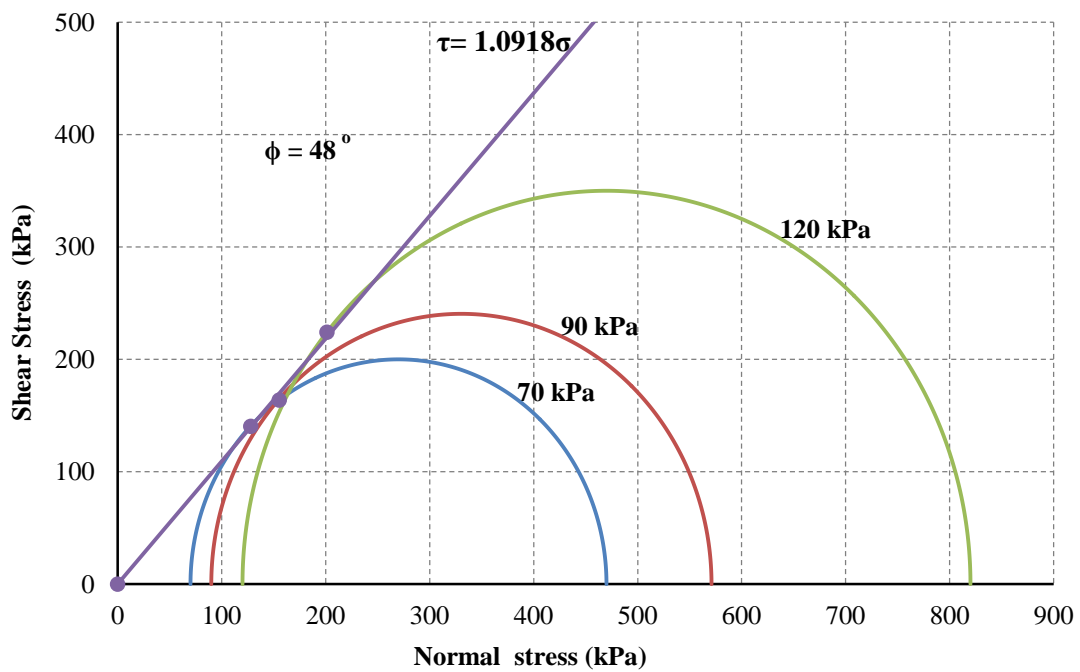


Figure 5.4: Mohr circles and failure envelop of recycled ballast from Km 17

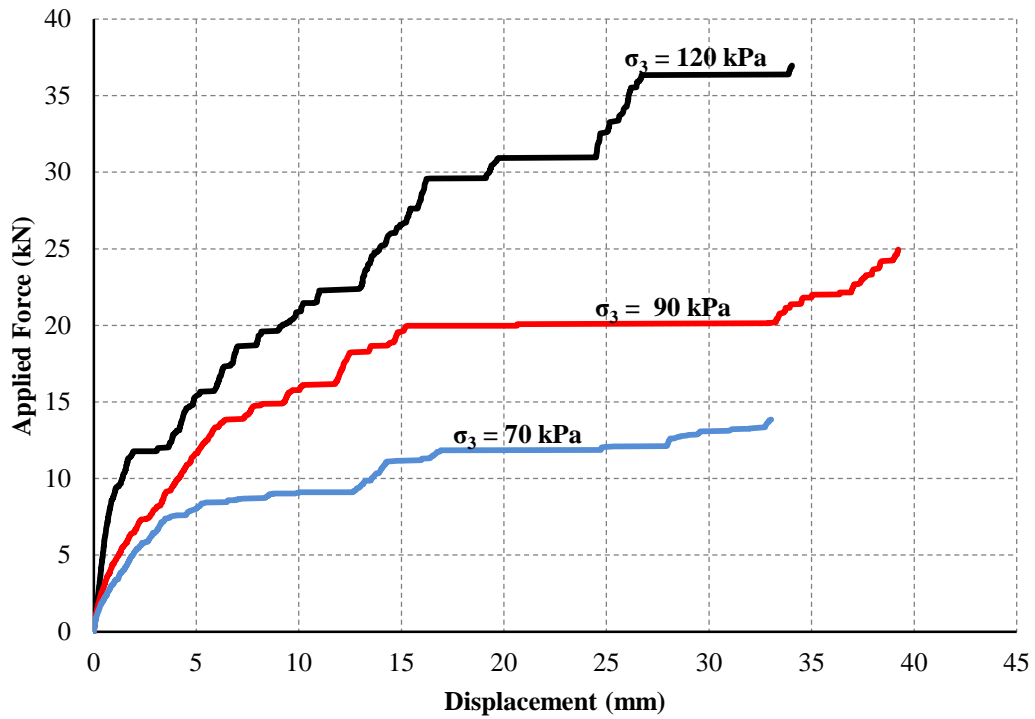


Figure 5.5: Shear test results for recycled ballast from Km 31

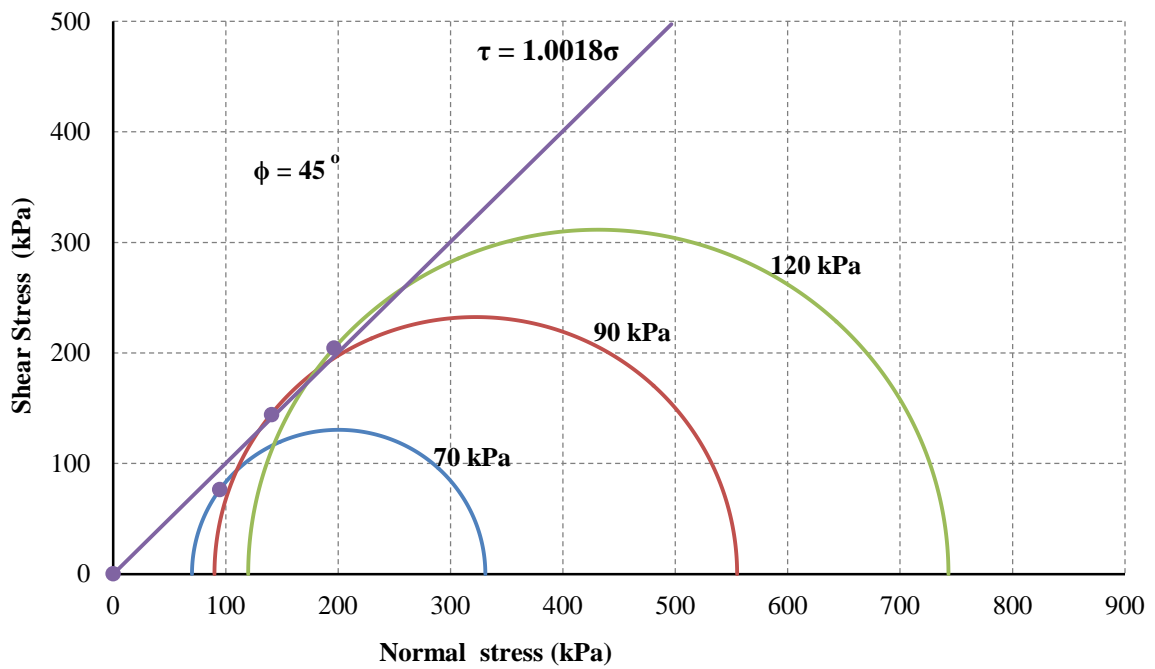


Figure 5.6: Mohr circles and failure envelop of recycled ballast from Km 31

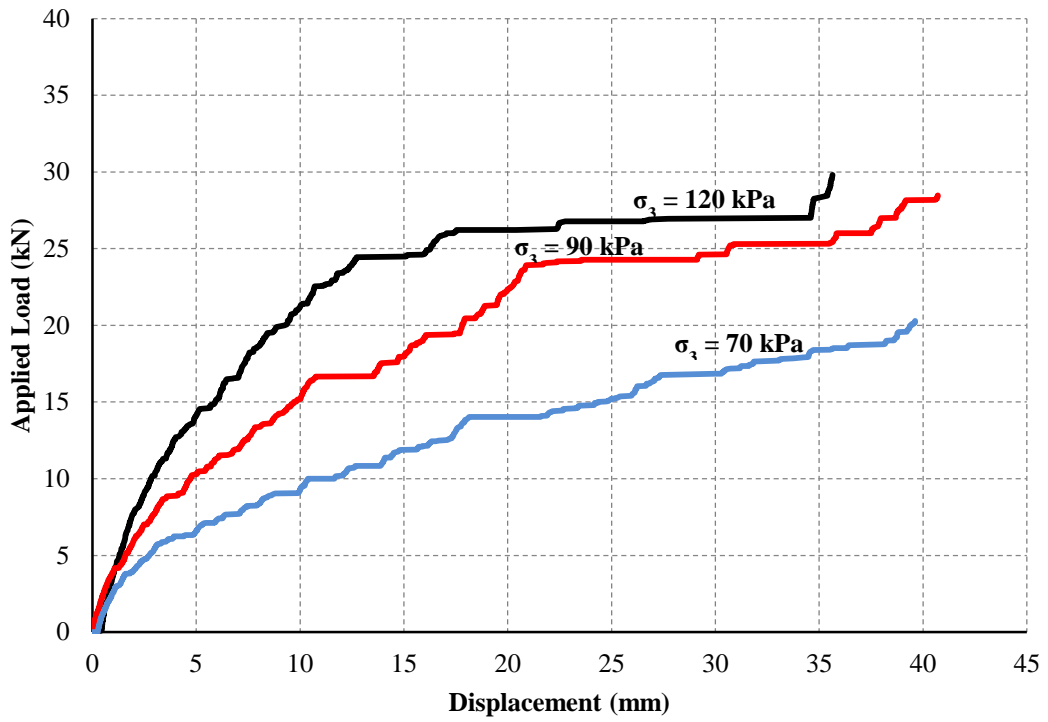


Figure 5.7: Shear test results for recycled ballast from Km 32

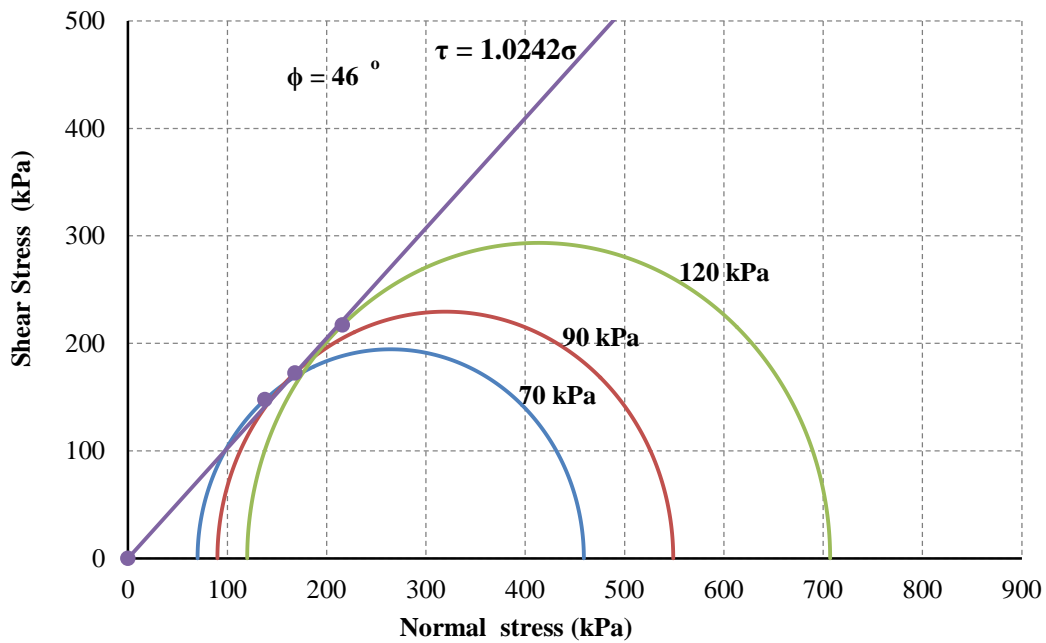


Figure 5.8: Mohr circles and failure envelop of recycled ballast from Km 32

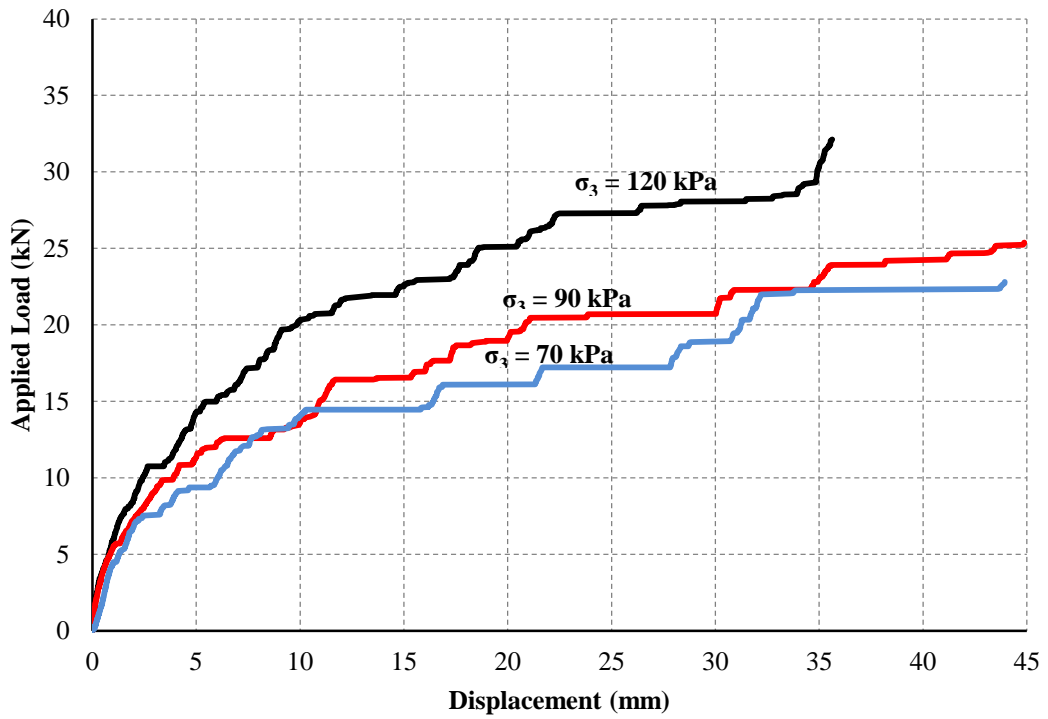


Figure 5.9: Shear test results of freshly crushed ballast

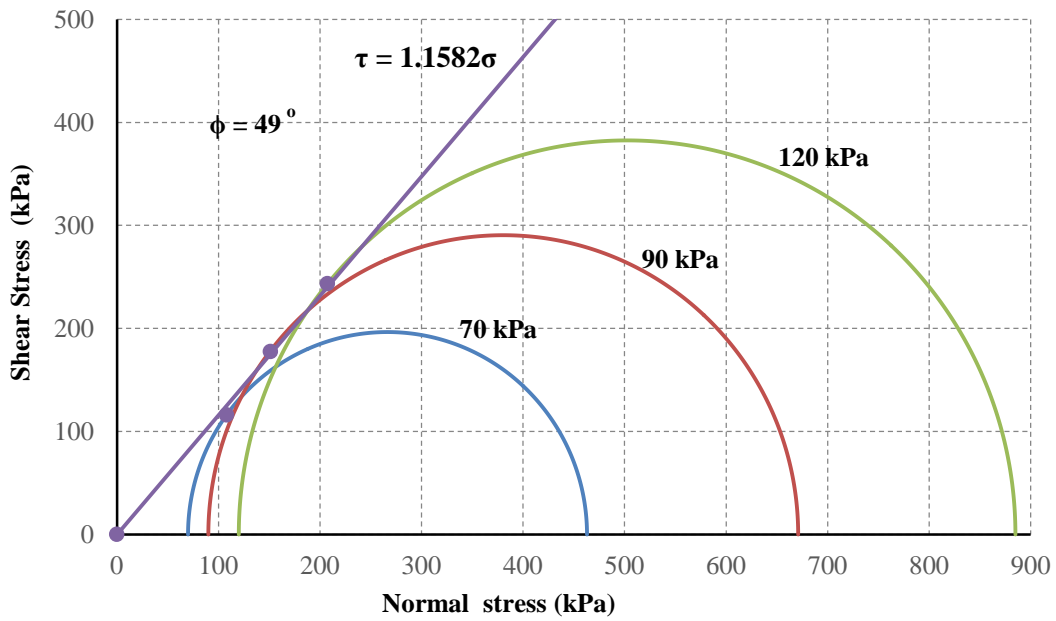


Figure 5.10: Mohr circles and failure envelop of freshly crushed ballast

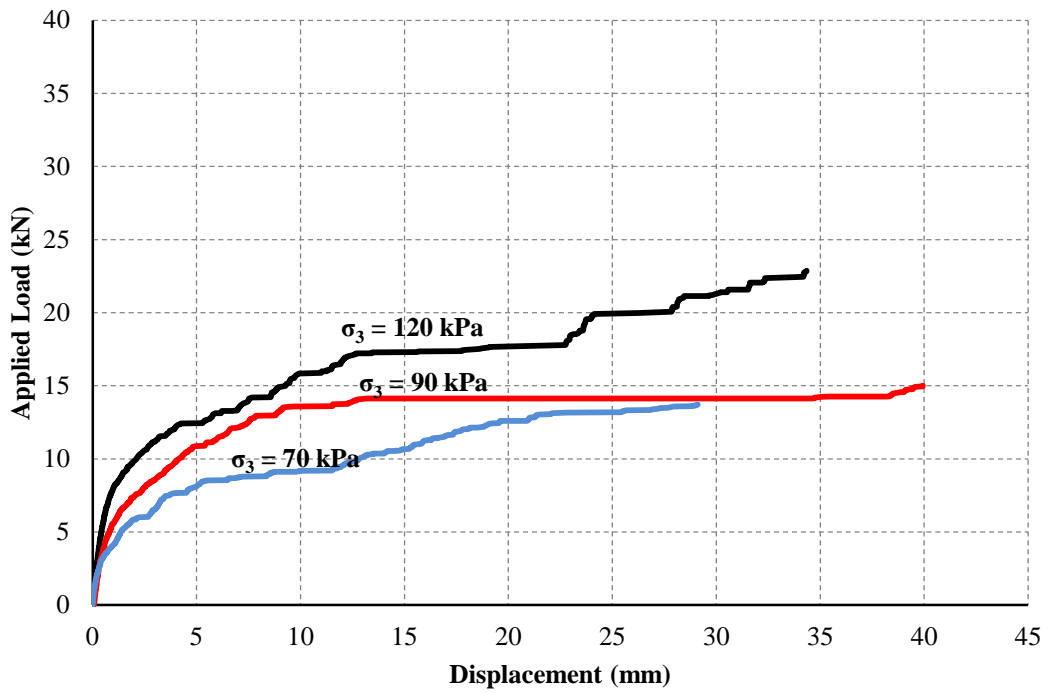


Figure 5.11: Shear test results of river pebbles

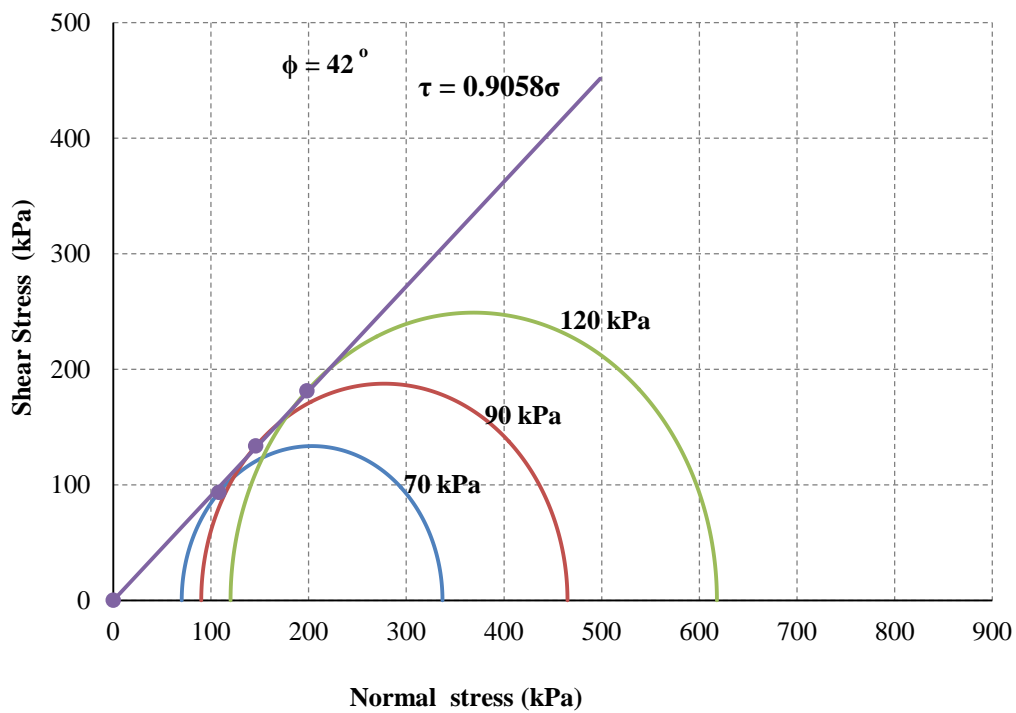


Figure 5.12: Mohr circles and failure envelop of river pebbles

### 5.3 SHAPE EFFECTS ON SHEAR STRENGTH

It is well known that high inter-particle contacts should usually result in a high friction angle within the sample (ASTM D 2850, ATM D 4767, Anochie-Boateng, 2007; Garg & Thompson, 1997). Aggregate interlock under static loading conditions also improves the material stiffness when the confining stress increases. Figures 5.13 to 5.15 show correlations of the internal friction angle with the sphericity computed by using the ballast surface area and volume, the roundness computed by using the ballast surface area and ellipsoid surface area and flatness ratio respectively. Overall, good correlations were observed. The trends of the plots agree with theory underplaying each of the shape indices. The highest correlation was found between the internal friction angle with the sphericity computed by using the ballast surface area and volume ( $R^2 = 0.904$ ), followed by the roundness computed by using the ballast surface area and ellipsoid surface area ( $R^2 = 0.759$ ) and the flatness ratio ( $R^2 = 0.544$ ).

The effect of ballast roundness on the shear strength properties of the ballast materials and the river pebbles is presented in Figure 5.14. The internal friction angle increases when the average roundness of the sample decreases from 1.3 to 1. The materials are grouped according to their degree of roundness. The pebble sample was used as a control for ballast material in its worst condition. Generally, the internal friction angle increases when the roundness of the particles is decreasing. One would expect that the recycled ballast (Km 9 and Km 31) would have the same internal friction angle because of their similar roundness values. However, the difference in frictional angle could be due to ballast breakdown creating fines and becoming flaky (Figure 5.15). The grinding of sharp edges of recycled ballast, during repeated loading, is considered the key reason for its reduced friction and decreasing roundness, leading to severe settlement as observed on the coal line. Thus, for the materials tested, lower inter-particle contacts or lower friction angle can be directly associated with a more rounded sample. Round ballast is usually smooth and because the particles do not have sharp corners (i.e. particles with high roundness), they cannot interlock, resulting in relatively lower internal friction angles.

This section only discuss results on roundness, sphericity and flatness ratio and did not cover other shape properties such as elongation and flat & elongated particles. In general, roundness increases frictional interlock between grains, which increases shear strength. The grinding of sharp edges of recycled ballast during repeated loading is considered the key reason for its reduced friction and decreasing roundness leading to possible settlement on the coal line.



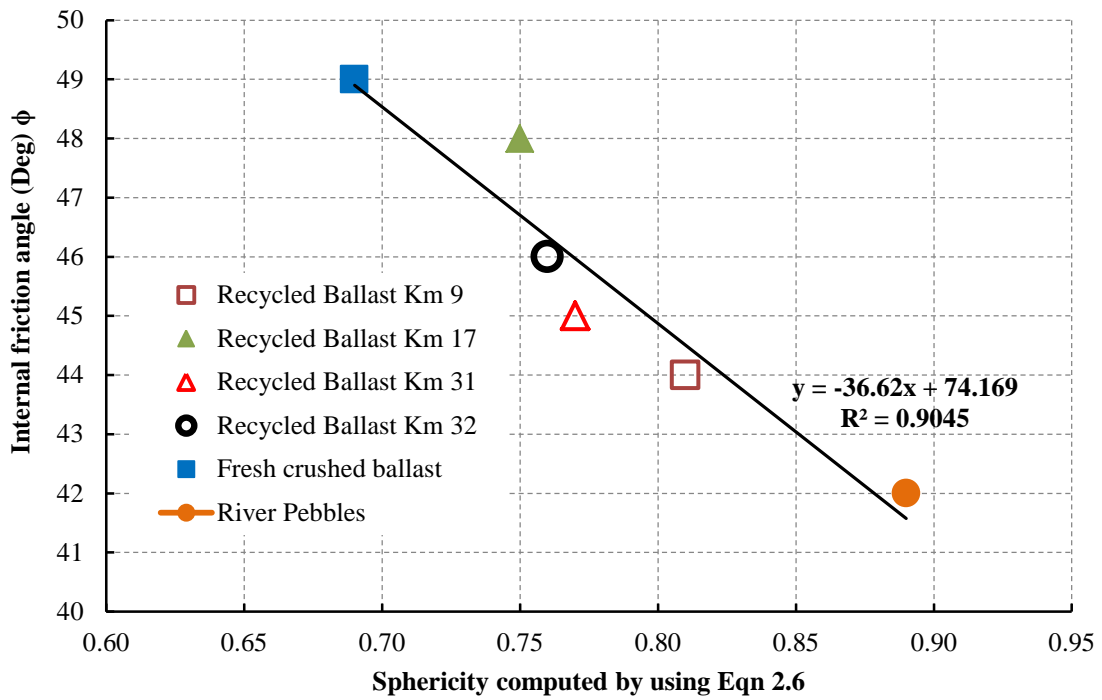


Figure 5.13: Effect of sphericity index on internal friction angle

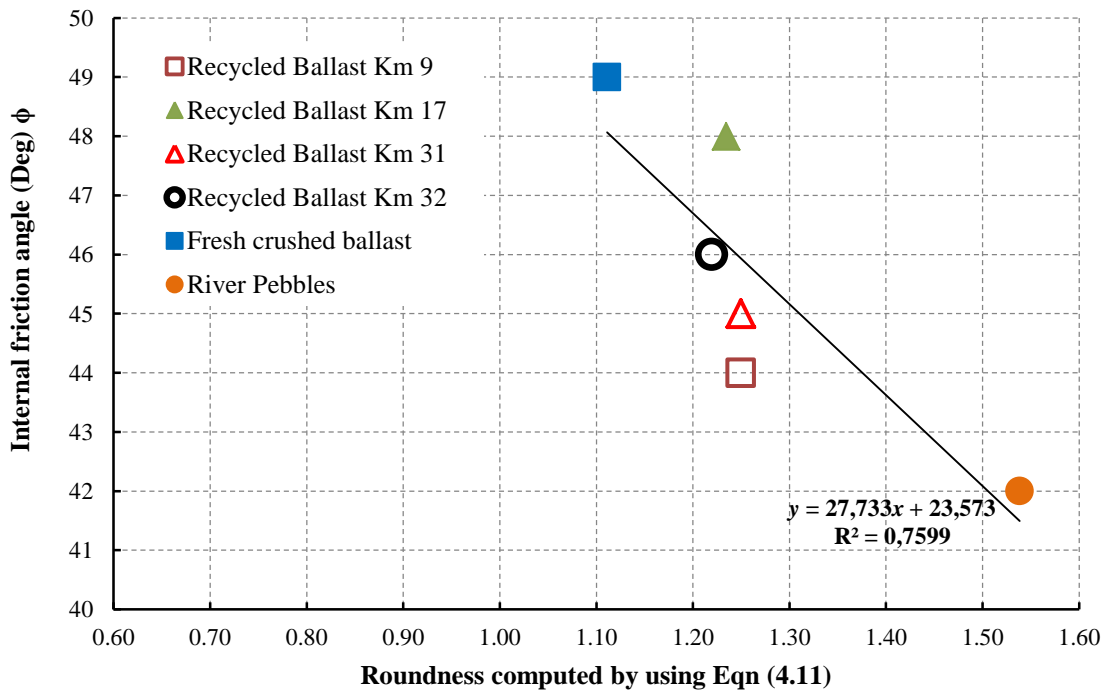
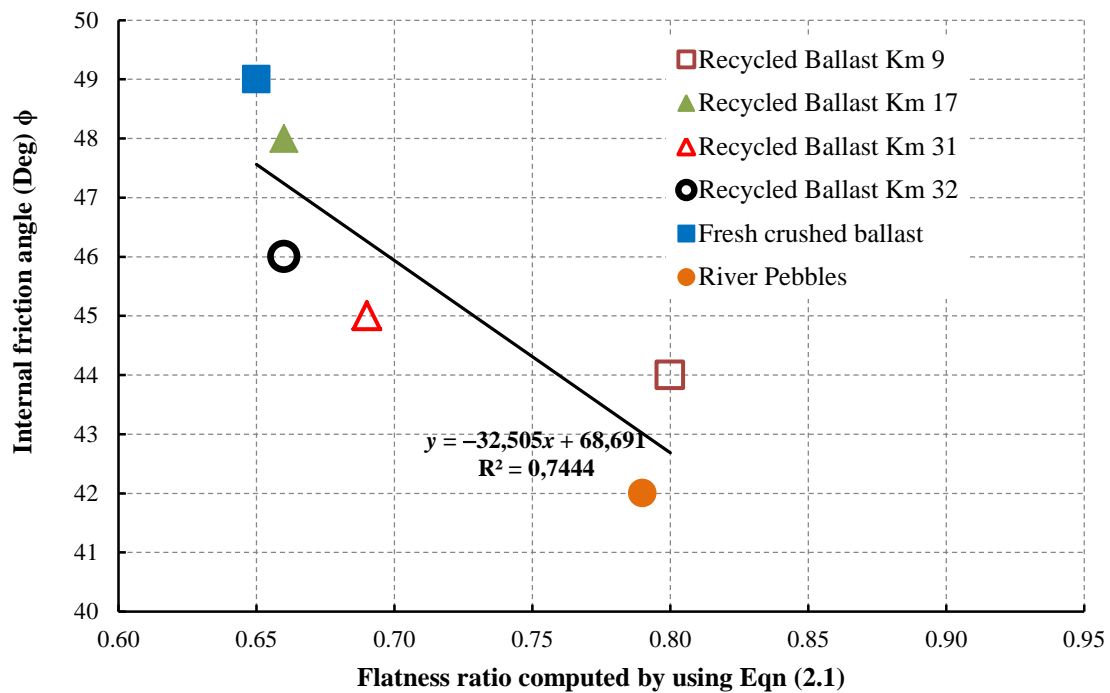


Figure 5.14: Effect of roundness index on internal friction angle



**Figure 5.15: Effect of flakiness index on internal friction angle**

#### 5.4 RESULTS AND DISCUSSION OF PERMANENT DEFORMATION

The following results were obtained from cyclic triaxial test and the discussions of permanent deformation results. Results from cyclic triaxial tests were used to illustrate that the failure under cyclic load is progressive and occurs at stress levels below those causing failure under static loading. Thus, the results to be presented here are only an indication of the type of behaviour that could occur in the field.

During the first loading of a granular material such as ballast, the strain develops rapidly and is only partially recovered upon unloading; each additional cycle contributes to another increment of plastic or permanent strain.

The cyclic test was carried out with the same cell pressure ( $\sigma_3 = 90$  kPa), with only an increase in the load. The samples were loaded at 90 kPa confining pressure and 100 kPa, then at 140 kPa axial loading. Figures 5.16 to 5.21 presents ballast response under cyclic loading. The first one was tested under 90 kPa axial pulse loading with 0.1-second load duration, and after 50 000 cycles, the repeated stress level was increased to 140 kPa for another 50 000 cycles.

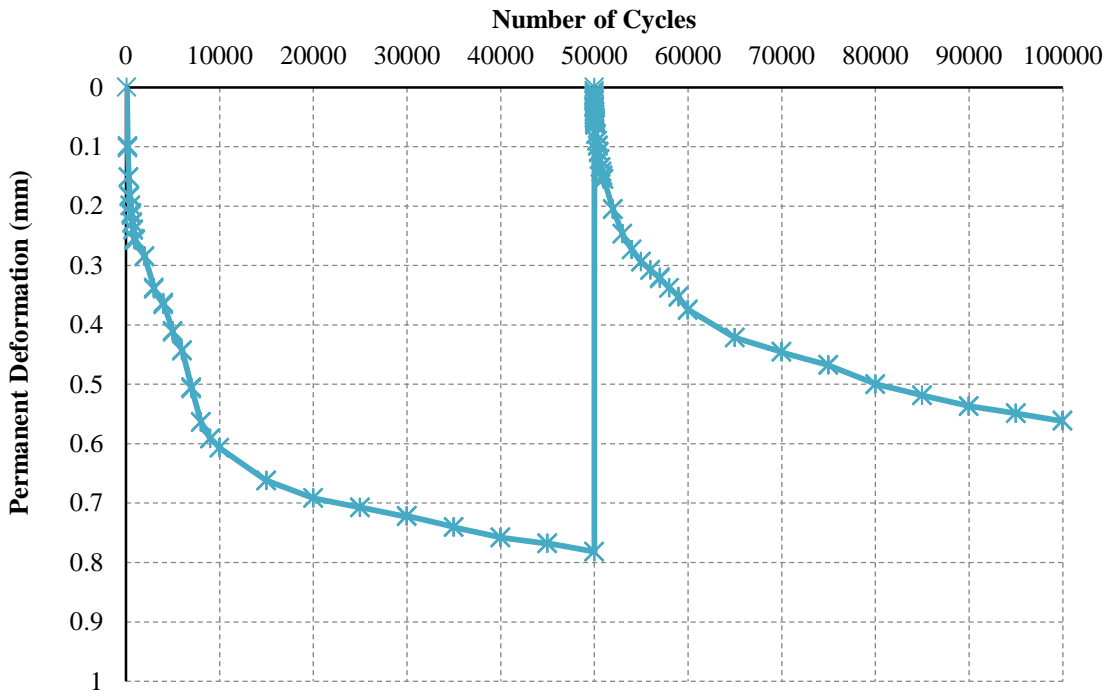


Figure 5.16: Measured permanent deformation of recycled ballast from Km 9

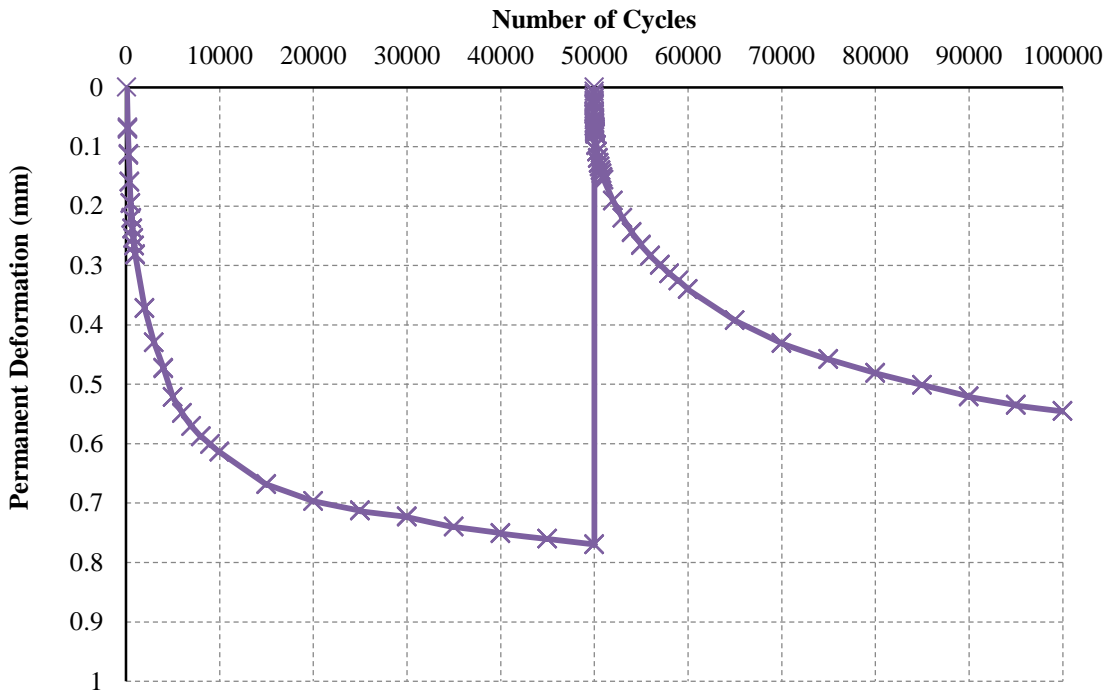


Figure 5.17: Measured permanent deformation of recycled ballast from Km 17

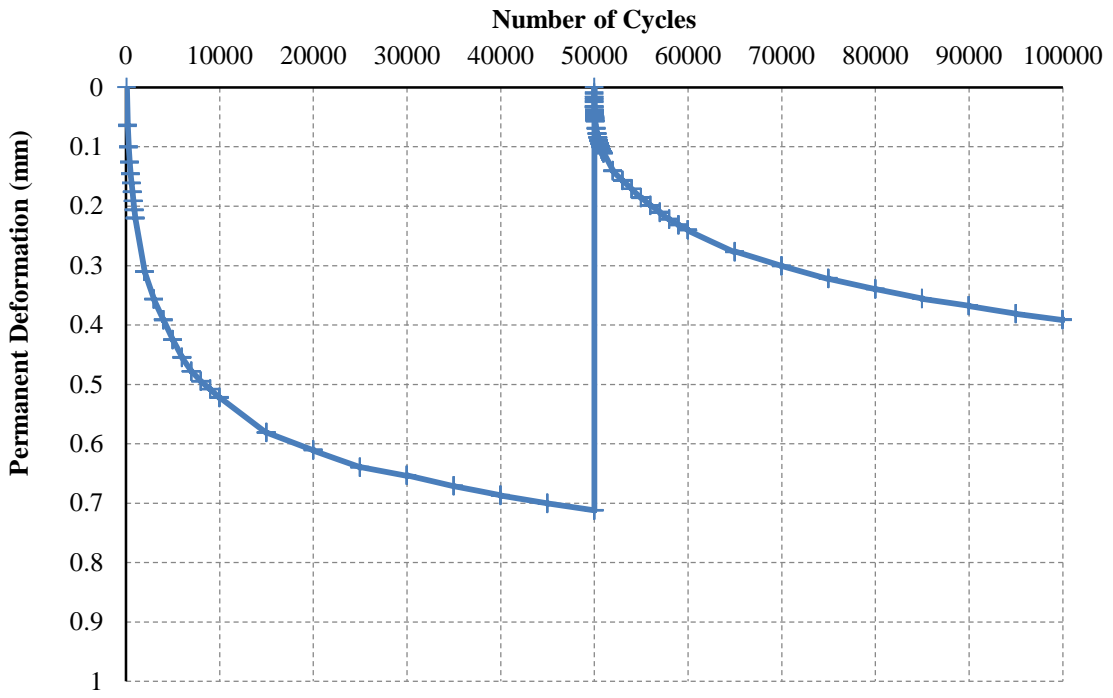


Figure 5.18: Measured permanent deformation of recycled ballast from Km 31

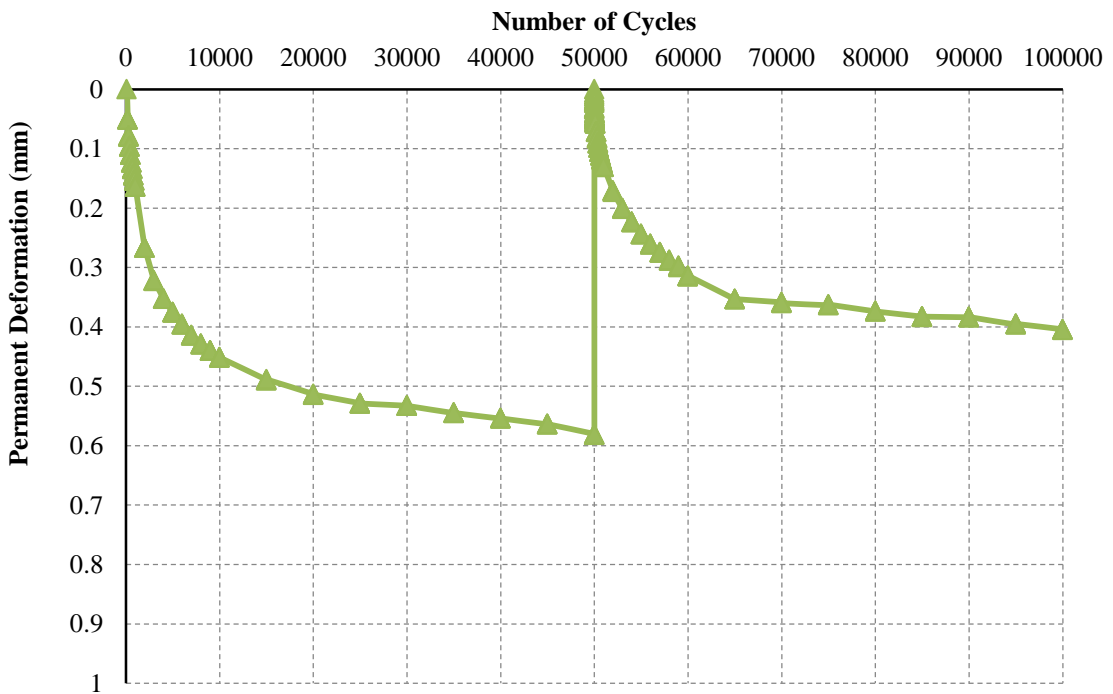


Figure 5.19: Measured permanent deformation of recycled ballast from Km 32

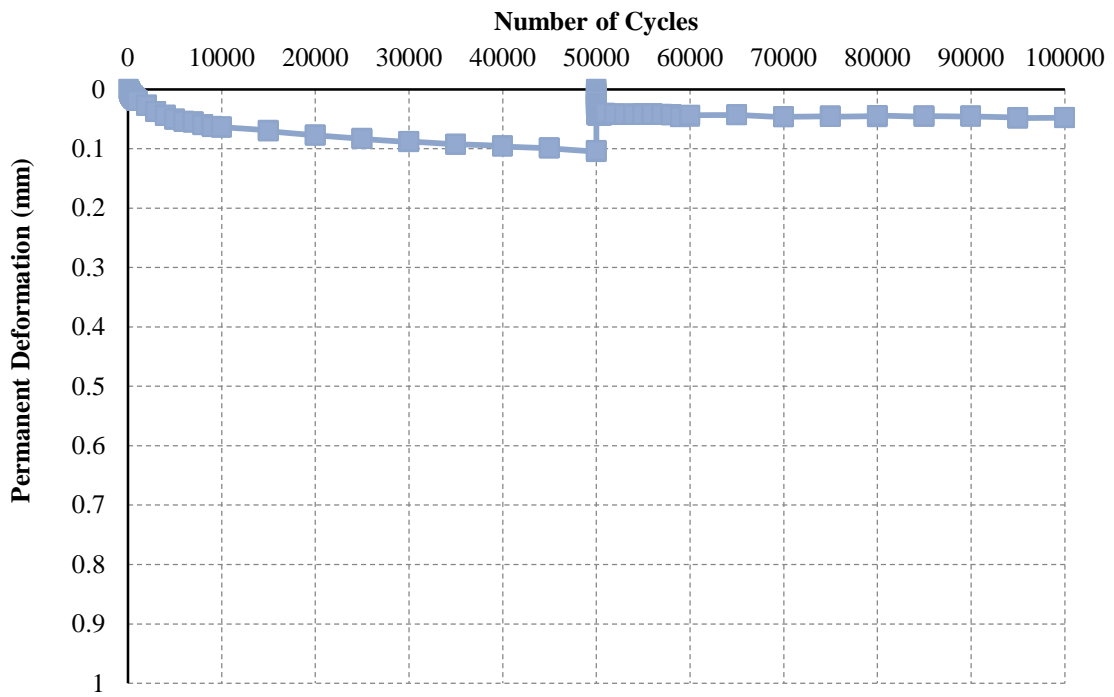


Figure 5.20: Measured permanent deformation of freshly crushed ballast

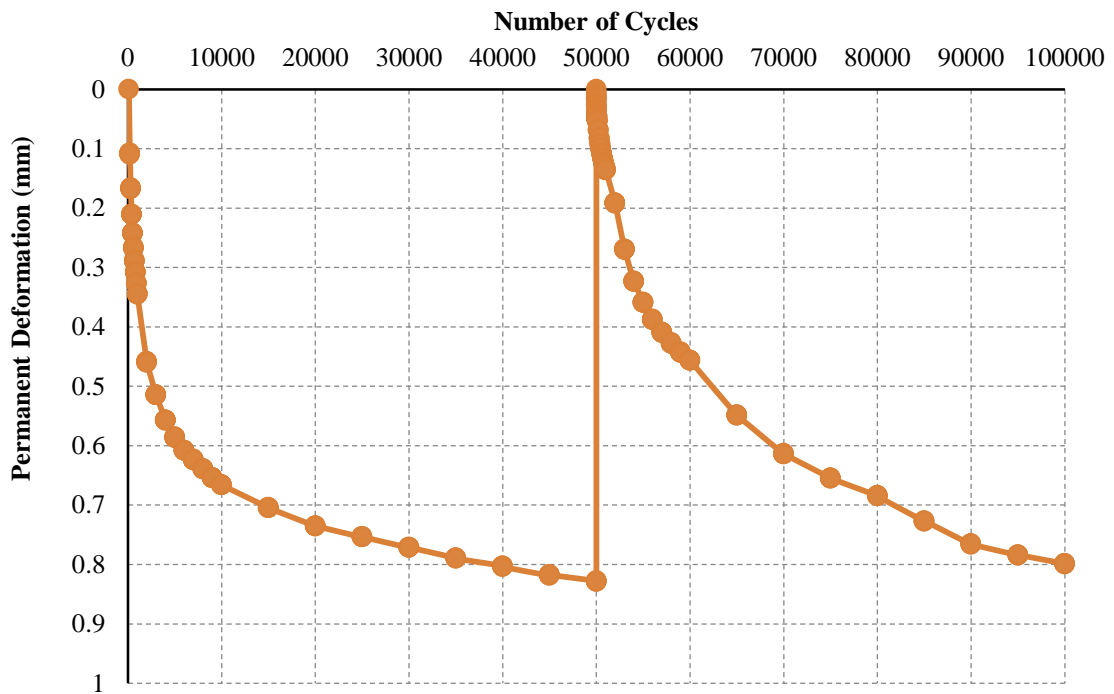
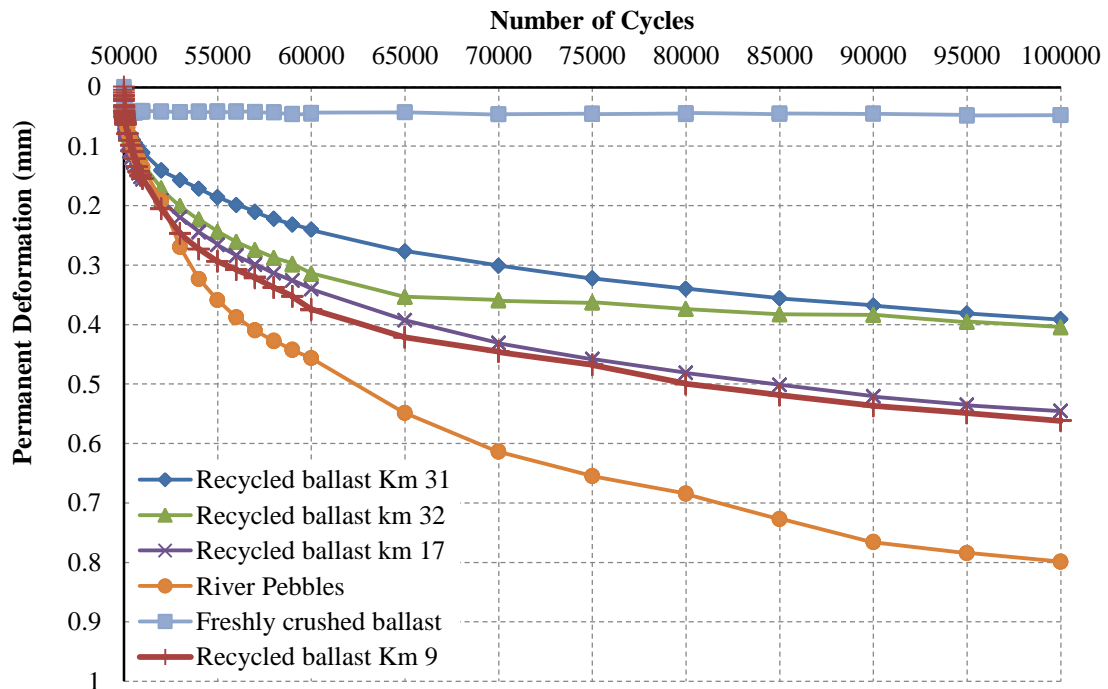


Figure 5.21: Measured permanent deformation of river pebbles

Table 5.1 presents a semi-logarithmic relationship of tested samples. As expected, the sample with the highest settlement on the second-stage test was round river pebbles, followed by recycled ballast Km 31, recycled ballast Km 17, recycled ballast Km 9, recycled ballast Km 32 and freshly crushed ballast. Figure 5.22 shows the highest permanent deformation was found in river pebbles sample, followed by the recycled ballast Km 31, recycled ballast Km 17, recycled ballast Km 9, recycled ballast Km 32 and freshly crushed ballast.

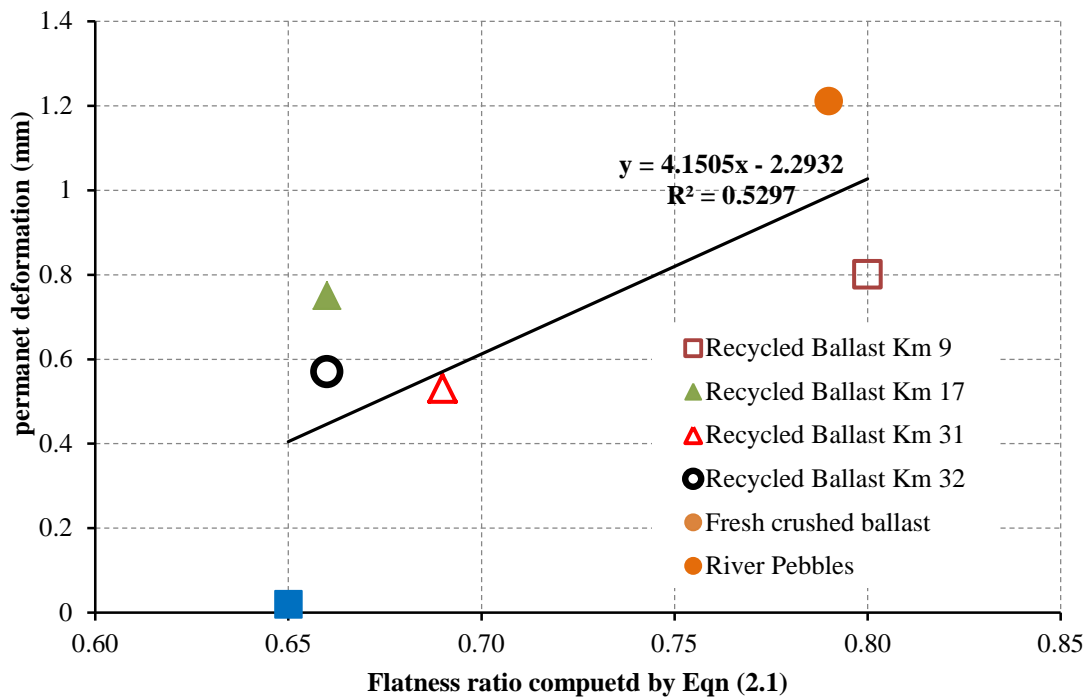
**Table 5.1: Semi-logarithmic relationship**

Sample description	<i>a</i>	<i>b</i>	$R^2$
River Pebbles	1.21	-12.96	0.89
Recycled ballast Km 31	0.53	-5.68	0.88
Recycled ballast Km 17	0.75	-8.03	0.87
Recycled ballast Km 9	0.8	-8.55	0.84
Recycled ballast Km 32	0.57	-6.06	0.77
Freshly crushed ballast	0.02	-0.14	0.16



**Figure 5.22: Second-stage permanent deformation of tested materials**

Figures 5.23 to 5.25 show correlations of the permanent deformation with the sphericity computed by using the ballast surface area and volume, the roundness computed by using the ballast surface area and ellipsoid surface area, and flatness ratio respectively. The trends of the plots agree with theory underlying each of the shape indices. The highest correlation was found between the permanent deformation with the sphericity computed by using the ballast surface area and volume ( $R^2 = 0.875$ ), followed by the roundness computed by using the ballast surface area and ellipsoid surface area ( $R^2 = 0.805$ ), and the flatness ratio ( $R^2 = 0.523$ ).



**Figure 5.23: Effect of flatness ratio on permanent deformation**

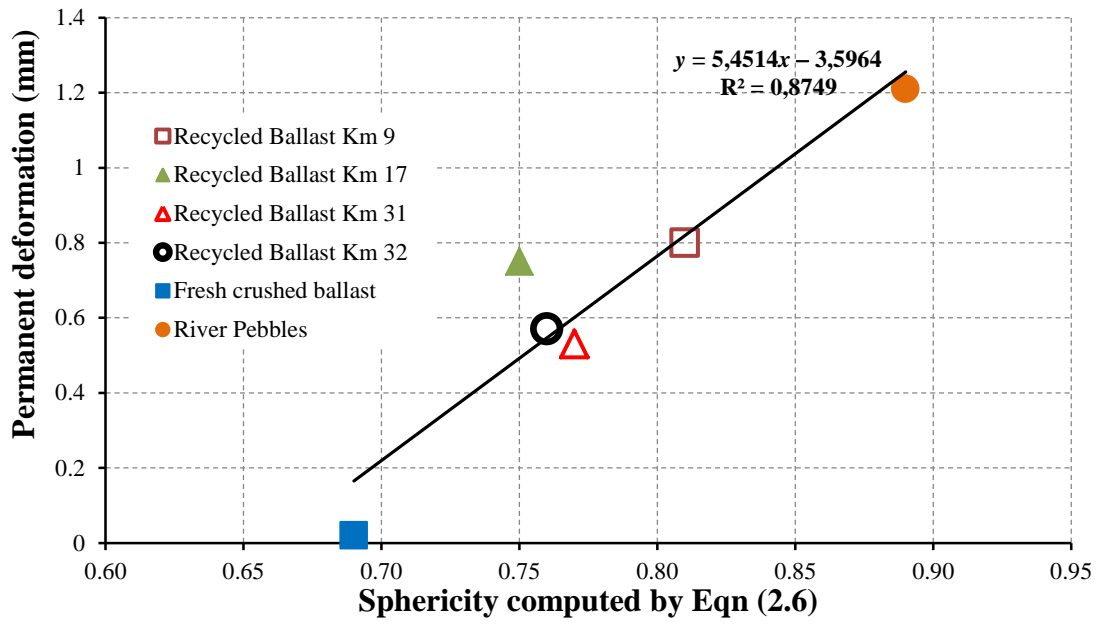


Figure 5. 24: Effect of sphericity index on permanent deformation

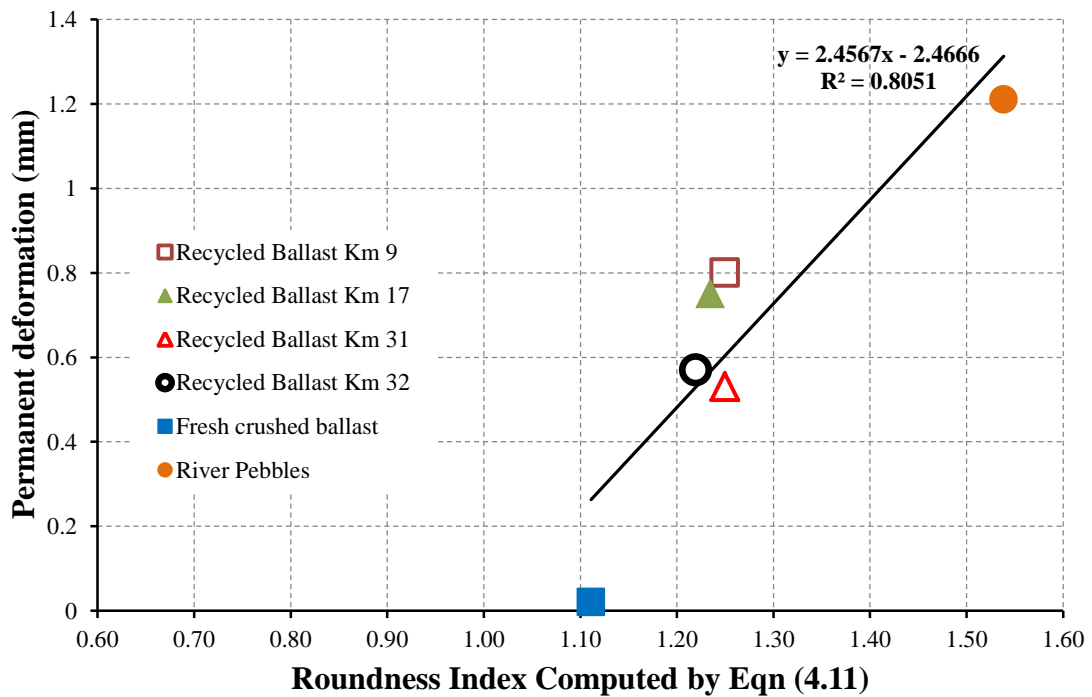


Figure 5.25: Effect of roundness index on permanent deformation



## **6 CONCLUSIONS AND RECOMMENDATIONS**

A modern 3D-laser scanning technique was used to determine the roundness parameter and link it with the internal frictional angle and settlement of the ballast materials. The approach was based on the use of the 3D-laser scanning technique to directly obtain the flakiness index, roundness and sphericity of ballast particles. A MATLAB<sup>TM</sup> code was developed for the processing of laser scan data, using the surface area of an ellipsoid to compute the roundness index and other shape properties derived from mathematical equations. The developed MATLAB<sup>TM</sup> code was found to be very useful in terms of the analysis.

### **6.1 CONCLUSIONS**

Based on the results presented in this dissertation, the following conclusions can be made:

#### **6.1.1 Development of shape descriptors to quantify ballast characteristics**

- The much-needed improvements in the measurement of the shape properties of ballast materials have been demonstrated in this study using the three dimensional laser-based scanning method.
- The laser scanning technique provides results that are more accurate when compared with the traditional methods for evaluating ballast shape properties and improves ballast selection for construction purposes.
- Statistical analysis results demonstrate a variation of 22% between fresh crushed ballast from the quarry and natural river pebbles, while recycled ballast from the field varies between 4 % and 9 %. These results will assist with quality control in the field, as well as to decide whether to maintain the existing recycled ballast or replace the ballast layer.
- The developed surface area relationship demonstrates that the use of automated and advanced techniques of scanning ballast materials would assist in accurate measurements of the ballast shape. The surface model can be used to estimate the particle surface area when the mass of and the specific gravity are known and used to compute the volume.

#### **6.1.2 The effect of ballast shape on performance-related properties**

- Based on the results presented in this study, it can be concluded that there is a strong correlation between the internal friction angle and roundness parameter of the ballast materials investigated.

- The results show that a roundness value of between 0.6 and 0.7 is typical for excessively rounded particles, while particles with high roundness have values of between 0.8 and 1.3.
- Because of the strong correlation between the internal friction angle and roundness parameter of the ballast materials investigated, the performance of the rail track structure can be linked to ballast shape properties.

## **6.2 RECOMMENDATIONS AND ASPECTS FOR FUTURE STUDY**

Based on the information contained in this dissertation, the following recommendations are made:

- A 3D-laser scanning technique can be used to determine the physical dimensions, surface area and volume properties of railway ballast to further determine shape indices. It is therefore important for the railway industry in South Africa to take this opportunity to improve and develop new guidelines and test methods for ballast in order to improve the performance of railway track structures.
- There is a need for automated techniques that is based on accurate measurements to quantify shape properties of railway ballast in order to mitigate human errors associated with the ballast shape properties.
- Results obtained from the laser scanning technique could be used for quality control in the quarries or aggregate production sources.
- It is anticipated that this study will lead to the development of new and improved national standards for ballast materials. These standards will have a significant impact on the track structure and the railway industry in an effort to provide better performing railway track structures to lower maintenance cost and improve safety on railway tracks.
- Another major contribution of the dissertation is the provision of a database of basic data to be used for on-going and future studies. Such studies could evaluate the ballast surface texture, which was outside the scope of this dissertation.
- Mathematical modelling of ballast particles using the Discrete-element method (DEM) should be considered using the stored shape library.

## 7 REFERENCES

American Society for testing and materials (ASTM) D2850-03a. 2003. *Standard test method for unconsolidated-undrained triaxial compression test on cohesive soils*. Annual Book of ASTM Standards.

American Society for testing and materials (ASTM) D4767-11. 2003. *Standard test method for consolidated-undrained triaxial compression test on cohesive soils*. Annual Book of ASTM Standards.

American Society for testing and materials ASTM C131. 2003. *Standard Test Method for: Resistance to degradation of Small Size Coarse by Abrasion and Impact in the Los Angeles Machine*. ASTM Annual Book of Standards, Section 4, Construction, Volume 89, road and Paving Material.

Anochie-Boateng J, Komba J and O'Connell J. 2011. Laser-based approach for determining flakiness index of aggregates used in pavements. *Proc. of the 30th Southern African transportation conference*. Pretoria.

Anochie-Boateng J, Komba J, Mukalega N and Maharaj A. 2010. Evaluation of 3D laser device for characterizing shape and surface properties of aggregates used in pavements. *Proc. Of the 29th Annual Southern African Transportation Conference*, Pretoria.

Anochie-Boateng JK, Komba JJ and Mvelase GM. 2011. Advanced and automated laser-based technique to evaluate aggregates. *Proc. of the International road Federation Congress*, Russia, pp. 22-24.

Anochie-Boateng JK, Komba JJ and Mvelase GM. 2013. Three-dimensional laser scanning technique to quantify aggregate and ballast shape properties. *Construction and Building Materials*, 43, pp. 389-398.

Anochie-Boateng JK, Komba JJ and Tutumluer E. 2012. Aggregate surface areas quantified through laser measurements for South African asphalt mixtures. *Transportation Engineering*, 138 (8), pp. 1-11.

Anochie-Boateng JK. 2007. *Advanced testing and characterization of transportation soils and bituminous sands*. PhD Thesis, University of Illinois at Urbana-Champaign USA.

Anochie-Boateng JK. 2014. *Test protocol for determining particle shape and surface properties of aggregate and ballast using laser scanning technique*. CSIR Built Environment. Technical manual CSIR/BE/IE/IR/2014/0038/C.

Arangie PBD. 1995. *The influence of ballast fouling on the functional behavior of the ballast pavement layer*. Master's Thesis, University of Pretoria SA.

Arangie, PBD. 1995. *The Influence of Ballast Fouling on the Functional Behaviour of the Ballast Pavement Layer*. Masters Theses. University of Pretoria.

Arasan, S, Hasiloglu, AS and Akbulut, S. 2010. Shape Properties of Natural and Crushed Aggregate using Image Analysis. *International Journal of Civil and Structural Engineering*, Volume 1, No 2, 2010, pp 221-233.

Asschenbrener, BC. 1956. A New Method of Expressing Particle Sphericity. *Journal of Sedimentary Petrology*, Vol 26, PP. 15-31.

Aursuckjj, B. 2007. *A Laboratory Study of Railway Ballast Behaviour under Traffic Loading and Tamping Maintenance*. PhD. Thesis, university of Nottingham.

Blatt,H. 1979. *Origin of Sedimentary rocks*. 2<sup>nd</sup> ed. Prentice-Hall.

Bowman, ET, Soga, K and Drummond W. 2001. Particle Shape Characterisation Using Fourier Descriptor Analysis. *Geotechnique*, Volume 51, Issue 6, Pages 545-554.

Fernlund, JMR. 2004. 3D Image Analysis Size and Shape Method Applied to the Evaluation of Los Angeles Test. *Engineering Geology Journal*, Volume 77, October, pp 57-67.

Folk RL. 1955. Student operator error in determining of angularity, sphericity and grain size. *Sedimentary Petrology*, 25, pp. 297-301.

Garg N and Thompson MR. 1977. Triaxial Characterization of Minnesota Road Research Project Granular Materials. *In Transportation Research Record 1577*, TRB, National Research Council, Washington, D.C., pp. 27-36.

Grabe, PJ and Clayton, CRI. 2005. Designing Railway Formation for the Future. *SAICE Journal*, May 2005.

Hai H. 2010. *Discrete element modeling of railroad ballast using imaging based aggregate morphology characterization*. Dissertation, University of Illinois at Urbana-Champaign, USA.

Hayakawa, Y and Oguchi, T. 2005. Evaluation of Gravel Sphericity and Roundness Based on Surface Area Measurement with a Laser Scanner. *Journal of Geology*, Volume 31, Issue 6, July 2005, pp 735-741.

Heyns, FJ. 2004. Additional Course Notes: *Geotechnical Application in Railway Track Design*. AFRICON (Pty) Ltd Training Academy, Pretoria, South Africa.

Huang, H. 2010. *Discrete Element Modelling of Railroad Ballast Using Image Based Aggregate Morphology Characterisation*. *PhD. Thesis*. University of Illinois.

Indraratna, B, Ionescu, D and Christie, D. 1998. Shear Behavior of Railway Ballast Based on Large Scale Triaxial Testing. *RTSA Journal*, Conference on Railway engineering, Darwin 20-23 June, pp 29.1-29.10.

Indraratna, B, Khabbaz, H and Salim, W. 2004. Ballast-Formation-Track Interaction Mechanism Based on Large Scale Laboratory Testing. *RTSA Journal*, Conference on Railway engineering, Darwin 20-23 June, pp 30.1-30.12.

Indraratna, B, Shahin, MA and Rujikiatkamjorn, C. 2006. *Stabilization of Rail Tracks and Underlying Soft Soil Formations*. University of Wollongong.

Indraratna, B and Salim, W. 2005. *Mechanics of Ballasted Rail Tracks: A Geotechnical Perspective*. 1<sup>st</sup> ed. Taylor and Francis Publishers.

Ionescu, D, Indraratna, B and Christie, D. 2004. Construction Potential of Recycled Railway Ballast Based on Large-Scale Triaxial Tests. *RTSA Journal*, Conference on Railway engineering, Darwin 20-23 June, pp 29.1-29.10.

Ionescu, D. 2006. Degradation of Characteristics of Ballast in the Field and their Measurements. *Proceedings, Conference on Railway Engineering*, Melbourne. pp 214-229

Janoo VC. 1998. *Quantification of shape, angularity, and surface texture of base course materials*. US Army Corps of Engineers. Cold Region Research and Engineering Laboratory. Special report 98-1.

Kaya, M. 2004. *A Study on the Stress-Strain Behaviour of Railroad ballast materials by use of parallel gradation technique*. PhD. Thesis, Middle East Technical University.

Komba, JJ. 2013. *Analytical and laser scanning techniques to determine shape properties of aggregates used in pavements*. Master's thesis, University of Pretoria, South Africa.

Krumbein WC. (1994). Measurement and geological significance of shape and roundness of sedimentary particles. *Sedimentary Petrology*, 11, pp. 64-72.

Kumar, PR. (2010). *Ballast specification for high axle load and high speed  $\geq 250$  mph*. Civil digital, seminar.

Kuo, CY and Freeman, RB. 2000. Imaging Indices for Quantification of Shape, Angularity, and Surface Texture of Aggregates. *Transportation Research Board 79th Annual Meeting*, Washington DC, January 2000, paper no: 000686.

Lanaro, F and Tolppanen, P. 2001. 3D Characterization of Course Aggregate. *Engineering Geology Journal*, Volume 65, 2002, pp 17-30.

Li D, Hyslip J, Sussmann T and Chrismer S. 2015. *Railway Geotechnics*. Taylor and Francis Group, New York.

Lin, CL and Miller, JD. 2005. 3D Characterization and Analysis of Particle Shape using X-Ray Micro tomography (XMT). *Elsevier Journal*, Volume 154, pp 61-69.

Lu, M and McDowell, GR. 2007. The Importance of Modelling Ballast Particle Shape in the Discrete Element Method. *Granular Matter Journal*, Volume 9, pp 69-80.

Masad, E, Al-Rousan, T, Bulton, J, Little, D and Tutumluer. E. 2007. *Test Methods for Characterizing Aggregate Shape, Texture and Angularity*. Transportation Research Board NCHRP Report, Report No 555, Washington.

Mora, CF. and Kwan, AKH. 1999. Sphericity, Shape Factor and Convexity Measurements of Course Aggregate for Concrete Using Digital Image Processing. *Cement and Concrete Research*. Volume 30, 2000, pp 351-358.

Murat Ozen. 2007. *Investigation of Relationship between Aggregate Shape Parameters and Concrete Strength Using Imaging Technique*. MSc thesis, Graduate school of natural and Applied Sciences of Middle East technical University.

Mvelase GM, Anochie-Boateng JK and Grabe PJ. 2012. Application of laser based technology to Quantify shape properties of railway ballast. *Proc. of the 31st Southern African transportation Conference*, Pretoria, pp. 12.

Rothman, W. 2009. Additional Course Notes: *Railway Infrastructure Maintenance Management (RIMM). Track Maintenance Management, A Spoornet Perspective*. University of Pretoria, South Africa.

Roussillon, T, Piegay, H, Sivignon, I, Tougne, L and Lavigne, F. 2008. Automatic Computation of Pebble Roundness Using Digital Imagery and Discrete Geometry. *Elsevier Journal, Computer and Geoscience*, 2009 pp1-9.

SABS 827, Standard Method for: *Sampling Aggregates*.

SABS 828, Standard Method for: *Preparation of test samples of aggregates*.

Sames, CW. 1966. *Morphometric data of some recent pebble associations and their Sedimentary Petrology*, 26, 15-31.

Selig, ET and Cantrell, DD. 2001. *Track Substructure Maintenance- -from Theory to Practice*. Prepared for American Railway Engineering and Maintenance-of-Way Association Annual Conference, Chicago Illinois.

Selig, ET and Waters, JM.1994.*Track Geotechnology and Substructure Management*. 1st ed. Thomas Telford, London.

Sneed, ED, and Folk, RL. 1958. Pebbles in the Lower Colorado River, Texas - A Study in Particle Morphogenesis. *Journal of Geology*, 66(2), 114-150.

Tolppanen P, Illerstrom A and Stephansson O. 1999. 3D Laser analysis of size, shape and roughness of railway ballast. Research in progress. *Proc. of the 7th Annual symposium, ICAR*. Austin.

Tolppanen, P, Illerstrom, A and Stephansson, O. 2008. *3D Laser Analysis of Size, Shape and Roughness of Railway Ballast*. Research in Progress, Royal Institute of Technology, Sweden.

Transnet Freight Rail. 2011. *Specification for the supply of stone*. Transnet Freight Rail technical document [S406].

Tutumluer E, Huang H and Hashash YMA. 2006. Aggregate shape effects on Ballast Tamping and railroad track lateral stability. *Proc. of the AREMA Annual conference*. Louisville, KY.

Tutumluer E, Huang H, Hashash Y and Ghaboussi J. 2007. Discrete element modelling of railroad track ballast settlement. *Proc. of the AREMA 2007 annual conference*. Chicago.

Tutumluer E, Qian, Y and Hashash YMA, Ghaboussi J and Davis D. 2011. Field validation discrete model for railroad ballast. *Proc. of the AREMA Annual conference*. Chicago.

Wadell H. (1933). Sphericity and roundness of rock particles. *Journal of Geology*, Volume 41, pp 310-331.



## 8 APPENDIX A: TRIAXIAL SAMPLE PREPARATION

- The rubber membrane was attached to the baseplate by means of the O-ring and insulating tape as shown in Figure A1.



**Figure A1: Attaching membrane to baseplate**

- The smooth surfaces of both end caps were cleaned. A thin layer of grease was applied onto the end cap surfaces. The aluminium-segregated discs were placed onto the greased surfaces. The hole in the top end plate was left exposed. Vacuum was applied through the hole. The segregated discs were evenly spaced in between as shown in Figure A2.



**Figure A2: Preparation of end caps**

- The split mould collar was placed into position. The geo-fabric was placed between the membrane and inside split mould as shown in figure A3. The purpose of the geo-fabric was to prevent damage of the membrane during placing the ballast and during the vibration process.





**Figure A3: Placing of the geofabric**

- The membrane was pulled over the collar and the second O-ring was pulled over the split mould collar as shown in Figure A4.



**Figure A4: Position of collar, geofabric and membrane**

- The weighted and graded amount of ballast was placed in the split mould after placing the initial layer by hand as shown in Figure A5.



**Figure A5: Placement of ballast**

- The split mould was filled to the top of the collar and vibrated for 30 seconds. The sample compacted to a lower level, then the collar was removed and ballast levelled by repositioning of ballast on the surface. The top end cap, with the segregated discs attached, was placed on top of the sample. The membrane was pulled over the end plate as shown in figure A6.





**Figure A6: Fitting of the top end plate**

- The sample height was measured with a steel ruler. The height of the ballast part was obtained by subtracting the total thickness of the two end caps and greased segregated discs from the measured height. A measurement was taken from the top of the end cap down to the surface of the material at four locations around the perimeter of the sample. Using this measurement and the weight of material added, the initial density of the material was found. The volume and density of the ballast sample were calculated and ranged from  $1\,593\text{ kg/m}^3$  to  $1\,714\text{ kg/m}^3$ . All samples for triaxial testing were prepared to an initial target density of  $1\,593\text{ kg/m}^3$ . This density was achievable for all grading and considered stable after the sample had been constructed.
- After fitting the second membrane, the sample was placed into position as shown in Figure A7. The triaxial chamber was tightened down. The chamber was pressurised, carefully avoiding applying the full confined pressure before removal of the vacuum. The vacuum pipe was ventilated to prevent any back-pressure.



**Figure A7: Completed ballast sample**

## 9 APPENDIX B: MATLAB CODE FOR PROCESSING LASER SCAN DATA

The main steps implemented in the MATLAB code are:

- Computing surface area for the ellipsoid;
- Determination of the ballast roundness, sphericity, flatness, elongation, shape factor;
- Classification of shape for the Zingg chart.

`% Ballast Analysis`

`% event data reserved - to be defined in a future version of MATLAB`

`% handles structure with handles and user data (see GUIDATA)`

```
set(handles.radiobutton1,'Value', 1);
set(handles.radiobutton2,'Value', 0);
set(handles.radiobutton3,'Value', 0);
axe = get(handles.edit1,'string');
axe1 = get(handles.edit2,'string');
sheet1 = str2num(cell2mat(get(handles.edit3,'string')));
sheet2 = str2num(cell2mat(get(handles.edit4,'string')));
sample1 = get(handles.edit5,'string');
x(:,1) = xlsread(cell2mat(axe(1,1)),sheet1,'B:B')./2;
x(:,2) = xlsread(cell2mat(axe(1,1)),sheet1,'C:C')./2;
x(:,3) = xlsread(cell2mat(axe(1,1)),sheet1,'D:D')./2;
x(:,4) = xlsread(cell2mat(axe(1,1)),sheet1,'E:E');
x(:,5) = xlsread(cell2mat(axe(1,1)),sheet1,'F:F');
cat = cell(length(x(:,1)),1);
% function for calculating surface area
for i=1:length(x(:,1));
x(i,6) = Surface_area(x(i,1),x(i,2),x(i,3));
end
% shape classification
shape = cell((length(x(:,1))),1);
for i=1:(length(x(:,1)))
if ((x(i,2)/x(i,1)) == 1) && ((x(i,3)/x(i,2)) == 1));
shape{i} = ['Sphere'];
elseif ((x(i,2)/x(i,1)) >= 2/3) && ((x(i,3)/x(i,2)) >= 2/3));
shape{i} = ['Cubic'];
```



```

elseif ((x(i,2)/x(i,1)) >= 2/3) && ((x(i,3)/x(i,2)) <= 2/3));
    shape{i} = ['Flaky'];
elseif ((x(i,2)/x(i,1)) <= 2/3) && ((x(i,3)/x(i,2)) <= 2/3));
    shape{i} = ['Flat & elongated'];
elseif ((x(i,2)/x(i,1)) <= 2/3) && ((x(i,3)/x(i,2)) >= 2/3));
    shape{i} = ['Elongated'];
else
    shape{i} = ['Undefined'];
end
end
names = cell(1,14);
names{1,1} = ['Part Number'];
names{1,2} = ['Category'];
names{1,3} = ['Long axis(a) L'];
names{1,4} = ['Intermediate axis(b) I'];
names{1,5} = ['Short axis(c) S'];
names{1,6} = ['Measured Surface Area(mm^2)'];
names{1,7} = ['Measured Volume (mm^3)'];
names{1,8} = ['Calculated Surface Area (mm^2)'];
names{1,9} = ['Roundness'];
names{1,10} = ['Shape'];
names{1,11} = ['Sphericity (Sph)'];
names{1,12} = ['Flatness (F)'];
names{1,13} = ['Elongation (E)'];
names{1,14} = ['Shape Factor (SF)'];
% the following line is for ratio calculation
x(:,7) = (x(:,4)./x(:,6));
% function for writing to an output excel file is written
count(:,1) = 1:length(x(:,1));
y1(:,1) = ((36.*pi.*(x(:,5).^2)).^(1/3))./x(:,4);
y1(:,2) = x(:,3)./x(:,2);
y1(:,3) = x(:,2)./x(:,1);
y1(:,4) = (x(:,3)/x(:,2))./(x(:,2)/x(:,1));
[W1, W2] = xlsread(cell2mat(axe(1,1)),sheet1,'A:A');
mus=1;

```

```
for i = 1:length(W2(:,1))
    if (strcmp(W2(i,1),") == 1)
        W2(i,1) = W2(mus,1);
    else
        mus = i;
        W2(i,1) = W2(mus,1);
    end
end
% if((length(x(:,1)) - length(W2(:,1)) ~= 0))
%
% end
```

## 10 APPENDIX C: BALLAST SCAN RESULTS

Table 8.1: Scanned particles of recycled ballast from Km 9

Category Sieve size	Long axis( <i>a</i> ) <i>L</i>	Intermediate axis( <i>b</i> ) <i>I</i>	Short axis( <i>c</i> ) <i>S</i>	Measured Surface Area(mm <sup>2</sup> )	Measured Volume (mm <sup>3</sup> )	Calculated Surface Area (mm <sup>2</sup> )	Roundness	Shape	Sphericity	Flatness ( <i>F</i> )	Elongation ( <i>E</i> )	Shape Factor ( <i>SF</i> )
53mm	49.60	35.99	28.31	19205.17	182234.72	17891.97	1.08	Cubic	0.81	0.79	0.73	1.08
53mm	44.59	34.57	24.38	16075.60	132516.40	14806.88	1.09	Cubic	0.78	0.71	0.78	0.91
37.5mm	31.26	30.21	23.82	12317.86	92824.88	10135.27	1.22	Cubic	0.80	0.79	0.97	0.82
37.5mm	37.11	25.60	22.25	10295.27	74449.93	9949.01	1.03	Cubic	0.83	0.87	0.69	1.26
37.5mm	29.94	29.36	24.14	9826.83	68520.43	9706.20	1.01	Cubic	0.82	0.82	0.98	0.84
26.5mm	20.74	17.14	14.31	4115.03	18660.56	3784.77	1.09	Cubic	0.83	0.83	0.83	1.01
26.5mm	33.09	23.32	16.79	7179.09	38338.85	7359.47	0.97	Cubic	0.77	0.72	0.70	1.02
26.5mm	32.37	23.25	16.56	6841.45	37081.18	7164.74	0.95	Cubic	0.79	0.71	0.72	0.99
26.5mm	20.26	20.03	18.87	5577.86	27612.98	4886.23	1.14	Cubic	0.79	0.94	0.99	0.95
26.5mm	29.99	22.98	20.09	6454.02	33611.75	7402.29	0.87	Cubic	0.78	0.87	0.77	1.14
26.5mm	24.12	21.01	14.75	4862.62	24556.40	4977.43	0.98	Cubic	0.84	0.70	0.87	0.81
26.5mm	20.54	17.09	12.53	3938.10	17820.45	3490.88	1.12	Cubic	0.84	0.73	0.83	0.88
19mm	20.64	15.07	13.02	3257.01	13099.25	3283.84	0.99	Cubic	0.83	0.86	0.73	1.18
13.2mm	11.83	10.97	7.39	1306.70	2719.13	1266.58	1.03	Cubic	0.72	0.67	0.93	0.73
13.2mm	11.28	9.18	6.48	1049.24	1913.78	1005.83	1.04	Cubic	0.71	0.71	0.81	0.87
9.5mm	7.22	5.72	4.88	454.30	613.13	440.51	1.03	Cubic	0.77	0.85	0.79	1.08
53mm	46.56	30.10	29.23	15825.38	137370.77	15439.55	1.02	Elongated	0.81	0.97	0.65	1.50
37.5mm	41.07	27.04	19.24	12334.36	82853.46	10410.95	1.19	Elongated	0.75	0.71	0.66	1.08
37.5mm	46.77	27.71	22.17	10946.99	70684.96	12658.84	0.86	Elongated	0.76	0.80	0.59	1.35
26.5mm	36.83	19.26	16.38	6871.12	34909.39	7020.50	0.98	Elongated	0.75	0.85	0.52	1.63
26.5mm	29.13	17.04	15.10	4945.97	21746.18	5101.32	0.97	Elongated	0.76	0.89	0.58	1.51

26.5mm	36.66	18.72	18.11	6844.32	32159.28	7255.75	0.94	Elongated	0.71	0.97	0.51	1.89
26.5mm	35.54	20.79	16.92	7099.51	39719.80	7264.86	0.98	Elongated	0.79	0.81	0.58	1.39
26.5mm	34.30	19.44	16.08	7332.18	41753.54	6577.64	1.11	Elongated	0.79	0.83	0.57	1.46
26.5mm	33.89	21.12	18.69	7346.04	39202.58	7427.74	0.99	Elongated	0.76	0.88	0.62	1.42
26.5mm	29.71	15.82	15.31	5713.03	26819.20	5000.80	1.14	Elongated	0.76	0.97	0.53	1.82
26.5mm	31.54	19.35	17.12	6576.03	33238.74	6316.73	1.04	Elongated	0.76	0.88	0.61	1.44
26.5mm	30.56	18.46	14.10	5899.90	27112.69	5401.23	1.09	Elongated	0.74	0.76	0.60	1.26
19mm	27.05	13.85	12.26	4307.82	19497.67	3775.75	1.14	Elongated	0.81	0.89	0.51	1.73
19mm	24.35	11.17	9.75	2800.61	8813.28	2684.69	1.04	Elongated	0.74	0.87	0.46	1.90
19mm	21.04	13.08	12.26	3311.71	11585.36	2946.74	1.12	Elongated	0.75	0.94	0.62	1.51
13.2mm	15.04	9.75	8.67	1497.04	3272.64	1537.12	0.97	Elongated	0.71	0.89	0.65	1.37
13.2mm	14.76	8.67	6.44	982.62	1473.99	1203.80	0.81	Elongated	0.64	0.74	0.59	1.27
9.5mm	9.69	5.98	4.88	625.70	1145.58	575.12	1.09	Elongated	0.85	0.82	0.62	1.32
9.5mm	10.33	5.88	4.63	537.83	682.87	585.33	0.92	Elongated	0.70	0.79	0.57	1.38
9.5mm	8.98	5.63	5.47	541.75	790.43	553.76	0.98	Elongated	0.76	0.97	0.63	1.55
37.5mm	32.49	28.84	15.23	7947.43	44478.04	8118.29	0.98	Flaky	0.76	0.53	0.89	0.60
37.5mm	33.53	28.98	18.47	11388.49	68621.02	9087.30	1.25	Flaky	0.71	0.64	0.86	0.74
37.5mm	32.09	26.53	16.46	8398.65	53056.65	7798.28	1.08	Flaky	0.81	0.62	0.83	0.75
26.5mm	25.79	24.77	11.60	5245.27	21289.15	5359.59	0.98	Flaky	0.71	0.47	0.96	0.49
26.5mm	28.46	25.02	7.30	4985.50	14010.95	5163.31	0.96	Flaky	0.56	0.29	0.88	0.33
26.5mm	30.55	23.80	13.01	6515.16	31940.49	6249.02	1.04	Flaky	0.75	0.55	0.78	0.70
26.5mm	37.11	27.08	13.10	5967.50	28501.09	8185.19	0.73	Flaky	0.76	0.48	0.73	0.66
26.5mm	29.63	20.96	7.84	4907.29	18951.24	4673.59	1.05	Flaky	0.70	0.37	0.71	0.53
26.5mm	26.40	21.12	13.01	5032.06	22363.50	5057.94	0.99	Flaky	0.76	0.62	0.80	0.77
26.5mm	21.22	18.35	11.23	3801.48	15330.11	3576.70	1.06	Flaky	0.79	0.61	0.86	0.71
26.5mm	20.93	17.92	11.27	3806.53	16529.09	3479.37	1.10	Flaky	0.82	0.63	0.86	0.73
26.5mm	23.57	19.06	12.64	4209.86	18445.08	4224.31	1.00	Flaky	0.80	0.66	0.81	0.82
26.5mm	19.31	18.45	11.56	3247.93	10312.99	3378.96	0.96	Flaky	0.71	0.63	0.96	0.66
19mm	25.04	17.76	10.15	3532.91	12593.06	3835.27	0.92	Flaky	0.74	0.57	0.71	0.81

19mm	19.73	15.61	9.94	2867.82	9869.64	2830.80	1.01	Flaky	0.78	0.64	0.79	0.81
19mm	25.60	18.99	6.19	3465.09	9986.07	3555.87	0.97	Flaky	0.65	0.33	0.74	0.44
19mm	20.31	16.97	6.64	2653.35	6945.42	2670.84	0.99	Flaky	0.66	0.39	0.84	0.47
19mm	20.07	14.78	8.17	2384.61	7032.82	2538.20	0.94	Flaky	0.74	0.55	0.74	0.75
19mm	17.93	16.11	6.97	2168.45	5849.29	2332.29	0.93	Flaky	0.72	0.43	0.90	0.48
19mm	19.81	13.95	8.86	2662.00	7204.45	2487.88	1.08	Flaky	0.68	0.64	0.70	0.90
13.2mm	18.97	12.94	5.77	1880.30	3628.46	1931.94	0.97	Flaky	0.61	0.45	0.68	0.65
9.5mm	7.30	7.09	2.24	435.16	439.61	385.48	1.12	Flaky	0.64	0.32	0.97	0.32
26.5mm	30.96	18.98	12.15	4936.65	21089.97	5203.30	0.95	Flat & elongated	0.75	0.64	0.61	1.04
26.5mm	33.14	19.23	10.96	5993.46	24773.39	5356.88	1.12	Flat & elongated	0.69	0.57	0.58	0.98
26.5mm	34.75	20.65	11.66	6166.93	26024.15	6024.81	1.02	Flat & elongated	0.69	0.56	0.59	0.95
26.5mm	31.72	18.64	12.24	5457.88	25651.53	5264.17	1.04	Flat & elongated	0.77	0.66	0.59	1.12
19mm	21.09	11.76	7.25	2125.88	4844.81	2139.67	0.99	Flat & elongated	0.65	0.62	0.56	1.11
13.2mm	13.96	8.66	5.68	1095.67	2023.20	1083.74	1.01	Flat & elongated	0.71	0.66	0.62	1.06
							<b>1.01</b>	<b>Mean</b>	<b>0.75</b>	<b>0.70</b>	<b>0.72</b>	<b>0.97</b>

**Table 8.2: Scanned particles of recycled ballast from Km 17**

Category Sieve size	Long axis( <i>a</i> ) <i>L</i>	Intermediate axis( <i>b</i> ) <i>I</i>	Short axis( <i>c</i> ) <i>S</i>	Measured Surface Area(mm <sup>2</sup> )	Measured Volume (mm <sup>3</sup> )	Calculated Surface Area (mm <sup>2</sup> )	Roundness	Shape	Sphericity	Flatness ( <i>F</i> )	Elongation ( <i>E</i> )	Shape Factor ( <i>SF</i> )
53.5mm	39.35	33.78	31.33	15372.22	133046.10	15202.32	1.01	Cubic	0.82	0.93	0.86	1.08
37.5mm	29.35	27.13	21.46	8136.48	48352.48	8457.02	0.96	Cubic	0.79	0.79	0.92	0.86
37.5mm	41.89	28.98	20.36	9943.85	62345.31	11406.43	0.87	Cubic	0.76	0.70	0.69	1.02
37.5mm	31.70	26.61	21.90	9653.81	66778.61	8943.40	1.08	Cubic	0.82	0.82	0.84	0.98
37.5mm	32.36	23.84	21.20	8394.12	50207.05	8295.22	1.01	Cubic	0.78	0.89	0.74	1.21
37.5mm	33.14	27.89	24.48	9546.82	62455.69	10175.45	0.93	Cubic	0.80	0.88	0.84	1.04
37.5mm	33.38	25.31	17.97	7706.77	45858.94	8108.29	0.95	Cubic	0.80	0.71	0.76	0.94
37.5mm	27.79	21.87	18.74	7213.77	44129.95	6491.56	1.11	Cubic	0.84	0.86	0.79	1.09
37.5mm	24.36	23.68	21.38	7281.86	44250.34	6725.87	1.09	Cubic	0.83	0.90	0.97	0.93
37.5mm	30.62	21.93	19.98	7416.72	43020.69	7276.66	1.02	Cubic	0.80	0.91	0.72	1.27
26.5mm	27.83	25.69	17.15	7583.48	39816.11	6938.14	1.10	Cubic	0.74	0.67	0.92	0.72
26.5mm	26.54	18.20	17.07	5476.69	30251.65	5276.05	1.04	Cubic	0.86	0.94	0.69	1.37
26.5mm	32.41	21.88	19.08	5761.79	25415.17	7409.46	0.78	Cubic	0.73	0.87	0.68	1.29
26.5mm	25.64	19.11	18.81	6339.21	33720.11	5609.28	1.14	Cubic	0.80	0.98	0.75	1.32
26.5mm	26.43	23.48	16.72	5681.23	30226.58	6169.18	0.92	Cubic	0.83	0.71	0.89	0.80
26.5mm	21.60	20.32	17.56	4841.18	19558.33	4932.43	0.98	Cubic	0.73	0.86	0.94	0.92
26.5mm	22.10	15.24	13.28	4045.93	17256.77	3532.33	1.15	Cubic	0.80	0.87	0.69	1.26
19mm	18.54	13.21	10.79	2385.75	7833.56	2496.36	0.95	Cubic	0.80	0.82	0.71	1.15
13.2mm	14.17	10.27	7.54	1411.45	3114.07	1407.49	1.00	Cubic	0.73	0.73	0.72	1.01
13.2mm	12.95	10.63	8.10	1418.28	3566.44	1392.03	1.02	Cubic	0.80	0.76	0.82	0.93
13.2mm	15.51	10.78	7.85	1585.56	4023.62	1599.12	0.99	Cubic	0.77	0.73	0.69	1.05
13.2mm	13.82	10.38	7.91	1475.70	3658.60	1424.24	1.03	Cubic	0.78	0.76	0.75	1.01
9.5mm	9.52	8.52	6.24	795.76	1473.71	819.26	0.97	Cubic	0.79	0.73	0.90	0.82
37.5mm	39.29	26.03	25.01	10869.70	71916.01	11250.54	0.96	Elongated	0.77	0.96	0.66	1.45
37.5mm	36.48	22.78	16.26	8333.45	49258.47	7740.20	1.08	Elongated	0.78	0.71	0.62	1.14
37.5mm	32.97	19.54	18.85	7227.07	41529.48	6957.28	1.04	Elongated	0.80	0.96	0.59	1.63
26.5mm	38.64	21.76	17.24	8837.67	56616.14	8113.61	1.09	Elongated	0.81	0.79	0.56	1.41

26.5mm	32.00	19.41	17.49	6892.91	36464.15	6482.36	1.06	Elongated	0.77	0.90	0.61	1.48
26.5mm	33.11	15.46	13.02	5636.24	26566.73	4974.93	1.14	Elongated	0.76	0.84	0.47	1.80
19mm	23.41	13.57	11.64	3394.46	12025.03	3204.69	1.06	Elongated	0.75	0.86	0.58	1.48
13.2mm	20.70	8.32	7.44	1921.59	4368.26	1699.80	1.14	Elongated	0.67	0.89	0.40	2.22
9.5mm	11.04	6.42	5.88	642.14	866.90	741.07	0.87	Elongated	0.68	0.92	0.58	1.57
63mm	51.95	40.33	23.43	17589.93	129949.99	18441.81	0.95	Flaky	0.71	0.58	0.78	0.75
63mm	36.90	35.88	22.94	15449.53	135908.65	12729.31	1.22	Flaky	0.83	0.64	0.97	0.66
37.5mm	37.45	31.78	18.21	11119.24	78103.63	10576.97	1.05	Flaky	0.79	0.57	0.85	0.67
37.5mm	41.82	30.22	14.44	10242.30	65495.91	10235.60	1.00	Flaky	0.77	0.48	0.72	0.66
37.5mm	37.95	31.54	19.15	11943.06	84523.18	10867.13	1.10	Flaky	0.78	0.61	0.83	0.73
37.5mm	36.67	24.55	15.78	7614.15	38557.07	8080.91	0.94	Flaky	0.72	0.64	0.67	0.96
37.5mm	35.97	28.56	12.83	8489.32	43406.14	8251.93	1.03	Flaky	0.70	0.45	0.79	0.57
37.5mm	31.90	26.33	16.03	7774.20	43528.55	7625.45	1.02	Flaky	0.77	0.61	0.83	0.74
37.5mm	28.56	25.50	16.14	7085.64	39921.55	6836.06	1.04	Flaky	0.80	0.63	0.89	0.71
37.5mm	29.72	27.43	18.00	7731.21	41919.78	7844.25	0.99	Flaky	0.75	0.66	0.92	0.71
26.5mm	26.71	22.83	13.86	5599.53	26506.22	5564.61	1.01	Flaky	0.77	0.61	0.85	0.71
26.5mm	26.47	19.55	9.86	4425.93	16552.47	4282.56	1.03	Flaky	0.71	0.50	0.74	0.68
26.5mm	29.18	22.06	13.99	5459.22	27967.20	5857.75	0.93	Flaky	0.82	0.63	0.76	0.84
26.5mm	24.83	18.93	10.86	4269.45	16963.85	4103.96	1.04	Flaky	0.75	0.57	0.76	0.75
26.5mm	26.17	24.74	12.32	5584.49	25892.95	5544.37	1.01	Flaky	0.76	0.50	0.95	0.53
26.5mm	23.22	20.38	11.46	4572.16	21473.58	4198.63	1.09	Flaky	0.82	0.56	0.88	0.64
26.5mm	24.85	20.80	13.35	5157.16	23506.49	4820.82	1.08	Flaky	0.77	0.64	0.84	0.77
26.5mm	29.82	21.06	12.57	5371.30	23041.90	5508.53	0.97	Flaky	0.73	0.60	0.71	0.84
26.5mm	25.55	21.33	11.56	5325.67	24022.71	4720.90	1.12	Flaky	0.76	0.54	0.84	0.65
26.5mm	25.77	21.84	12.01	5684.35	28327.49	4915.62	1.16	Flaky	0.79	0.55	0.85	0.65
26.5mm	25.75	18.87	8.60	4213.59	15968.11	3882.00	1.09	Flaky	0.73	0.46	0.73	0.62
26.5mm	28.10	24.85	8.07	4998.37	17683.81	5189.09	0.96	Flaky	0.66	0.32	0.88	0.37
26.5mm	29.17	25.13	9.02	5526.61	19748.18	5567.24	0.99	Flaky	0.64	0.36	0.86	0.42
26.5mm	21.59	20.27	10.59	3736.33	15295.88	3815.07	0.98	Flaky	0.80	0.52	0.94	0.56
26.5mm	20.61	20.42	10.61	3685.91	14748.44	3699.11	1.00	Flaky	0.79	0.52	0.99	0.52
26.5mm	23.26	19.26	12.19	4383.07	21572.55	4142.17	1.05	Flaky	0.86	0.63	0.83	0.76
26.5mm	25.72	21.85	5.72	3863.14	9570.25	3979.21	0.97	Flaky	0.56	0.26	0.85	0.31
19mm	21.46	15.44	5.97	2672.27	7036.51	2518.94	1.06	Flaky	0.66	0.39	0.72	0.54

19mm	18.35	16.55	9.48	2688.04	8072.79	2731.10	0.98	Flaky	0.72	0.57	0.90	0.64	
19mm	16.32	14.67	8.37	1991.74	5743.90	2147.09	0.93	Flaky	0.78	0.57	0.90	0.64	
19mm	16.71	15.04	6.60	1808.92	4555.48	2038.70	0.88	Flaky	0.73	0.44	0.90	0.49	
19mm	13.83	13.33	8.07	1598.41	4153.60	1723.63	0.93	Flaky	0.78	0.61	0.96	0.63	
19mm	20.07	18.02	7.94	2735.43	7198.32	2936.84	0.93	Flaky	0.66	0.44	0.90	0.49	
13.2mm	11.46	8.75	4.33	768.82	1205.07	827.87	0.93	Flaky	0.71	0.50	0.76	0.65	
13.2mm	14.87	10.74	5.30	1244.72	2625.53	1308.50	0.95	Flaky	0.74	0.49	0.72	0.68	
13.2mm	11.41	9.50	6.16	1125.02	2262.97	1014.57	1.11	Flaky	0.74	0.65	0.83	0.78	
9.5mm	11.46	8.75	4.40	771.72	1213.72	833.25	0.93	Flaky	0.71	0.50	0.76	0.66	
26.5mm	34.71	21.59	13.79	6859.18	35210.33	6640.76	1.03	Flat & elongated	0.76	0.64	0.62	1.03	
19mm	28.97	18.95	10.06	3871.57	13602.99	4557.21	0.85	Flat & elongated	0.71	0.53	0.65	0.81	
19mm	24.16	15.31	8.94	3043.76	9179.38	3170.42	0.96	Flat & elongated	0.70	0.58	0.63	0.92	
19mm	24.89	16.58	9.47	3381.62	11563.05	3528.44	0.96	Flat & elongated	0.73	0.57	0.67	0.86	
13.2mm	22.47	13.47	7.24	2409.94	5822.21	2499.76	0.96	Flat & elongated	0.65	0.54	0.60	0.90	
13.2mm	18.09	11.93	4.92	1697.39	3107.43	1656.53	1.02	Flat & elongated	0.61	0.41	0.66	0.63	
9.5mm	12.69	7.74	4.20	844.75	1279.59	815.34	1.03	Flat & elongated	0.67	0.54	0.61	0.89	
9.5mm	14.45	8.52	3.41	793.71	1035.60	928.98	0.85	Flat & elongated	0.62	0.40	0.59	0.68	
9.5mm	11.73	6.63	3.30	573.92	680.08	622.78	0.92	Flat & elongated	0.65	0.50	0.57	0.88	
<b>1.00</b>									<b>Mean</b>	<b>0.75</b>	<b>0.66</b>	<b>0.77</b>	<b>0.89</b>



**Table 8.3: Scanned particles of recycled ballast from Km 31**

Category Sieve size	Long axis( <i>a</i> ) <i>L</i>	Intermediate axis( <i>b</i> ) <i>I</i>	Short axis( <i>c</i> ) <i>S</i>	Measured Surface Area(mm <sup>2</sup> )	Measured Volume (mm <sup>3</sup> )	Calculated Surface Area (mm <sup>2</sup> )	Roundness	Shape	Sphericity	Flatness ( <i>F</i> )	Elongation ( <i>E</i> )	Shape Factor ( <i>SF</i> )
53mm	50.11	36.19	25.41	16172.83	123335.22	17156.74	0.94	Cubic	0.74	0.70	0.72	0.97
37.5mm	30.86	30.47	23.88	9820.92	61760.83	10119.17	0.97	Cubic	0.77	0.78	0.99	0.79
37.5mm	32.03	28.46	22.24	10211.00	69163.66	9523.20	1.08	Cubic	0.80	0.78	0.89	0.88
37.5mm	38.24	31.45	24.28	10735.83	70421.88	12252.50	0.88	Cubic	0.77	0.77	0.82	0.94
37.5mm	33.20	22.42	20.39	8161.50	46301.69	7963.53	1.02	Cubic	0.76	0.91	0.68	1.35
37.5mm	31.18	23.91	20.40	7540.12	43140.08	7900.32	0.95	Cubic	0.79	0.85	0.77	1.11
37.5mm	33.05	28.69	23.79	9990.91	68374.26	10179.56	0.98	Cubic	0.81	0.83	0.87	0.96
37.5mm	27.30	26.93	21.15	8628.70	53666.24	7918.42	1.09	Cubic	0.80	0.79	0.99	0.80
37.5mm	27.28	22.16	15.62	5701.16	26788.06	5860.67	0.97	Cubic	0.76	0.70	0.81	0.87
37.5mm	36.02	29.94	20.12	10654.95	76649.45	10261.12	1.04	Cubic	0.82	0.67	0.83	0.81
37.5mm	28.78	27.76	23.19	8718.19	55232.16	8864.57	0.98	Cubic	0.80	0.84	0.96	0.87
37.5mm	35.49	25.08	19.77	8377.41	48242.34	8886.00	0.94	Cubic	0.76	0.79	0.71	1.12
37.5mm	24.16	21.47	18.46	5699.08	32049.63	5722.86	1.00	Cubic	0.86	0.86	0.89	0.97
37.5mm	27.74	22.51	18.87	6690.89	39337.72	6635.77	1.01	Cubic	0.84	0.84	0.81	1.03
37.5mm	33.65	23.39	16.96	8193.67	44988.89	7514.23	1.09	Cubic	0.75	0.73	0.70	1.04
26.5mm	28.12	20.53	13.99	5307.01	25115.58	5395.61	0.98	Cubic	0.78	0.68	0.73	0.93
26.5mm	21.98	21.84	17.68	5030.53	25017.08	5273.66	0.95	Cubic	0.82	0.81	0.99	0.81
26.5mm	38.23	31.44	24.27	10757.63	70368.03	12244.31	0.88	Cubic	0.77	0.77	0.82	0.94
26.5mm	23.43	18.08	17.64	4672.68	20960.26	4863.54	0.96	Cubic	0.79	0.98	0.77	1.26
26.5mm	23.49	18.03	14.02	4397.20	20935.38	4266.53	1.03	Cubic	0.84	0.78	0.77	1.01
26.5mm	21.55	18.39	13.00	3812.39	16450.52	3888.32	0.98	Cubic	0.82	0.71	0.85	0.83
19mm	18.11	14.43	10.58	2475.87	8097.19	2573.28	0.96	Cubic	0.79	0.73	0.80	0.92
19mm	13.59	12.97	8.96	1644.54	4449.82	1754.75	0.93	Cubic	0.80	0.69	0.95	0.72
13.2mm	12.98	11.54	8.70	1630.69	4537.05	1534.22	1.06	Cubic	0.81	0.75	0.89	0.85
13.2mm	10.99	8.03	6.85	887.82	1556.66	925.02	0.96	Cubic	0.73	0.85	0.73	1.17
9.5mm	8.12	7.07	5.93	675.32	1255.27	620.66	1.09	Cubic	0.83	0.84	0.87	0.96
37.5mm	39.34	24.74	21.80	10234.31	66192.18	10096.65	1.01	Elongated	0.77	0.88	0.63	1.40

37.5mm	32.95	21.61	20.61	7445.42	40413.66	7781.78	0.95	Elongated	0.76	0.95	0.66	1.45	
26.5mm	36.26	19.13	16.93	6628.93	34070.81	7017.94	0.94	Elongated	0.77	0.89	0.53	1.68	
26.5mm	38.78	21.68	15.80	7647.93	45912.02	7788.08	0.98	Elongated	0.81	0.73	0.56	1.30	
19mm	24.89	16.00	12.14	3843.91	13840.74	3836.95	1.00	Elongated	0.73	0.76	0.64	1.18	
37.5mm	35.69	29.42	19.05	9115.14	52962.87	9800.60	0.93	Flaky	0.75	0.65	0.82	0.79	
37.5mm	38.56	31.51	18.25	12578.89	79387.83	10775.68	1.16	Flaky	0.71	0.58	0.82	0.71	
37.5mm	37.36	29.92	15.87	9018.83	50027.79	9534.72	0.94	Flaky	0.73	0.53	0.80	0.66	
37.5mm	40.25	30.11	17.44	9701.21	60160.89	10591.64	0.92	Flaky	0.77	0.58	0.75	0.77	
37.5mm	31.51	30.53	19.42	9075.75	55053.58	9220.94	0.98	Flaky	0.77	0.64	0.97	0.66	
37.5mm	40.35	29.69	17.16	10127.00	61508.48	10436.56	0.97	Flaky	0.74	0.58	0.74	0.79	
37.5mm	35.01	29.84	18.13	9550.54	56854.17	9532.93	1.00	Flaky	0.75	0.61	0.85	0.71	
37.5mm	34.52	30.65	18.74	9328.16	56112.70	9763.35	0.95	Flaky	0.76	0.61	0.89	0.69	
37.5mm	28.05	22.26	14.10	5811.21	30722.14	5727.67	1.01	Flaky	0.82	0.63	0.79	0.80	
37.5mm	34.67	29.29	15.14	8369.52	42876.57	8651.05	0.97	Flaky	0.71	0.52	0.84	0.61	
37.5mm	34.67	29.27	15.13	8371.31	42876.09	8643.38	0.97	Flaky	0.71	0.52	0.84	0.61	
26.5mm	26.91	20.61	13.46	5906.36	31235.25	5125.24	1.15	Flaky	0.81	0.65	0.77	0.85	
26.5mm	29.73	23.91	11.83	6190.45	26617.24	5912.30	1.04	Flaky	0.70	0.49	0.80	0.61	
26.5mm	28.91	20.42	11.67	4982.00	22170.82	5087.71	0.98	Flaky	0.77	0.57	0.71	0.81	
26.5mm	26.92	20.59	13.45	5905.43	31238.66	5122.86	1.15	Flaky	0.81	0.65	0.76	0.85	
26.5mm	21.38	20.84	11.01	3901.90	16379.04	3931.38	0.99	Flaky	0.80	0.53	0.97	0.54	
26.5mm	20.08	18.80	10.99	3228.17	13308.95	3451.03	0.93	Flaky	0.84	0.58	0.94	0.62	
19mm	21.54	16.22	9.27	3024.11	9712.73	3039.14	1.00	Flaky	0.73	0.57	0.75	0.76	
19mm	18.73	17.64	8.13	2864.33	8801.62	2748.15	1.04	Flaky	0.72	0.46	0.94	0.49	
19mm	16.67	16.65	10.12	2381.03	7902.34	2621.16	0.91	Flaky	0.81	0.61	1.00	0.61	
19mm	17.99	13.68	8.66	2052.17	5940.87	2239.84	0.92	Flaky	0.77	0.63	0.76	0.83	
19mm	20.06	15.01	7.55	2154.59	5532.84	2494.05	0.86	Flaky	0.70	0.50	0.75	0.67	
9.5mm	10.42	8.75	4.71	771.81	1379.82	788.44	0.98	Flaky	0.78	0.54	0.84	0.64	
9.5mm	11.28	9.50	4.85	773.03	1059.73	908.40	0.85	Flaky	0.65	0.51	0.84	0.61	
37.5mm	35.73	23.47	15.61	7773.34	43625.39	7622.35	1.02	Flat & elongated	0.77	0.66	0.66	1.01	
37.5mm	45.94	29.01	17.67	11396.10	74983.37	11606.53	0.98	Flat & elongated	0.75	0.61	0.63	0.96	
19mm	26.17	16.73	7.42	3538.23	8844.27	3419.84	1.03	Flat & elongated	0.58	0.44	0.64	0.69	
19mm	22.41	14.08	8.94	2892.31	9537.56	2793.19	1.03	Flat & elongated	0.75	0.63	0.63	1.01	
								<b>0.98</b>	<b>Mean</b>	<b>0.77</b>	<b>0.69</b>	<b>0.80</b>	<b>0.89</b>

**Table 8.4: Scanned particles of recycled ballast from Km 32**

Category Sieve size	Long axis(a) <i>L</i>	Intermediate axis(b) <i>I</i>	Short axis(c) <i>S</i>	Measured Surface Area(mm <sup>2</sup> )	Measured Volume (mm <sup>3</sup> )	Calculated Surface Area (mm <sup>2</sup> )	Roundness	Shape	Sphericity	Flatness ( <i>F</i> )	Elongation ( <i>E</i> )	Shape Factor ( <i>SF</i> )
63mm	46.66	35.92	25.57	17043.28	147951.99	16152.48	1.05	Cubic	0.79	0.71	0.77	0.92
37.5mm	39.93	31.99	23.49	12362.06	89111.06	12605.39	0.98	Cubic	0.78	0.73	0.80	0.92
37.5mm	39.30	34.60	23.14	12716.65	87591.03	13068.46	0.97	Cubic	0.75	0.67	0.88	0.76
37.5mm	35.23	27.43	25.17	10572.87	73864.23	10715.88	0.99	Cubic	0.81	0.92	0.78	1.18
37.5mm	34.57	30.68	26.07	10901.32	73139.95	11613.73	0.93	Cubic	0.78	0.85	0.89	0.96
37.5mm	29.15	22.44	16.35	6431.03	33532.60	6379.59	1.01	Cubic	0.78	0.73	0.77	0.95
37.5mm	31.82	26.44	18.30	8066.60	43962.13	8120.94	0.99	Cubic	0.75	0.69	0.83	0.83
37.5mm	31.18	23.91	20.40	7540.12	43140.08	7900.32	0.95	Cubic	0.79	0.85	0.77	1.11
37.5mm	28.88	26.92	22.07	10104.48	73773.96	8447.77	1.19	Cubic	0.84	0.82	0.93	0.88
37.5mm	27.45	24.43	18.48	6996.09	41867.57	6883.29	1.02	Cubic	0.83	0.76	0.89	0.85
37.5mm	42.41	30.20	24.71	13869.52	105410.45	13060.11	1.06	Cubic	0.78	0.82	0.71	1.15
26.5mm	27.84	18.77	12.75	5711.89	27898.58	4813.53	1.19	Cubic	0.78	0.68	0.67	1.01
26.5mm	29.09	20.17	15.37	4997.41	21038.55	5737.85	0.87	Cubic	0.74	0.76	0.69	1.10
26.5mm	22.75	16.33	15.78	3545.79	12558.76	4170.20	0.85	Cubic	0.74	0.97	0.72	1.35
26.5mm	27.13	20.49	15.15	5082.05	24579.20	5438.16	0.93	Cubic	0.80	0.74	0.76	0.98
26.5mm	24.66	22.08	20.55	6297.21	33528.96	6313.29	1.00	Cubic	0.80	0.93	0.90	1.04
26.5mm	19.69	16.49	14.01	3638.82	17048.64	3503.61	1.04	Cubic	0.88	0.85	0.84	1.01
19mm	20.33	18.70	15.19	3542.92	13010.70	4094.08	0.86	Cubic	0.76	0.81	0.92	0.88
19mm	18.98	16.75	11.43	2929.40	9552.39	3088.37	0.95	Cubic	0.74	0.68	0.88	0.77
13.2mm	17.30	12.27	8.54	1848.93	4649.97	1993.76	0.93	Cubic	0.73	0.70	0.71	0.98
53.5mm	45.71	27.86	19.81	13320.15	95283.58	11798.12	1.12	Elongated	0.76	0.71	0.61	1.17
37.5mm	52.83	32.20	25.04	16061.94	121590.61	16448.88	0.98	Elongated	0.74	0.78	0.61	1.28
37.5mm	33.61	21.96	18.98	6335.68	34801.40	7627.92	0.83	Elongated	0.81	0.86	0.65	1.32
37.5mm	41.50	24.94	17.70	10309.88	65577.52	9563.08	1.08	Elongated	0.76	0.71	0.60	1.18
37.5mm	43.15	24.58	24.42	11072.77	72424.90	11576.49	0.95	Elongated	0.76	0.99	0.57	1.74

37.5mm	38.43	23.86	20.73	9196.37	59042.59	9418.85	0.98	Elongated	0.80	0.87	0.62	1.40
26.5mm	31.40	19.30	13.55	5171.42	23001.46	5589.63	0.93	Elongated	0.76	0.70	0.61	1.14
26.5mm	33.30	21.71	15.98	7356.28	42622.15	6877.14	1.08	Elongated	0.80	0.74	0.65	1.13
26.5mm	30.18	17.30	14.87	5717.90	30481.58	5264.23	1.09	Elongated	0.83	0.86	0.57	1.50
13.2mm	16.43	9.94	7.95	1580.68	3810.03	1600.09	0.99	Elongated	0.75	0.80	0.61	1.32
63mm	53.26	36.83	24.17	17121.43	146216.40	17860.24	0.96	Flaky	0.78	0.66	0.69	0.95
63mm	53.27	38.98	18.70	16363.72	103862.71	16871.07	0.97	Flaky	0.65	0.48	0.73	0.66
63mm	48.98	42.94	18.71	16332.51	104405.04	16957.46	0.96	Flaky	0.66	0.44	0.88	0.50
37.5mm	31.35	27.48	16.64	7540.51	44675.54	7894.74	0.95	Flaky	0.81	0.61	0.88	0.69
37.5mm	31.32	27.47	16.63	7531.01	44575.07	7882.29	0.95	Flaky	0.81	0.61	0.88	0.69
37.5mm	31.36	27.51	16.63	7538.41	44658.25	7897.59	0.95	Flaky	0.81	0.60	0.88	0.69
37.5mm	25.74	23.66	15.47	6409.80	34898.85	5842.48	1.10	Flaky	0.81	0.65	0.92	0.71
37.5mm	31.76	27.68	14.27	7428.36	42072.97	7521.86	0.99	Flaky	0.79	0.52	0.87	0.59
37.5mm	30.43	28.57	16.44	7742.48	45415.70	7894.40	0.98	Flaky	0.80	0.58	0.94	0.61
37.5mm	28.72	23.64	15.33	6549.76	33910.32	6338.72	1.03	Flaky	0.77	0.65	0.82	0.79
37.5mm	32.19	27.71	17.17	7802.43	43784.77	8229.78	0.95	Flaky	0.77	0.62	0.86	0.72
37.5mm	27.59	26.64	7.62	5537.25	18173.97	5356.31	1.03	Flaky	0.60	0.29	0.97	0.30
26.5mm	31.43	29.61	19.68	9352.39	56052.26	9053.20	1.03	Flaky	0.76	0.66	0.94	0.71
26.5mm	32.72	23.12	10.07	5400.44	21082.87	5936.81	0.91	Flaky	0.68	0.44	0.71	0.62
26.5mm	24.37	21.36	12.87	4556.71	19495.28	4759.26	0.96	Flaky	0.77	0.60	0.88	0.69
26.5mm	37.19	26.64	17.45	8285.63	44908.03	9065.54	0.92	Flaky	0.74	0.65	0.72	0.91
26.5mm	28.28	25.00	14.33	6807.91	35815.87	6333.68	1.08	Flaky	0.77	0.57	0.88	0.65
26.5mm	28.26	24.94	14.30	6812.06	35815.54	6312.26	1.08	Flaky	0.77	0.57	0.88	0.65
26.5mm	29.93	22.67	13.46	5133.18	21785.85	6003.18	0.85	Flaky	0.73	0.59	0.76	0.78
26.5mm	30.16	24.85	11.12	5661.93	24385.98	6042.50	0.93	Flaky	0.72	0.45	0.82	0.54
26.5mm	32.37	25.64	14.53	6527.85	30649.62	7254.31	0.90	Flaky	0.73	0.57	0.79	0.72
26.5mm	28.14	24.79	11.43	5623.41	26230.87	5738.26	0.98	Flaky	0.76	0.46	0.88	0.52
26.5mm	25.05	24.39	11.33	4364.90	17907.05	5124.15	0.85	Flaky	0.76	0.46	0.97	0.48
26.5mm	24.58	22.71	10.48	4575.62	17992.56	4628.35	0.99	Flaky	0.73	0.46	0.92	0.50
19mm	20.95	20.29	6.88	2431.48	6451.20	3226.36	0.75	Flaky	0.69	0.34	0.97	0.35
13.2mm	17.65	15.86	7.61	2248.21	5590.32	2341.87	0.96	Flaky	0.68	0.48	0.90	<b>0.53</b>
37.5mm	50.15	30.62	15.88	13128.36	84666.51	12547.12	1.04	Flat & elongated	0.71	0.52	0.61	0.85
26.5mm	37.51	22.35	14.44	7175.92	33890.57	7426.90	0.97	Flat & elongated	0.71	0.65	0.60	1.08

26.5mm	32.18	20.07	11.76	5893.47	26325.47	5530.29	1.06	Flat & elongated	0.73	0.59	0.62	0.94
19mm	28.80	18.87	8.30	4176.07	12794.91	4245.16	0.98	Flat & elongated	0.63	0.44	0.66	0.67
19mm	26.79	17.44	5.32	3499.79	8855.24	3341.14	1.05	Flat & elongated	0.59	0.31	0.65	0.47
							<b>0.98</b>	<b>Mean</b>	<b>0.76</b>	<b>0.66</b>	<b>0.78</b>	<b>0.87</b>

**Table 8.5: Scanned particles of freshly crushed**

Category Sieve size	Long axis( <i>a</i> ) <i>L</i>	Intermediate axis( <i>b</i> ) <i>I</i>	Short axis( <i>c</i> ) <i>S</i>	Measured Surface Area(mm <sup>2</sup> )	Measured Volume (mm <sup>3</sup> )	Calculated Surface Area (mm <sup>2</sup> )	Roundness	Shape	Sphericity	Flatness ( <i>F</i> )	Elongation ( <i>E</i> )	Shape Factor ( <i>SF</i> )
53.5mm	30.35	28.40	25.84	12134.94	94931.72	9984.27	1.22	Cubic	0.83	0.91	0.94	0.97
53.5mm	39.69	33.90	25.23	13716.68	109764.70	13559.61	1.01	Cubic	0.81	0.74	0.85	0.87
37.5mm	38.70	29.18	25.42	11824.83	83995.70	12061.40	0.98	Cubic	0.78	0.87	0.75	1.15
37.5mm	35.58	27.09	20.15	9765.47	60218.64	9475.68	1.03	Cubic	0.76	0.74	0.76	0.98
37.5mm	33.43	27.85	25.60	10701.12	72095.51	10510.68	1.02	Cubic	0.78	0.92	0.83	1.10
26.5mm	27.61	21.04	18.14	6307.84	31270.14	6181.00	1.02	Cubic	0.76	0.86	0.76	1.13
26.5mm	26.86	23.33	16.11	5775.69	26321.16	6098.57	0.94	Cubic	0.74	0.69	0.87	0.80
19mm	21.32	18.59	16.64	3892.70	13104.28	4455.04	0.88	Cubic	0.69	0.89	0.87	1.03
19mm	19.44	15.41	13.18	2897.54	10072.00	3201.33	0.91	Cubic	0.78	0.86	0.79	1.08
19mm	13.68	11.28	9.51	1635.93	4043.03	1651.91	0.99	Cubic	0.75	0.84	0.83	1.02
9.5mm	5.97	4.08	2.91	226.17	202.30	229.73	0.98	Cubic	0.74	0.71	0.68	1.05
9.5mm	9.32	6.95	6.77	683.54	1012.94	737.08	0.93	Cubic	0.71	0.97	0.75	1.31
9.5mm	9.53	6.47	6.13	688.45	1146.72	675.65	1.02	Cubic	0.77	0.95	0.68	1.40
53.5mm	54.29	33.50	22.81	16901.27	134034.13	16556.13	1.02	Elongated	0.75	0.68	0.62	1.10
53.5mm	65.49	30.32	30.11	22076.81	191927.32	21026.35	1.05	Elongated	0.73	0.99	0.46	2.15
53.5mm	51.95	34.41	29.20	17399.59	147214.53	18337.99	0.95	Elongated	0.77	0.85	0.66	1.28
37.5mm	46.53	26.58	19.75	11352.66	72116.30	11593.97	0.98	Elongated	0.74	0.74	0.57	1.30
26.5mm	39.63	17.30	15.64	7186.40	34337.89	6857.87	1.05	Elongated	0.71	0.90	0.44	2.07
26.5mm	31.50	20.46	15.95	6991.30	38000.63	6303.28	1.11	Elongated	0.78	0.78	0.65	1.20
26.5mm	42.79	17.57	16.66	7965.29	41299.33	7662.04	1.04	Elongated	0.73	0.95	0.41	2.31
26.5mm	49.95	19.14	17.35	9256.94	44963.24	9458.24	0.98	Elongated	0.66	0.91	0.38	2.36

19mm	21.10	13.16	12.94	3032.94	9296.70	3060.44	0.99	Elongated	0.70	0.98	0.62	1.58
19mm	21.91	13.00	10.60	2997.89	10151.78	2809.15	1.06	Elongated	0.76	0.82	0.59	1.38
19mm	20.11	12.95	12.62	3084.73	10295.24	2873.30	1.08	Elongated	0.74	0.97	0.64	1.51
13.2mm	21.94	11.75	8.66	1989.81	4880.17	2387.16	0.83	Elongated	0.70	0.74	0.54	1.38
9.5mm	17.44	6.25	4.73	824.59	1050.90	985.18	0.84	Elongated	0.61	0.76	0.36	2.11
63mm	41.29	39.87	25.15	16376.25	146255.33	15703.84	1.04	Flaky	0.82	0.63	0.97	0.65
53.5mm	43.93	42.87	22.83	16550.70	113594.89	16677.26	0.99	Flaky	0.69	0.53	0.98	0.55
53.5mm	48.57	37.91	11.28	15306.83	85397.15	13270.30	1.15	Flaky	0.61	0.30	0.78	0.38
53.5mm	48.77	40.13	16.82	14686.64	89167.54	15450.91	0.95	Flaky	0.66	0.42	0.82	0.51
53.5mm	46.36	33.69	11.98	12453.91	69067.13	11638.88	1.08	Flaky	0.65	0.36	0.73	0.49
37.5mm	38.45	32.56	21.03	12231.15	75147.22	11734.81	1.04	Flaky	0.70	0.65	0.85	0.76
37.5mm	34.06	23.34	6.36	6223.28	19473.02	5587.12	1.11	Flaky	0.56	0.27	0.69	0.40
19mm	21.71	16.45	10.14	2816.95	8196.34	3211.53	0.88	Flaky	0.70	0.62	0.76	0.81
19mm	16.54	14.58	3.53	1895.67	3145.61	1690.30	1.12	Flaky	0.55	0.24	0.88	0.27
13.2mm	11.62	9.48	4.81	790.24	1320.54	926.66	0.85	Flaky	0.74	0.51	0.82	0.62
13.2mm	16.44	11.86	3.98	1469.96	2883.22	1432.64	1.03	Flaky	0.67	0.34	0.72	0.47
13.2mm	14.52	13.35	6.54	1373.48	2660.65	1640.97	0.84	Flaky	0.68	0.49	0.92	0.53
9.5mm	9.15	7.77	4.18	541.92	675.70	615.70	0.88	Flaky	0.69	0.54	0.85	0.63
53.5mm	64.70	39.08	25.46	24538.05	219311.47	22515.27	1.09	Flat & elongated	0.72	0.65	0.60	1.08
37.5mm	52.38	32.06	15.08	13432.13	80809.43	13294.05	1.01	Flat & elongated	0.67	0.47	0.61	0.77
37.5mm	40.50	25.60	10.56	9450.28	46993.56	7924.47	1.19	Flat & elongated	0.67	0.41	0.63	0.65
37.5mm	43.91	27.68	11.57	8794.51	39073.41	9323.79	0.94	Flat & elongated	0.63	0.42	0.63	0.66
37.5mm	53.35	25.63	16.64	13005.93	71014.86	11858.90	1.10	Flat & elongated	0.64	0.65	0.48	1.35
26.5mm	40.60	24.15	12.41	8189.06	38977.65	7965.59	1.03	Flat & elongated	0.68	0.51	0.59	0.86
26.5mm	37.01	17.69	8.18	4758.66	15430.95	5060.77	0.94	Flat & elongated	0.63	0.46	0.48	0.97
26.5mm	35.11	23.12	9.50	5530.96	19058.32	6220.69	0.89	Flat & elongated	0.62	0.41	0.66	0.62
26.5mm	40.95	22.41	6.18	5582.70	17273.41	6394.00	0.87	Flat & elongated	0.58	0.28	0.55	0.50
19mm	27.54	14.63	8.87	3361.96	9698.25	3435.69	0.98	Flat & elongated	0.65	0.61	0.53	1.14
19mm	28.56	15.89	7.14	3424.29	8571.97	3517.09	0.97	Flat & elongated	0.59	0.45	0.56	0.81
13.2mm	20.09	10.03	5.26	1602.00	3300.54	1623.45	0.99	Flat & elongated	0.67	0.52	0.50	1.05
13.2mm	19.04	10.96	5.38	1593.37	3498.75	1665.61	0.95	Flat & elongated	0.70	0.49	0.58	0.85
13.2mm	18.68	9.66	4.27	1354.33	2147.61	1383.70	0.98	Flat & elongated	0.59	0.44	0.52	0.85
9.5mm	14.50	6.67	4.17	775.92	1012.22	823.70	0.94	Flat & elongated	0.63	0.63	0.46	1.36

9.5mm	10.54	6.22	3.63	565.09	709.31	557.12	1.01	Flat & elongated	0.68	0.58	0.59	0.99	
9.5mm	9.50	4.93	2.74	393.56	383.11	385.78	1.02	Flat & elongated	0.65	0.56	0.52	1.07	
9.5mm	9.12	4.63	2.46	360.85	337.50	341.75	1.05	Flat & elongated	0.65	0.53	0.51	1.05	
9.5mm	15.77	5.56	3.12	648.34	566.01	706.95	0.92	Flat & elongated	0.51	0.56	0.35	1.59	
								<b>0.99</b>	<b>Mean</b>	<b>0.69</b>	<b>0.65</b>	<b>0.66</b>	<b>0.98</b>

**Table 8.6: Scanned particles of river pebbles**

Category Sieve size	Long axis(a) <i>L</i>	Intermediate axis(b) <i>I</i>	Short axis(c) <i>S</i>	Measured Surface Area(mm <sup>2</sup> )	Measured Volume (mm <sup>3</sup> )	Calculated Surface Area (mm <sup>2</sup> )	Roundness	Shape	Sphericity	Flatness ( <i>F</i> )	Elongation ( <i>E</i> )	Shape Factor ( <i>SF</i> )
63mm	41.57	40.13	31.06	20206.34	234415.57	17711.39	1.14	Cubic	0.91	0.77	0.97	0.80
53.5mm	41.09	31.26	28.80	15353.07	165724.62	14197.33	1.09	Cubic	0.95	0.92	0.76	1.21
26.5mm	33.41	22.45	15.66	6973.21	46851.88	6990.20	1.00	Cubic	0.90	0.70	0.67	1.04
26.5mm	28.99	21.28	15.50	6245.12	39421.92	5960.06	1.05	Cubic	0.90	0.73	0.73	0.99
26.5mm	29.23	19.58	16.17	6470.63	39220.11	5798.61	1.11	Cubic	0.86	0.83	0.67	1.23
26.5mm	29.25	20.03	13.73	5855.86	34230.28	5432.37	1.08	Cubic	0.87	0.69	0.68	1.00
19mm	18.55	14.75	11.02	2788.53	12924.01	2719.22	1.02	Cubic	0.96	0.75	0.80	0.94
19mm	16.40	14.72	10.23	2661.69	11309.97	2375.51	1.12	Cubic	0.92	0.70	0.90	0.77
19mm	19.23	13.02	10.63	2867.70	12201.60	2525.66	1.14	Cubic	0.89	0.82	0.68	1.21
19mm	15.55	14.88	10.39	2390.64	9928.23	2317.75	1.03	Cubic	0.93	0.70	0.96	0.73
19mm	13.14	12.92	9.85	1887.11	6923.06	1796.16	1.05	Cubic	0.93	0.76	0.98	0.78
13.2mm	12.46	9.91	9.62	1480.99	5127.62	1423.92	1.04	Cubic	0.97	0.97	0.80	1.22
13.2mm	16.55	11.47	10.36	1838.29	5939.78	2032.90	0.90	Cubic	0.86	0.90	0.69	1.30
13.2mm	11.57	9.60	8.59	1234.60	3691.96	1232.09	1.00	Cubic	0.94	0.89	0.83	1.08
13.2mm	12.91	9.62	9.29	1495.99	4469.54	1405.40	1.06	Cubic	0.88	0.97	0.75	1.29
13.2mm	10.96	10.57	9.14	1266.23	3470.04	1312.94	0.96	Cubic	0.88	0.86	0.96	0.90
53.5mm	47.59	30.89	30.08	16512.11	166185.17	16232.87	1.02	Elongated	0.89	0.97	0.65	1.50
37.5mm	51.09	29.35	19.73	14314.31	126345.86	13448.18	1.06	Elongated	0.85	0.67	0.57	1.17
37.5mm	45.09	26.13	23.00	12202.71	101164.83	12049.23	1.01	Elongated	0.86	0.88	0.58	1.52
26.5mm	38.96	19.22	15.21	7577.52	46268.61	7103.21	1.06	Elongated	0.82	0.79	0.49	1.60

26.5mm	28.25	17.34	16.15	5829.46	36607.04	5217.45	1.11	Elongated	0.91	0.93	0.61	1.52
26.5mm	28.11	16.58	14.70	5394.35	30049.05	4796.96	1.12	Elongated	0.87	0.89	0.59	1.50
26.5mm	30.86	19.46	14.83	6152.96	36929.68	5779.61	1.06	Elongated	0.87	0.76	0.63	1.21
26.5mm	34.45	19.68	15.15	7196.22	43672.54	6462.95	1.11	Elongated	0.83	0.77	0.57	1.35
19mm	18.97	11.95	10.76	2645.26	10985.91	2379.15	1.11	Elongated	0.90	0.90	0.63	1.43
19mm	20.66	11.95	10.57	2636.92	10270.76	2530.98	1.04	Elongated	0.87	0.88	0.58	1.53
19mm	21.09	12.98	10.13	2721.29	10972.53	2654.96	1.02	Elongated	0.88	0.78	0.62	1.27
19mm	23.87	13.77	12.79	3420.59	14647.93	3459.65	0.99	Elongated	0.85	0.93	0.58	1.61
19mm	23.50	14.24	13.86	3499.31	15954.01	3646.78	0.96	Elongated	0.88	0.97	0.61	1.61
13.2mm	17.51	10.92	9.64	1959.47	7053.97	1981.88	0.99	Elongated	0.91	0.88	0.62	1.41
63mm	50.49	44.69	29.74	23333.78	284150.05	21652.09	1.08	Flaky	0.90	0.67	0.89	0.75
63mm	50.07	44.39	24.35	21444.77	241348.39	19553.29	1.10	Flaky	0.87	0.55	0.89	0.62
53.5mm	47.36	37.14	19.96	14588.05	130807.64	15034.90	0.97	Flaky	0.85	0.54	0.78	0.69
37.5mm	43.12	29.51	19.61	12708.93	104678.42	11630.90	1.09	Flaky	0.85	0.66	0.68	0.97
26.5mm	28.74	20.95	13.96	6099.44	36733.69	5568.70	1.10	Flaky	0.88	0.67	0.73	0.91
37.5mm	51.48	30.91	16.72	13352.61	108125.91	13169.11	1.01	Flat & elongated	0.82	0.54	0.60	0.90
							<b>1.05</b>	<b>Mean</b>	<b>0.89</b>	<b>0.79</b>	<b>0.71</b>	<b>1.11</b>



**Table 8.7: Summary of average results of scanned particles**

<b><u>Recycled ballast from Km 9</u></b>				
<b>Sieve Size</b>	<b>Average of Roundness</b>	<b>Average of Sphericity</b>	<b>Average of Elongation (E)</b>	<b>Average of Flatness (F)</b>
13.2mm	0.97	0.68	0.71	0.69
19mm	1.01	0.73	0.69	0.64
26.5mm	1.00	0.76	0.72	0.70
37.5mm	1.06	0.78	0.81	0.72
53mm	1.06	0.80	0.72	0.82
9.5mm	1.02	0.74	0.72	0.75
<b>Averages</b>	1.01	<b>0.75</b>	<b>0.72</b>	<b>0.70</b>
<b><u>Recycled ballast from Km 17</u></b>				
13.2mm	1.01	0.72	0.65	0.70
19mm	0.95	0.73	0.58	0.78
26.5mm	1.02	0.76	0.64	0.79
37.5mm	1.01	0.78	0.74	0.78
53.5mm	1.01	0.82	0.93	0.86
63mm	1.06	0.77	0.61	0.87
9.5mm	0.93	0.69	0.60	0.67
<b>Averages</b>	1.00	<b>0.75</b>	<b>0.66</b>	<b>0.77</b>
<b><u>Recycled ballast from Km 31</u></b>				
13.2mm	1.01	0.77	0.80	0.81
19mm	0.96	0.74	0.60	0.79
26.5mm	0.99	0.79	0.70	0.78
37.5mm	0.99	0.77	0.71	0.81
53mm	0.94	0.74	0.70	0.72
9.5mm	0.96	0.75	0.63	0.85
<b>Averages</b>	0.98	<b>0.77</b>	<b>0.69</b>	<b>0.80</b>

<b><u>Recycled ballast from Km 32</u></b>				
13.2mm	0.95	0.74	0.75	0.66
19mm	0.91	0.68	0.52	0.82
26.5mm	0.97	0.76	0.65	0.77
37.5mm	0.99	0.78	0.71	0.80
53.5mm	1.12	0.76	0.71	0.61
63mm	0.98	0.72	0.57	0.77
<b>Averages</b>	0.98	<b>0.76</b>	<b>0.66</b>	<b>0.78</b>
<b><u>Freshly crushed ballast</u></b>				
13.2mm	0.92	0.68	0.50	0.65
19mm	0.98	0.69	0.73	0.71
26.5mm	0.98	0.69	0.68	0.58
37.5mm	1.03	0.69	0.61	0.68
53.5mm	1.04	0.72	0.64	0.74
63mm	1.04	0.82	0.63	0.97
9.5mm	0.95	0.66	0.68	0.57
<b>Averages</b>	0.99	<b>0.69</b>	<b>0.65</b>	<b>0.66</b>
<b><u>Round river pebbles</u></b>				
13.2mm	0.99	0.90	0.91	0.78
19mm	1.04	0.90	0.82	0.73
26.5mm	1.08	0.87	0.77	0.64
37.5mm	1.04	0.84	0.69	0.61
53.5mm	1.02	0.90	0.81	0.73
63mm	1.10	0.89	0.66	0.91
<b>Averages</b>	1.05	<b>0.89</b>	<b>0.79</b>	<b>0.71</b>